BOSONIC FIELD METHODS FOR UNQUENCHED LATTICE QCD

by

Jaebeom Yoo

B.S. in Physics,

Kyungpook National University, Korea, 1997

Submitted to the Graduate Faculty of

Arts and Sciences in partial fulfillment

of the requirements for the degree of

Doctor of Philosophy

University of Pittsburgh

2003

UNIVERSITY OF PITTSBURGH

FACULTY OF ARTS AND SCIENCES

This dissertation was presented

by

Jaebeom Yoo

It was defended on

August 21, 2003

and approved by

H. Anthony Duncan, Professor, Physics and Astronomy

Joseph F. Boudreau, Associate Professor, Physics and Astronomy

Robert Coalson, Professor, Chemistry

James A. Mueller, Associate Professor, Physics and Astronomy

Raymond S. Willey, Professor Emeritus, Physics and Astronomy

Dissertation Director: H. Anthony Duncan, Professor, Physics and Astronomy

BOSONIC FIELD METHODS FOR UNQUENCHED LATTICE QCD

Jaebeom Yoo, PhD

University of Pittsburgh, 2003

Two new algorithms of particular interest in unquenched lattice quantum chromodynamic simulations (lattice QCD) are studied: the all-point quark propagator algorithm for extracting full quark propagators, and the combined truncated determinant/multiboson algorithm for simulating full dynamical QCD. In each case, a detailed study of the statistical properties and efficiency of the algorithm is made, allowing optimization of the relevant parameters, as well as an application of the algorithm to a problem of physical interest in lattice QCD. In the first case, the all-point method is applied to the problem of extracting parameters of the QCD chiral Lagrangian from lattice QCD measurements of hadronic correlators. In the second case, the truncated determinant/ multiboson method is used to search for a potential Sharpe-Singleton chiral phase in the strong-coupling region of unquenched QCD.

TABLE OF CONTENTS

LIST OF TABLES

LIST OF FIGURES

1.0 INTRODUCTION TO LATTICE GAUGE THEORY

Quantum chromodynamics(QCD) is the theory of strong interactions between hadronic particles. The full analytic solution of the theory has never been found. In some field theories such as QED (quantum electrodynamics, the quantized field theory of interacting electrons and photons), calculations of the physical observables can be done perturbatively to any given accuracy with analytical methods since the coupling constant is small. That is, one first expands equations for the physical observables in order of the small coupling constant, and then does analytic calculations term by term in the expansion. However, although it becomes small in the high momentum regime, the effective coupling constant of QCD becomes large in the low momentum regime, excluding perturbative calculations for low momentum quantities. In order to perform controlled nonperturbative calculations in QCD, one instead puts the fields on a space-time lattice for computational simulations. The continuous space-time is replaced by a finite four-dimensional discrete set of points, which is called a lattice. Then, quantum fields are defined on the points in a lattice, or on the links connecting adjacent points [1]. The desired physical results for a continuum space-time are then recovered by extrapolation to the limit where the lattice spacing (the distance between adjacent points on the lattice) is taken to zero (or in practice, much smaller than the important physical distance scales in the problem).

In Quantum Field Theory, physical observables are extracted from correlation functions of fields, which can be calculated by the functional integral method. Putting fields on a lattice with the physical lattice spacing a regularizes those functional integrals with the momentum cutoff of order $\simeq 1/a$. Field correlators are calculated numerically using computers, as we shall explain below [1, 2, 3, 4, 5].

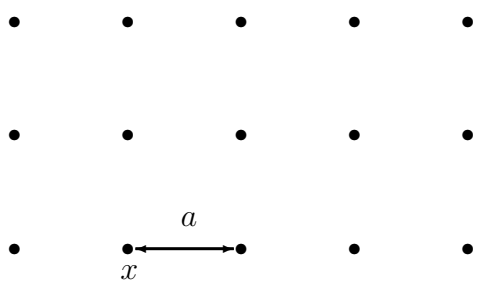

Figure 1.1: A lattice

1.1 GAUGE FIELDS ON A LATTICE

Before considering Quantum Chromodynamics on a lattice, let us begin with a pure gauge theory based on a $SU(3)$ gauge group, on a lattice. In the continuous four-dimensional Euclidean space, the nonabelian gauge theory has the action

$$S_g = \frac{1}{4}\int d^4x\, F^a_{\mu\nu}F^a_{\mu\nu} = -\frac{1}{2g^2}\int d^4x\, \mathrm{Tr}F_{\mu\nu}F_{\mu\nu}\,, \tag{1.1}$$

where the field strength tensor $F^a_{\mu\nu}$ is defined with gauge field A^a_μ as

$$F^a_{\mu\nu} = \partial_\mu A^a_\nu - \partial_\nu A^a_\mu + g f_{abc} A^b_\mu A^c_\nu, \tag{1.2}$$

where g is a coupling constant, $a = 1, \ldots, 8$ is a color index, and $\mu, \nu = 1, 2, 3, 4$ are Euclidean space-time indices. It is convenient to use a matrix form of the field strength, defined as $F_{\mu\nu} = -igF^a_{\mu\nu}(x)T^a$ with T^a, a =1,. . . ,8 the generators of $SU(3)$.

In order to regularize functional integrals in this theory on a lattice, one needs to put the gauge fields on a lattice, write the action in terms of the lattice language, and calculate path integrals of correlation functions with a lattice version of the action. $F_{\mu\nu}$ in the gauge action S_g is a complicated function of the gauge field A_μ. Fortunately there is a simple relation between A_μ and $F_{\mu\nu}$, which is used to define a lattice action.

The continuum theory has a relation which relates a line integral over a closed loop of A_μ to a surface integral of $F_{\mu\nu}$ enclosed by the same loop:

$$\mathrm{P}\, \mathrm{e}^{-\oint A_\mu \, dx_\mu} = \mathrm{e}^{-\iint F_{\mu\nu} \, d\sigma^{\mu\nu}} \,, \tag{1.3}$$

where P on the left indicates that the integration is path ordered along the loop (this is essential in the nonabelian case as A_μ is a matrix, $A_\mu \equiv -igA_\mu^a T^a$). This relation allows the lattice action(basically the square of the field strength $F_{\mu\nu}$) to be written in terms of loop integrals of A_μ around the elementary squares(plaquette) on the lattice.

Define an operator(referred to in the following as a "link variable") connecting two points $x, x+\hat{\mu}$ on the lattice(with $\hat{\mu}$ the unit vector in the μ direction) as

$$U_{x,\mu} \equiv \mathrm{e}^{-\int dx_\mu \, A_\mu(x)} = \mathrm{e}^{-aA_\mu(x+\frac{a}{2}\hat{\mu})} \,, \tag{1.4}$$

where the integration is done along the path from x and $x+\hat{\mu}$, and so link variables have a direction. Each link variable is a unitary matrix, with the hermitian conjugate (or inverse) representing the path integral along the reversed link.

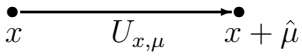

Consider the ordered product $U_{x,\mu\nu}$ of the four SU(3) matrix link variables along the smallest square (called a plaquette) with length of side a in the $\hat{\mu}, \hat{\nu}$ plane (see Fig. 1.2) [3]:

$$U_{x,\mu\nu} \equiv U_{x,\nu}^\dagger \, U_{x+\nu,\mu}^\dagger \, U_{x+\mu,\nu} \, U_{x,\mu} \tag{1.5}$$

Noting the relation (1.3), this becomes in the continuum limit $a \to 0$

$$U_{x,\mu\nu} = \mathrm{e}^{-a^2 F_{\mu\nu}(x)}, \tag{1.6}$$

from which one can get

$$\mathrm{Tr}(U_{x,\mu\nu} + U_{x,\mu\nu}^\dagger) = 2\,\mathrm{Tr}\,(1) + a^4 \mathrm{Tr}(F_{\mu\nu}(x)^2) + O(a^6) \tag{1.7}$$

Now with these new lattice link variables one can express the gauge action on the lattice [1]:

$$S_g = \sum_p \beta(1 - \frac{1}{3}\mathrm{Re}\,\mathrm{Tr} U_p) \,, \tag{1.8}$$

where $\beta = \frac{6}{g^2}$, and the sum is over all plaquettes p. It should be noted that the lattice gauge action (1.8) is constructed without the complicated definition (1.2) of $F_{\mu\nu}$ in terms of A_μ and derivatives of A_μ.

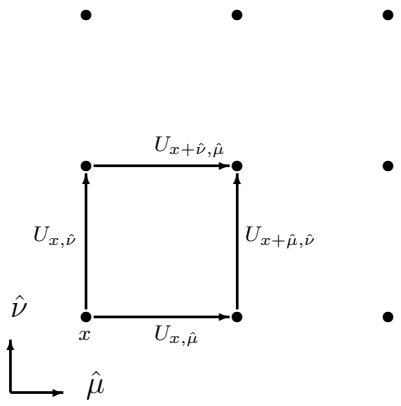

Figure 1.2: A plaquette

1.2 PATH INTEGRAL IN FIELD THEORY

In this section let us see how a path integral in a continuum field theory becomes a multi-dimensional integral in the corresponding lattice theory. As an example, the free field of a scalar particle on a lattice is considered [4].

The Lagrangian for a real scalar field ϕ is written as

$$\mathcal{L} = \frac{1}{2}(\partial_\mu \phi)^2 + \frac{1}{2}m^2\phi^2 \,. \tag{1.9}$$

The theory is quantized by the path integral, which is a sum over all configurations

$$Z = \int [d\phi]\, \mathrm{e}^{-S} \,, \tag{1.10}$$

where S is the action of each field configuration:

$$S = \int d^4x\, \mathcal{L} \,. \tag{1.11}$$

On the lattice the derivatives of ϕ are replaced by the ratio of nearest neighbor differences to the lattice spacing a

$$\partial_\mu \phi_x \to (\phi_{x+\hat{\mu}} - \phi_x)/a \,. \tag{1.12}$$

The action is a sum

$$S = a^4 \sum_{<xy>} (\phi_x - \phi_y)^2/(2a^2) + a^4 \sum_x m^2 \phi_x^2/2\,, \tag{1.13}$$

where $< xy >$ represents the set of all nearest-neighbor pairs of lattice sites. The action S can be written as an quadratic form in ϕ with the $V \times V$ matrix M with the lattice volume V:

$$S = \frac{1}{2} \sum_{xy} \phi_x M_{xy} \phi_y\,, \tag{1.14}$$

where M in this case is a finite-dimensional real symmetric matrix. Consequently, on the lattice the path integral is an ordinary multidimensional integral:

$$Z = \int [d\phi] \mathrm{e}^{-S} \propto \frac{1}{\det(M)}\,. \tag{1.15}$$

Let us calculate the propagator of ϕ:

$$< \phi_x \phi_y > \;\equiv\; \frac{1}{Z} \int D\phi\, \phi_x \phi_y \mathrm{e}^{-S}\,. \tag{1.16}$$

This integral can be easily calculated by introducing an external source J_x coupled to the field ϕ_x in the action:

$$S[J] = \frac{1}{2} \sum_{xy} \phi_x M_{xy} \phi_y - \sum_x J_x \phi_x\,. \tag{1.17}$$

This can be made a quadratic form as follows:

$$S[J] = \frac{1}{2} \sum_{xy} \left[\phi_x - \sum_z M^{-1}_{xz} J_z \right] M_{xy} \left[\phi_y - \sum_z M^{-1}_{yz} J_z \right] - \frac{1}{2} \sum_{xy} J_x M^{-1}_{xy} J_y\,. \tag{1.18}$$

The propagator of field ϕ is obtained by differentiating $S[J]$ with the external source J (and then setting J=0).

$$\frac{1}{Z} \int D\phi\, \phi_x \phi_y \mathrm{e}^{-S} = \frac{1}{Z} (\frac{\partial}{\partial J_x} \frac{\partial}{\partial J_y}) \int D\phi\, \mathrm{e}^{-S[J]}\,. \tag{1.19}$$

As one changes the integration variable ϕ to $\phi_x - \sum_z M^{-1}_{xz} J_z$, the integral (1.19) can be easily done:

$$< \phi_x \phi_y >= \frac{1}{Z}(\frac{\partial}{\partial J_x}\frac{\partial}{\partial J_y})\mathrm{e}^{\frac{1}{2}\sum_{xy} J_x M^{-1}_{xy} J_y}|_{J=0} \tag{1.20}$$

This gives

$$< \phi_x \phi_y >= M^{-1}_{xy} \,. \tag{1.21}$$

The propagator of ϕ is the inverse of the matrix M on the lattice. Similarly, one can calculate correlators of any number of ϕ as averages of products of matrix elements of M^{-1}. In general, propagators in lattice field theory amount to inverses of (very large) matrices, and the important physical quantities (correlators) to products of elements of these propagators.

1.3 QUARK FIELDS ON A LATTICE

In QCD quarks are represented by fermionic fields that have spinor and color degrees of freedom. Quark fields are defined on a four dimensional lattice of discrete points. To understand the specific problems of fermion fields on a lattice, let us first put a free fermion field on a lattice. The continuum theory of a fermion field ψ with mass m has the Lagrangian

$$\mathcal{L}_q = \bar{\psi}(i\gamma^\mu \partial_\mu + m)\psi \,, \tag{1.22}$$

where γ^μ are the 4x4 Dirac matrices. The above Lagrangian contains a first order derivative with respect to space and time. A derivative $\partial f(x)$ is the limit of the ratio of $f(x+\epsilon) - f(x)$ to ϵ as ϵ tends to zero. Once this limit is taken, the derivative ∂ is associated with a single point x and becomes an exactly antihermitian operator(recall that $i\partial$ is the hermitian momentum operator in quantum mechanics)

The naive lattice version of the derivative is to just replace ϵ by the lattice spacing a in the continuum definition, which can be done in two possible ways. Define forward and backward derivatives as

$$\partial^f \equiv \frac{f(x+a)-f(x)}{a}$$
$$\partial^b \equiv \frac{f(x)-f(x-a)}{a}\,, \tag{1.23}$$

respectively. However, neither of them is an antihermitian operator. By combining both of them, one can obtain an antisymmetrized lattice derivative

$$\frac{1}{2}(\partial^f+\partial^b)f(x) = \frac{f(x+a)-f(x-a)}{2a} \tag{1.24}$$

Note that the middle point x is skipped. Using this definition of the lattice derivative one can write a Lagrangian of the fermions on a lattice:

$$\mathcal{L}_q = \bar{\psi}(\frac{1}{2}i\gamma^\mu(\partial^f_\mu+\partial^b_\mu)+m)\psi\,, \tag{1.25}$$

where $\frac{1}{2}\gamma^\mu(\partial^f_\mu+\partial^b_\mu)$ is the Dirac operator for free fermions on a lattice. Unfortunately, the above lattice regularization of the derivative operator(although preserving the desired antisymmetry) leads to an unwanted proliferation of fermionic states in the continuum limit, sometimes called the doubling problem.

For example, the above Lagrangian gives the propagator of the free fermion field as

$$<\psi(x)\bar{\psi}(y)>=\int_{\pi/a}^{\pi/a}\frac{d^4\,p}{(2\pi)^4}\frac{-i\sum\gamma_\mu\bar{p}_\mu+m}{\sum_\mu\bar{p}^2+m^2}\;\mathrm{e}^{ipx}\,, \tag{1.26}$$

where an infinite volume lattice is considered for simplicity, and $\bar{p}_\mu=\frac{1}{a}\sin(p_\mu a)$.

The lattice momentum $\bar{p}_\mu$ in the denominator of (1.26) is a sine function of p_μ. Thus, the above integral gets equal contributions from all 16 corners $p_\mu=(0,\pi/a)$ in which $\sin(p_\mu)\simeq 0$. But the corner at (0,0,0,0) only has a correct continuum limit as smooth fields in the continuum limit correspond to $p_\mu\sim 0$, not π/a. The 15 other contributions are unphysical. Interestingly one can show that by skipping the middle point in defining the lattice derivative, the Dirac operator has additional symmetries [2]. In particular, one can show that the above Dirac operator has unphysical modes which wildly oscillate from point to point on the lattice

so that the lattice derivative is a bad approximation to the continuum one [2]. Since the operators

$$\hat{Q}_\mu : \psi_x \to (-1)^{x_\mu} \gamma_\mu \gamma^5 \psi_x \tag{1.27}$$

commute with the Dirac operator and anticommute with each other, one can show that for a given eigenfunction u of the Dirac operator with eigenvalue λ, the 16 functions

$$u\,,\ \ \hat{Q}_\mu u\,,\ \ \hat{Q}_{[\mu}\hat{Q}_{\nu]}u\,,\ \ \hat{Q}_{[\mu}\hat{Q}_{\nu}\hat{Q}_{\rho]}u\,,\ \ \hat{Q}_{[\mu}\hat{Q}_{\nu}\hat{Q}_{\rho}\hat{Q}_{\sigma]}u \tag{1.28}$$

form a degenerate 16-plet. The origin of this unwanted degeneracy is that, in order to make the lattice derivative antisymmetric, one uses fields at $x + a$ and $x - a$, skipping x, which induces this additional symmetry of the lattice Dirac operator. This is the "doubling problem"(although more accurately the problem in four dimensional space-time is one of a 16 fold multiplication of fermionic states).

Wilson proposed a solution to this problem by adding an artificial term proportional to a, and therefore, vanishing in the continuum limit [1]. That is,

$$\frac{1}{2} i\gamma^\mu(\partial^f_\mu + \partial^b_\mu) \ \ \longrightarrow \ \ \frac{1}{2} i\gamma^\mu(\partial^f_\mu + \partial^b_\mu) - \frac{1}{2} a\, \partial^f_\mu \partial^b_\mu \tag{1.29}$$

This Dirac operator of free fermions has the correct continuum limit as a tends to zero.

In the continuum QCD the quark part in the Lagrangian includes a gauge field:

$$\mathcal{L}_q = \bar{\psi} i\gamma^\mu(\partial_\mu + A_\mu)\psi \equiv \bar{\psi} \not{D} \psi \tag{1.30}$$

The gauge covariant derivative D can be understood in terms of parallel transporters, following the analogy with General Relativity. To define the derivative requires to subtract two values of the field separated by a small distance. To do that, a field at one point needs to be

parallel dragged to the other. With a fixed gauge field the Dirac operator in the continuum theory can be written as a limit of discrete derivatives as follows:

$$\begin{aligned} -iD\psi(x) &= (\partial_\mu + A_\mu)\psi(x) \\ &= \lim_{\delta x_\mu \to 0} \frac{\psi(x+\delta x_\mu) - \psi(x) + A_\mu(x)\,\delta x_\mu\,\psi(x)}{\delta x_\mu} \\ &= \lim_{\delta x_\mu \to 0} \frac{(1 + A_\mu(x)\,\delta x_\mu)\psi(x+\delta x_\mu) - \psi(x)}{\delta x_\mu} \\ &= \lim_{\delta x_\mu \to 0} \frac{U(x, x+\delta x_\mu)^\dagger \psi(x+\delta x_\mu) - \psi(x)}{\delta x_\mu}, \end{aligned} \tag{1.31}$$

where one can see that the link variable $U(x, x+\delta x_\mu) \equiv \mathrm{e}^{-A_\mu \delta x_\mu}$ acts as a parallel transporter. Thus, the operator

$$U(xy) = \mathrm{P}\,\mathrm{e}^{-\int_x^y A_\mu(x)\,dx_\mu}\,, \tag{1.32}$$

where the integral is done along the path, can be considered as a parallel transporter for x and y separated finitely along a certain curve.

As seen above, considering a link variable as a parallel transporter, a gauge covariant derivative can be defined. It is used to define the lattice counterpart of the gauge covariant derivative of fermion fields. One can write a naive lattice quark Lagrangian with a fixed gauge field:

$$\mathcal{L}_q = \bar{\psi}(\frac{1}{2} i\gamma^\mu(\nabla^b_\mu + \nabla^f_\mu) + m)\psi\,, \tag{1.33}$$

where ∇^f and ∇^b are gauge covariant forward and backward derivatives(recall Eq. (1.23)). This action has the same doubling problem as do free fermions. To cure the problem, adding the Wilson term just as for free quarks one can write the lattice Dirac operator with a fixed gauge field:

$$D = \frac{1}{2}\left(i\gamma^\mu(\nabla^b_\mu + \nabla^f_\mu) - a\nabla^f\nabla^b\right) \tag{1.34}$$

Rescaling the quark field, one can have the lattice quark action of a simple form:

$$S = \sum_x \{(\bar{\psi}(x)\psi(x) - \kappa \sum_\mu (\bar{\psi}_x[1+\gamma_\mu]\psi(x+\hat{\mu}))\} \equiv \sum_{xy} (\bar{\psi}_y Q_{yx} \psi_x) \tag{1.35}$$

where Q is called the Wilson-Dirac operator, and κ is called the hopping parameter and is varied to change the bare quark mass in the action. In a theory of a free quark, it is related to the mass of the quark by $m = \frac{1}{2\kappa} - \frac{1}{2\kappa_c}$ with $\kappa_c = \frac{1}{8}$. In a theory of interacting quarks and gluons, the value of κ for which the renormalized quark mass is zero, κ_c, is called the critical kappa. In the real world, κ for the light up and down quarks is very close to κ_c.

In the previous section we obtained the lattice gauge action. Combining the quark action with it yields the complete QCD action on a lattice:

$$S_{QCD} = \sum_p \beta(1 - \frac{1}{3}\mathrm{Re}\,\mathrm{Tr}U_p) + \sum_{yx} \bar{\psi}_y Q_{yx} \psi_x \,. \tag{1.36}$$

A hadronic correlator $G[\psi, \bar{\psi}]$ is calculated by the path integral

$$< G[\psi, \bar{\psi}] > = \frac{\int DU D\bar{\psi} D\psi \, G[\psi, \bar{\psi}] \, \mathrm{e}^{-S_{QCD}}}{Z} \,, \tag{1.37}$$

where the normalization constant Z is

$$Z = \int DU D\bar{\psi} D\psi \, \mathrm{e}^{-S_{QCD}} \,. \tag{1.38}$$

Whereas the integral over gauge link fields U in (1.37) is a standard integral(over the Haar measure of $SU(3)$), the $D\psi$, $D\bar{\psi}$ fermionic integrals have to be defined formally in terms of anticommuting Grassmann variables (to preserve the anticommuting property of fermion fields), as described below.

1.4 FERMION DETERMINANT

In order to ensure the proper Pauli statistics, fermionic path integrals are defined with anticommuting Grassmann variables. Consider ψ and $\bar{\psi}$ as independent Grassmann variables, $\psi^2 = \bar{\psi}^2 = 0$. Integrals of Grassmann variables $\psi, \bar{\psi}$ are defined by

$$\int d\psi = \int d\bar{\psi} = 0\,, \quad \int d\psi\, \psi = \int d\bar{\psi}\, \bar{\psi} = 1\,. \tag{1.39}$$

Let us consider a simple example with only two Grassmann variables ψ_1, ψ_2 (with their conjugates). Let M be a general two dimensional matrix. The two dimensional fermionic path integral is

$$\int D\bar{\psi} D\psi\, e^{-\bar{\psi}_m M_{mn} \psi_n} \equiv \int d\bar{\psi}_1 d\bar{\psi}_2 d\psi_1 d\psi_2\; \mathrm{e}^{-M_{11}\bar{\psi}_1\psi_1 - M_{12}\bar{\psi}_1\psi_2 - M_{21}\bar{\psi}_2\psi_1 - M_{22}\bar{\psi}_2\psi_2}\,. \tag{1.40}$$

Using the definition (1.39) one can show (by expanding the exponential)

$$\int D\bar{\psi} D\psi\, e^{-\bar{\psi}_m M_{mn} \psi_n} = \det(M)\,. \tag{1.41}$$

In general, the Grassmann integral over fermionic fields can be regarded simply as a formal shorthand for the determinant of the matrix defining the fermionic part of the action. In the case of QCD, this is the Wilson-Dirac matrix Q in (1.36). With the Grassmann integrals one first integrates out quark fields in functional integrals (1.37), which yields

$$< \psi(x)\bar{\psi}(y) > \propto \int DU\, \mathrm{det}Q[U]\, (Q^{-1})_{xy} \mathrm{e}^{-S_g}\,, \tag{1.42}$$

where the inverse Q^{-1} of the Wilson-Dirac operator is the quark propagator. In the first step to evaluating field correlations, one generates gauge configurations with the Monte Carlo simulation according to the probability weight:

$$P[U] \propto \mathrm{det}Q[U] \mathrm{e}^{-S_g}\,. \tag{1.43}$$

The determinant $\mathrm{det}Q[U]$ is called an quark determinant. It contains the contributions from closed (internal) quark loops. However, a direct calculation of $\mathrm{det}Q[U]$ is impossible, as Q is typically a *very* large matrix. The multidimensional integral (1.42) is completely conventional but obviously immensely complex. As an example, evaluation of this integral on a 40^4 lattice

with two light quarks (up and down) involves an integration over 81920000 real variables (8 components of each of $4x40^4$ link variables for the SU(3) gauge group), where the integrand requires evaluation of the determinant of the 61440000 dimensional matrix Q ! Remarkably, developments in both algorithms and supercomputer technology will make such calculations feasible in the next decade.

To evaluate the path integrals (1.37) in QCD with the Monte Carlo method, one might think that one could first generate gauge configurations with the pure gauge action only, and then include the quark determinant (assuming one could actually calculate it!) as a prefactor when calculating physical correlators (averages of products of quark propagators). This direct approach does not work because the quark determinant fluctuates too strongly with the gauge configurations generated from the pure gauge action [3], inducing huge statistical errors in the measured quantities.

The quenched approximation to QCD consists of ignoring the effect of the closed quark loops in the quark determinant by setting $\det[Q]$ to a constant so one just generates gauge configurations without the quark determinant $\det Q[U]$. In Feynman graph language (perturbation theory) this corresponds to ignoring graphs with closed internal quark loops.

An unquenched QCD simulation, in which the quark determinant is included properly, is extremely expensive due to the huge size of the matrices involved. There are several algorithms for unquenched QCD simulations such as the Hybrid Monte Carlo method, the Multiboson method, etc.

1.5 TWO BOSONIC FIELD METHODS IN THIS THESIS

QCD path integrals involve integrals over anticommuting Grassmann variables. The results from Grassmann integrals in hadronic correlators appear in two forms: quark propagators and the quark determinant.

The conventional method to calculate a quark propagator is to use matrix linear solvers. This method gives a quark propagator with one source(where a quark is created). Calculation of some hadronic observables, however, requires quark propagators from any source point to any sink point(where a quark destroyed). In unquenched simulations, to extract

the full physical content from each gauge configuration is also important, given the huge computational investment in generating these configurations. Due to the large size of the Wilson-Dirac matrix, the conventional method is impractical for all-point propagators. A bosonic field method is developed to calculate all-point quark propagators using Monte Carlo techniques.

The probability weight of gauge configurations in full QCD simulation includes the quark determinant. One needs to convert the quark determinant to bosonic integrals for Monte Carlo simulations. Present algorithms work well only for heavy quarks, and the performances become poor at light quarks. The truncated determinant approximation method, which includes the infrared part of the quark determinant only, has been shown to be very effective with light quarks [18]. The exact algorithm of the TDA algorithm combined with the multiboson method as suggested by [18, 32], is studied for the possibility to reduce the computational cost of unquenched simulation of light quarks.

2.0 ALL POINT PROPAGATORS

2.1 THE NEED FOR ALL-POINT PROPAGATORS

Once gauge configurations are generated from the Monte Carlo simulation of the path integral of the gauge field, one performs the calculation of the quark part in the path integral (1.37) of the hadronic correlator with each gauge configuration. For example, consider the pion propagator, using $\bar{\psi}\gamma_5\psi$ as the interpolating field for the pion. The path integral giving this propagator is

$$< \bar{\psi}_x\gamma_5\psi_x\,\bar{\psi}_y\gamma_5\psi_y > \;\equiv\; \int D\bar{\psi}D\psi DU\;\bar{\psi}_x\gamma_5\psi_x\,\bar{\psi}_y\gamma_5\psi_y\,\mathrm{e}^{-S_{QCD}}\,. \tag{2.1}$$

Calculation of the Grassmann integral over the quark fields gives

$$< \bar{\psi}_x\gamma_5\psi_x\,\bar{\psi}_y\gamma_5\psi_y > \;=\; -\int DU\;\mathrm{Tr}\,\left[Q^{-1}_{xy}(U)\gamma_5 Q^{-1}_{yx}(U)\gamma_5\right]\,\det(Q)\,\mathrm{e}^{-S_g}\,. \tag{2.2}$$

With a fixed gauge configuration, the Feynman diagram of the quark fields can be drawn as in Fig. 2.1. The two lines in the figure represent the quark propagator Q^{-1}. The pion is created at point x, and destroyed at point y. In order to calculate the quark diagram one has to calculate the quark propagator Q^{-1} with each gauge configuration. The average value and the error of the propagator can be obtained from the statistical analysis of the measurement from each gauge configuration. The average value of the propagator is

$$< \bar{\psi}_x\gamma_5\psi_x\,\bar{\psi}_y\gamma_5\psi_y > \;=\; -\sum_i \frac{1}{N}\mathrm{Tr}\,\left[Q^{-1}_{xy}(U_i)\gamma_5 Q^{-1}_{yx}(U_i)\gamma_5\right]\,, \tag{2.3}$$

where U_i are N gauge configurations generated from the Monte Carlo simulation of (1.43). Similarly, to obtain this quark propagator with a fixed gauge configuration is necessary in the computation of any other hadronic correlator(whether for mesons, baryons, etc).

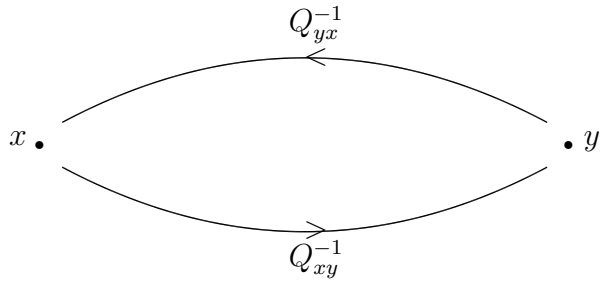

Figure 2.1: The Feynman graph for the pion propagator, $< \bar{\psi}_x \gamma_5 \psi_x \, \bar{\psi}_y \gamma_5 \psi_y >$ (a pion is created at x, and destroyed at y).

With a fixed gauge configuration the path integral giving the quark propagator is written as the fermionic (Grassmann) integral:

$$< \psi_x \bar{\psi}_y > \equiv \frac{\int D\bar{\psi} D\psi \, \psi_x \bar{\psi}_y \, \mathrm{e}^{-\bar{\psi} Q \psi}}{Z} = Q_{xy}^{-1} \,, \tag{2.4}$$

where the lattice points x and y are called a source(where the quark is created) and sink (where the quark is destroyed), respectively and the normalization constant is

$$Z = \int D\bar{\psi} D\psi \, \mathrm{e}^{-\bar{\psi} Q \psi} \,. \tag{2.5}$$

This integral cannot be evaluated using the Monte Carlo technique because it involves abstract anticommuting Grassmann numbers so the concept of a probability is not applicable here. Thus, instead, one has to find a way to compute the matrix Q^{-1} in some other way.

The conventional method to calculate a quark propagator makes use of matrix inversions to obtain Q^{-1}, but is designed to calculate not the whole matrix of the quark propagator Q^{-1}, but only one row or column of the matrix. With y fixed, the propagator Q_{xy}^{-1} is the solution of the linear equation:

$$\sum_x Q_{yx} X_x = e_y \,, \;\; X_x = Q_{xy}^{-1} \,, \tag{2.6}$$

where the elements of the column vector e are zero except $e_y = 1$ at sink point y. Thus, matrix inversion algorithms such as conjugate gradient, biconjugate gradient, etc, which find

the solution of Eq. (2.6) iteratively, can be used to find the quark propagators with a delta function source(or sink), where the quark is created(or destroyed) at a single point. The advantage of this method is that although one cannot calculate a full quark propagator(i.e. all source points to all sink points), but needs to fix the source point, a propagator obtained in this manner is exact to the machine precision so that there is no statistical error associated with calculation of quark propagators.

However, for some hadronic observables one needs a propagator from any source point to any sink point, namely an all-point quark propagator, such as a hadronic correlator in momentum space. As a simple example, consider

$$\int d^4x d^4y \, \mathrm{e}^{ip(x-y)} \langle 0|\bar{\psi}\gamma_5\psi(x)\,\bar{\psi}\gamma_5\psi(y)|0\rangle, \tag{2.7}$$

which is the pion propagator in momentum space: the integral over x and y clearly requires all-point quark propagators. The pion form factor is an even more complicated example of a hadronic correlator requiring all-point propagators. To extract the pion formfactor, we need the following 3-point function:

$$\begin{aligned} J_{t_0 t_1 t_2}(\vec{q}) &= \sum_{\vec{w}\vec{x}\vec{y}\vec{z}} e^{i\vec{q}\cdot(\vec{x}-\vec{y})} f^{\mathrm{sm}}(\vec{z}) f^{\mathrm{sm}}(\vec{w}) \\ &< \bar{\psi}(\vec{z}+\vec{x},t_2)\gamma_5\psi(\vec{x},t_2)\bar{\psi}(\vec{y},t_1)\gamma_0\psi(\vec{y},t_1)\bar{\psi}(\vec{w},t_0)\gamma_5\psi(0,t_0) > \end{aligned} \tag{2.8}$$

where f^{sm} is a spatial wavefunction to maximize the overlap of the pion field $\psi\gamma_5\psi$ with the ground state.

To calculate an all-point propagator with the conventional conjugate gradient method is completely impractical. A typical lattice volume(the number of all lattice points) V is $\sim 10^4$. With the latest Pentium processor one quark inversion takes from a few minutes to a few hours depending on the complexity of the quark action, the lattice size and the quark mass. Thus, one cannot practically calculate an all-point quark propagator with this method. On the other hand, it is important to extract the full content of information from each gauge configuration, especially for the unquenched QCD simulation, since generating gauge configurations with the quark determinant is computationally very expensive. Since the conventional method calculates the quark propagator with one source point, one uses

only a small amount of physical content from each gauge configuration. On the other hand, an all-point quark propagator contains the maximum information which a single gauge configuration yields.

2.2 PSEUDOFERMION FIELDS

A quark propagator with a fixed gauge configuration on a lattice is the inverse of the Wilson-Dirac operator as a finite dimensional matrix. Consider the propagator of two complex bosonic fields on the lattice:

$$< \phi_x \phi_y^\dagger > \equiv \frac{\int D\phi^\dagger D\phi \, \phi_x \phi_y^\dagger \, e^{-\phi^\dagger H^2 \phi}}{Z} \,, \tag{2.9}$$

where H is the hermitian Wilson-Dirac operator defined as $H = \gamma_5 Q$,

$$\phi^\dagger H^2 \phi \equiv \sum_{z,w} \phi_z^\dagger (H^2)_{zw} \phi_w,$$

and the normalization factor is

$$Z = \int D\phi^\dagger D\phi \, e^{-\phi^\dagger H^2 \phi} \,. \tag{2.10}$$

Since the operator H is hermitian, H^2 is nonnegative. For a finite quark mass H does not have zero modes so H^2 is positive definite. The above integral is therefore a well defined multidimensional gaussian integral. This bosonic path integral gives

$$< \phi_x \phi_y^\dagger > = H_{xy}^{-2} \,. \tag{2.11}$$

The lattice points x and y in Eq. (2.11) are discrete indices labeling fields, not continuous variables. Thus, one can multiply the matrix H on both sides of Eq. (2.11) from the right. This gives

$$\begin{aligned} \sum_z < \phi_x \phi_z^\dagger > \, H_{zy} &= < \phi_x (\phi^\dagger H)_y > \\ &= H_{xy}^{-1} \\ &= (Q^{-1})_{xy} \gamma_5 \,. \end{aligned} \tag{2.12}$$

As H^{-1}(modulo a trivial factor of γ_5) is the quark propagator from any point x to any other point y, the all-point quark propagator can therefore be obtained by inverting the hermitian Wilson-Dirac operator H^2 with bosonic fields [3, 6, 7] (originally suggested by Michael and Peisa in the context of static quark systems in [6]). That is, one can calculate a propagator of fermionic quark fields using bosonic fields. These bosonic fields used in calculating a quark propagator are called pseudofermion fields. One notes that this integral involves the complex bosonic fields and the positive definite exponential factor. So the Monte Carlo techniques used to evaluate multidimensional integrals can be applied to this bosonic correlator.

Let us apply this pseudofermion method to the calculation of pion propagators in momentum space. The pion propagator with a fixed gauge configuration becomes

$$\begin{aligned} < \bar{\psi}_x \gamma_5 \psi_x \, \bar{\psi}_y \gamma_5 \psi_y > &= -\mathrm{Tr}\, H^{-1}_{xy} H^{-1}_{yx} \\ &= -\sum_{a,b,\alpha,\beta} H^{-1}_{xa\alpha,yb\beta} H^{-1}_{yb\beta,xa\alpha} \,, \end{aligned} \tag{2.13}$$

where the indices (a, b), and (α, β) are for the color and spin, respectively. In terms of a pseudofermion field ϕ,

$$-\sum_{a,b,\alpha,\beta} H^{-1}_{xa\alpha,yb\beta} H^{-1}_{yb\beta,xa\alpha} = -\sum_{a,b,\alpha,\beta} < \phi_{xa\alpha} \widetilde{\phi}^{\dagger}_{yb\beta} >< \phi_{yb\beta} \widetilde{\phi}^{\dagger}_{xa\alpha} > , \tag{2.14}$$

where $\widetilde{\phi} \equiv H\phi$. This is a product of two separate path integrals. This can be written as a single path integral(but over two independent fields) by introducing another pseudofermion field χ:

$$-\mathrm{Tr}\, H^{-1}_{xy} H^{-1}_{yx} = -\sum_{a,b,\alpha,\beta} < \phi_{xa\alpha} \widetilde{\phi}^{\dagger}_{yb\beta} \, \chi_{yb\beta} \widetilde{\chi}^{\dagger}_{xa\alpha} > \, . \tag{2.15}$$

Rearranging the pseudofermion fields, one has

$$\begin{aligned} < \bar{\psi}_x \gamma_5 \psi_x \, \bar{\psi}_y \gamma_5 \psi_y > &= -\sum_{a,b,\alpha,\beta} < (\widetilde{\phi}^{\dagger}_{yb\beta} \chi_{yb\beta}) \, (\widetilde{\chi}^{\dagger}_{xa\alpha} \phi_{xa\alpha}) > \\ &\equiv - < (\widetilde{\phi}^{\dagger} \cdot \chi)_y \, (\widetilde{\chi}^{\dagger} \cdot \phi)_x > \, . \end{aligned} \tag{2.16}$$

Note that the factor depending on x and the factor depending on y are separated. This fact is used to obtain the pion propagator in momentum space. The pion propagator on a lattice can be defined as

$$\Delta_{ps-ps}(p) \equiv \frac{1}{V}\sum_{x,y} \mathrm{e}^{ip(x-y)} < \bar{\psi}_x\gamma_5\psi_x\,\bar{\psi}_y\gamma_5\psi_y > \ . \tag{2.17}$$

Using Eq. (2.16), one can Fourier-transform the x-dependent factor and the y-dependent factor separately. This gives

$$\Delta_{ps-ps}(p) = -\frac{1}{V} < (\widetilde{\phi}^\dagger\cdot\chi)(-p)\,(\widetilde{\chi}^\dagger\cdot\phi)(p) > , \tag{2.18}$$

where

$$\begin{aligned}(\widetilde{\phi}^\dagger\cdot\chi)(-p) &= \sum_x \mathrm{e}^{-ipx}(\widetilde{\phi}^\dagger\cdot\chi)_x\,,\\ (\widetilde{\chi}^\dagger\cdot\phi)(p) &= \sum_x \mathrm{e}^{ipx}(\widetilde{\chi}^\dagger\cdot\phi)_x\,.\end{aligned}$$

The calculation of the integral (2.18) gives the pion propagator in momentum space. Namely, the pion correlator in momentum space is calculated with this pseudofermion correlator as an integral over bosonic rather than fermionic fields. Evaluating the pion propagator in this way ensures that the maximum physical information is extracted from each gauge configuration.

The multidimensional integral (2.18) is done with the Monte Carlo method. One updates the field ϕ_x, and χ_x at site x according to the Boltzmann factor e^{-S} at one site at a time for all sites on the lattice. A complete update over the entire sites is called a sweep. As one continues sweeps, one measures

$$-\frac{1}{V}(\widetilde{\phi}^\dagger\cdot\chi)(-p)\,(\widetilde{\chi}^\dagger\cdot\phi)(p)\,. \tag{2.19}$$

The pseudofermion action is quadratic with ϕ and χ. Moreover, it is local. That is, the part of action depending on x can be written in terms of field values at neighboring sites. Thus, the update can be implemented with the standard local heatbath algorithm.

The part of the action depending on ϕ_x at x has of the form:

$$S(\phi_x) = \phi_x^\dagger A\phi_x - 2\mathrm{Re}\left[\phi_x^\dagger b_x\right]\ , \tag{2.20}$$

where

$$A = (1+16\kappa^2)\mathbf{1}\,, \tag{2.21}$$

$$b_x = 2\kappa \sum_{\mu} U_{x-\hat{\mu},\nu}\,\phi_{x-\hat{\mu}} - \kappa^2 \sum_{|\mu|\neq|\nu|} (1+\gamma_\mu)(1-\gamma_\nu) U^\dagger_{x\mu} U^\dagger_{x+\hat{\mu},\nu}\,\phi_{x+\hat{\mu}+\hat{\nu}}\,. \tag{2.22}$$

b_x does not depend on ϕ_x This $S(\phi_x)$ becomes

$$S(\phi_x) = A|\phi_x - \frac{1}{A} b_x|^2 + C \tag{2.23}$$

with an irrelevant constant term C. One needs to update the field ϕ_x at x according to $\mathrm{e}^{-S(\phi_x)}$. Let ξ_x be an random gaussian vector generated with the probability density proportional to $\mathrm{e}^{-\xi_x^\dagger \xi_x}$. The new field ϕ is obtained with this random gaussian vector as follows:

$$\phi_x^{new} = \frac{1}{\sqrt{A}}\xi_x + \frac{1}{A} b_x\,. \tag{2.24}$$

One does this local update for all of the sites on the lattice. After a sweep, one measures Eq. (2.19). The simulation proceeds as follows:

- generate pseudofermion fields ϕ and χ with the probability weight of $\mathrm{e}^{-\phi^\dagger H^2 \phi}$ and $\mathrm{e}^{-\chi^\dagger H^2 \chi}$, respectively.
- calculate and Fourier-transform the overlap fields $\widetilde{\phi}^\dagger \cdot \chi$, and $\widetilde{\chi}^\dagger \cdot \phi$.
- measure the product field, (2.19), of the two overlap fields.

This pseudofermion method was tested with a configuration on a 6^4 lattice. Since the start of the run, the fields $\phi\,, \chi$ are updated for 1000 sweeps without measuring the propagator in order for the field to reach the thermal equilibrium. After the first 1000 sweeps the pion propagator was measured after every sweep. (In a real simulation, the propagator is measured less frequently to ensure decorrelation: here the measurement is done at every sweep in order to check the autocorrelation time.) A total of 20000 sweeps was performed.

The correlation between the updated configurations is expressed in terms of the auto-correlation function, which is defined for a given quantity A as

$$C_{AA}(t) \equiv \overline{(A_i - \overline{A})(A_{i+t} - \overline{A})}\,, \tag{2.25}$$

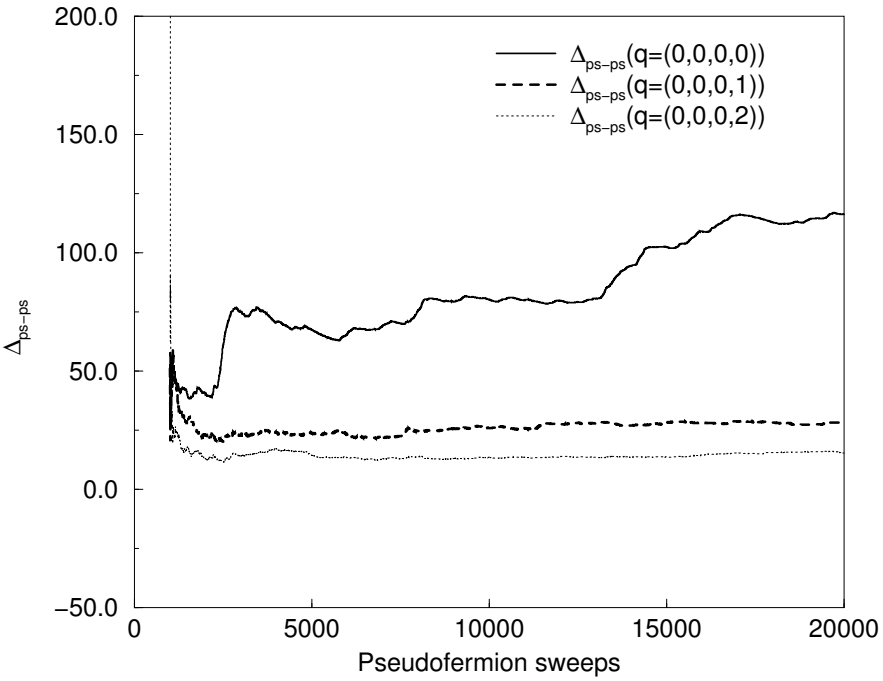

Figure 2.2: Cumulative averages of the pseudoscalar correlator

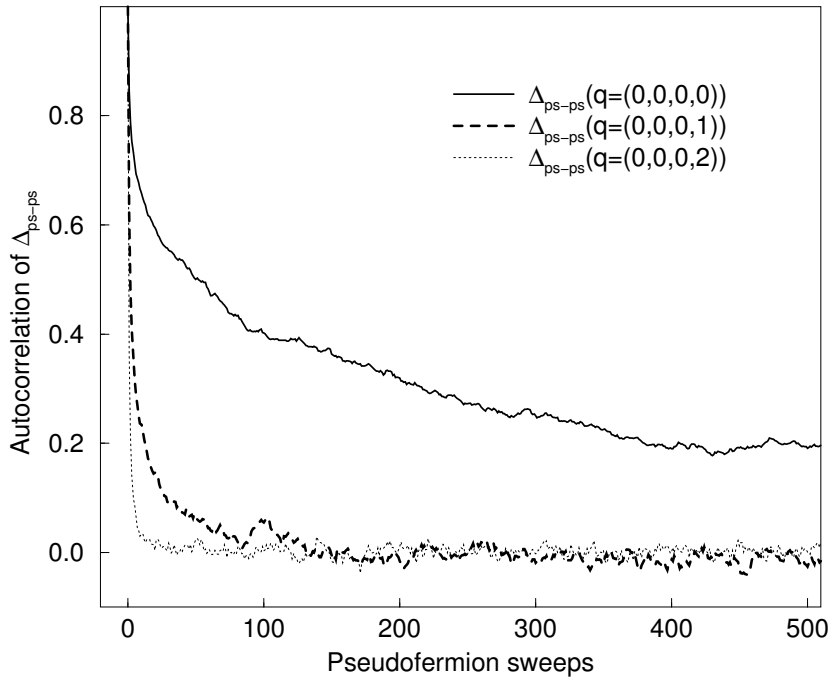

Figure 2.3: Autocorrelations of the pseudoscalar correlator

where the bars over the quantities means their averages, and $i, i+t$ are simulation times. The normalized autocorrelation function is

$$\rho_A(t) \equiv \frac{C_{AA}(t)}{C_{AA}(0)} \,. \tag{2.26}$$

The statistical error of A is related to the integrated autocorrelation time τ_{int}, defined as [8]

$$\tau_{int} \equiv \frac{1}{2} + \sum_{t=1}^{\infty} \rho_A(t) \,. \tag{2.27}$$

When each measurement of A_i is statistically independent, the variance of $\overline{A}$ is

$$\sigma_{A0}^2 \equiv \frac{1}{N-1} \overline{(A_i - \overline{A})^2} \,. \tag{2.28}$$

With the correlation, the true variance of $\overline{A}$ increases by a factor $2\tau_{int}$:

$$\sigma_A^2 = 2\tau_{int}\sigma_{A0}^2 \,. \tag{2.29}$$

Fig. 2.2 shows the cumulative average of the pion propagators $\Delta(q^2)$ in momentum space, (2.17) at the three points $q_\mu = (0,0,0,0)$, $q_\mu = (0,0,0,1)$, and $q_\mu = (0,0,0,2)$ as the update proceeds, and Fig. 2.3 shows their normalized autocorrelation functions. From these graphs one can see the different behavior between the zero momentum mode and the nonzero momentum modes. The cumulative averages of the nonzero momentum modes become flat just after several thousands sweeps, and the autocorrelations drop very fast. However, the cumulative averages of the zero mode still oscillates even at the 20000 sweep, and the autocorrelation has a long tail over hundreds of sweeps. The integrated autocorrelation times at the three momentum points were measured as 171, 4, and 1 sweeps, in order of increasing momentum.

2.3 MODE SHIFTING

The presence of small eigenvalues of H(and very small eigenvalues of H^2 !) for light quarks induces long autocorrelations of the lowest momentum modes in the pseudofermion Monte Carlo simulation. This problem can be greatly reduced by defining a modified operator H_s in which the smallest eigenvalues(which causes long correlations) are shifted to larger values [9].

Let λ_i and $|\lambda_i\rangle, i = 1, \ldots N$, be the eigenvalues and the eigenvectors of the N lowest modes of H. Let us define the shifted hermitian Wilson-Dirac operator to remove the lowest modes from H as follows:

$$H_s \equiv H + \sum_{i=1}^{N} (\lambda_i^s - \lambda_i)|\lambda_i\rangle\langle\lambda_i| \,, \tag{2.30}$$

where $\lambda_i^{(s)}$ is defined as 1 for negative λ_i and +1 for positive λ_i. The eigenvalues of the N lowest eigenmodes of the shifted operator H are now +1, or −1 depending on the sign of λ_i, so that these lowest eigenmodes have been removed from the original operator H.

Let us reconstruct the operator H^{-1} with this shifted operator:

$$\begin{aligned} H^{-1} &= \left(\frac{1}{\lambda_i^2} |\lambda_i\rangle\langle\lambda_i| \right) H \\ &= \left[H_s^{-2} - \sum_{i=1}^{N} (1 - \frac{1}{\lambda_i^2}) |\lambda_i\rangle\langle\lambda_i| \right] H. \end{aligned} \tag{2.31}$$

Evaluating H_s^{-2} with the pseudofermion field yields

$$H_{xy}^{-1} = < \phi_{\mathbf{x}} \widetilde{\phi}_{\mathbf{y}}^{\dagger} > - \sum_{i=1}^{N} (\lambda_i - \frac{1}{\lambda_i}) \langle x|\lambda_i\rangle\langle\lambda_i|y\rangle \,, \tag{2.32}$$

where $\widetilde{\phi} \equiv H_s \phi$. The pseudofermion simulation inverts not H^2 with small eigenvalues but H_s^2 with the shifted modes. The pion propagator in momentum space with these pseudofermion

fields becomes

$$\begin{aligned}\Delta_{ps-ps}(p) &= \sum_{x,y} \mathrm{e}^{ip(x-y)}\{< (\widetilde{\phi}\cdot\chi)_x(\widetilde{\chi}\cdot\phi)_y \\ &- \sum_{i}^{N}(\lambda_i - \frac{1}{\lambda_i})\left[(\widetilde{\chi}\cdot v_i)_x(v_i\cdot\chi)_y + (v_i\cdot\phi)_x(\widetilde{\phi}\cdot v_i)_y\right] > \\ &+ \sum_{i,j}^{N}(\lambda_i - \frac{1}{\lambda_i})(\lambda_j - \frac{1}{\lambda_j})(v_i\cdot v_j)_x(v_j\cdot v_i)_y\}\,, \end{aligned} \tag{2.33}$$

where v_i is the eigenvector of H with the eigenvalue λ_i. The N lowest modes of the operator H are exactly calculated and included in the action so that one expects that the long autocorrelation of the zero mode of the pion propagator is removed. These lowest eigenmodes should be calculated before the simulation of the pseudofermions.

First, the test runs with up to 10 shifted modes were performed with the same gauge configuration used in the previous section to check the computational cost and their efficiency using a PC with the Xeon 2.8GHz CPU. As before, the total sweeps were 20000, and the propagator was measured at each sweep after the first 1000 sweeps. The exact computational costs for the updates and measurements were measured in units of time/site for each mode-shift. The time to update one site, and the time to measure the pion correlator divided by the number of sites are shown in Fig. 2.4 as the number of the shifted modes is changed from 0 to 10. In this figure, the zero-mode shift means the pure heatbath. Their integrated autocorrelations are shown in Fig. 2.5. From Fig. 2.4 one can see that the measurement time increases very sharply compared to the update time as the number of the shifted modes increases. For more than 5 shifted modes the measurement takes longer than the update. The integrated autocorrelation times drop very fast with only a few lowest eigenmodes included, whereas for more than three shifted modes they change little. Since the computational cost increases with more shifted modes, the case of three shifted modes has been chosen to compare the mode-shifted method with an alternative approach to reducing long autocorrelations, the overrelaxation method, which will be described in the forthcoming section.

With the 3 shifted modes the cumulative averages and the autocorrelations of the same gauge configuration were calculated. Fig. 2.6 shows the cumulative averages of the pion

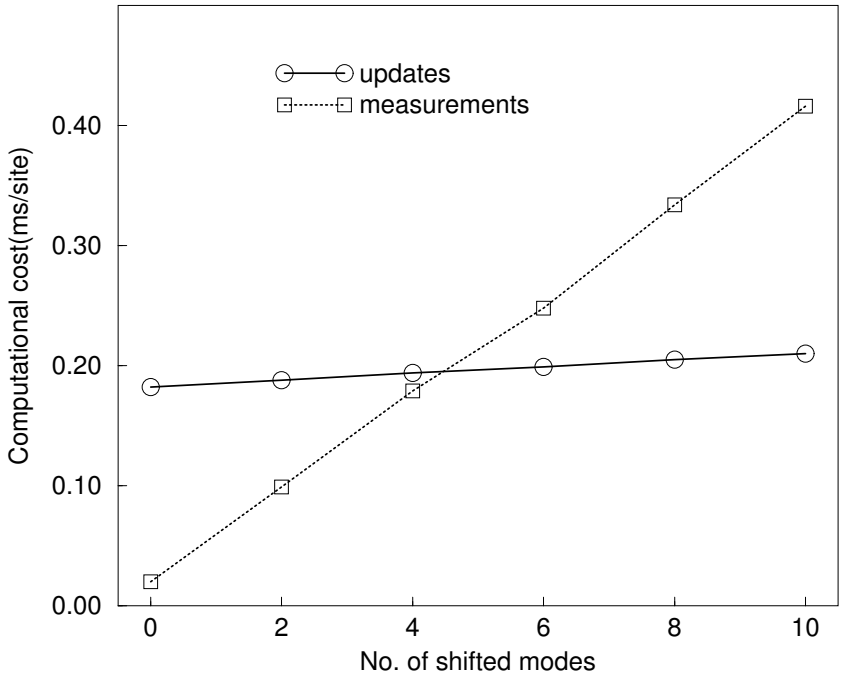

Figure 2.4: Computational cost of the updates and the measurements of the mode-shifted method.

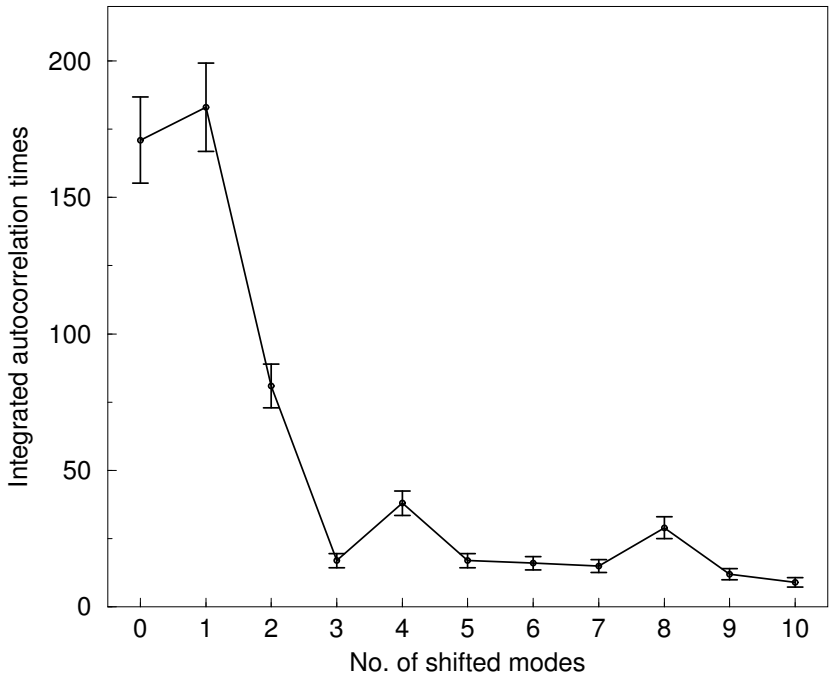

Figure 2.5: Integrated autocorrelations with the mode-shifted method.

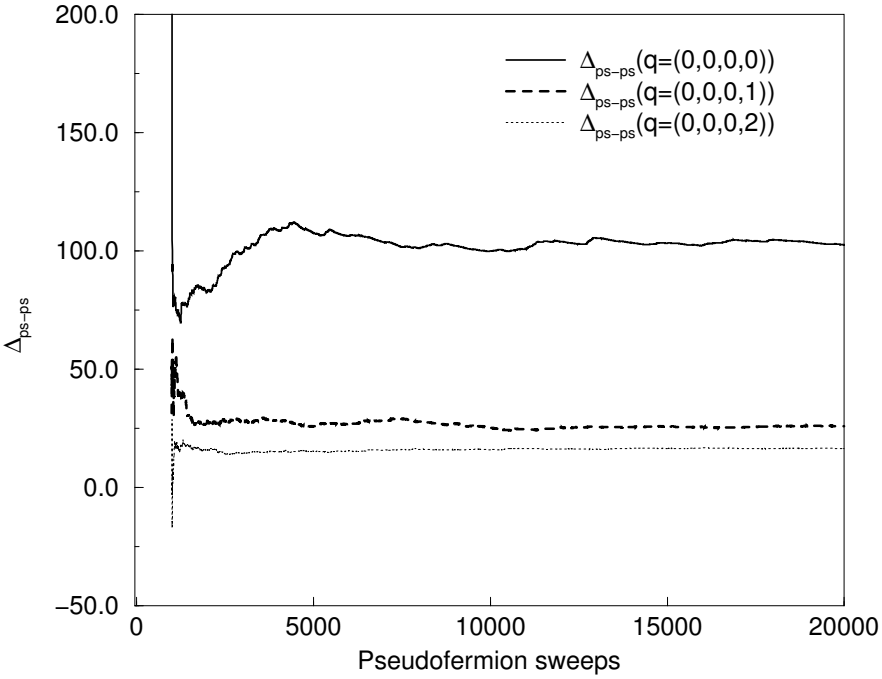

Figure 2.6: Cumulative averages of the pseudoscalar correlator with the 3 mode shifted Wilson-Dirac operator

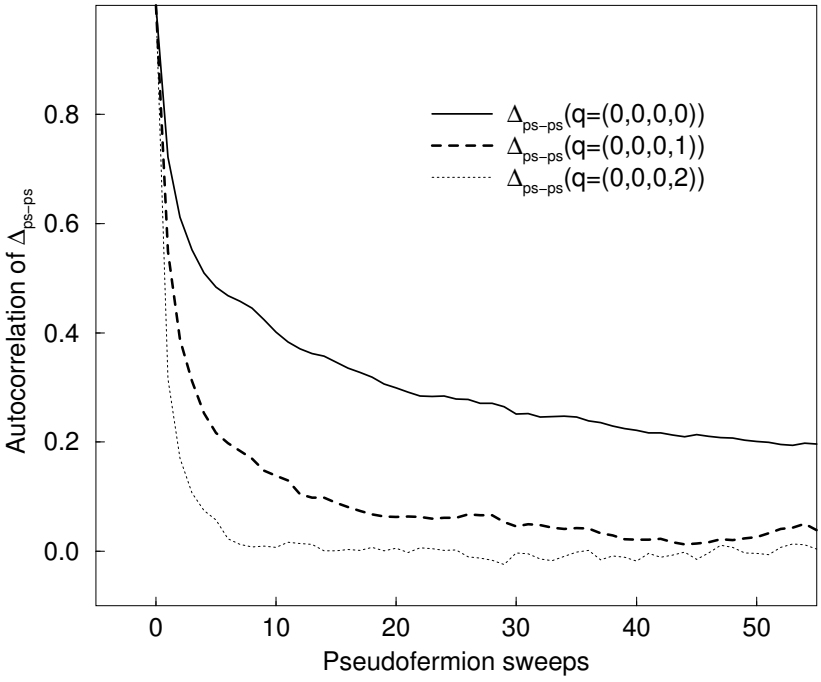

Figure 2.7: Autocorrelations of the pseudoscalar correlator with the 3 mode shifted Wilson-Dirac operator

propagator at the three points, $q_\mu = (0,0,0,0)$, $q_\mu = (0,0,0,1)$, and $q_\mu = (0,0,0,2)$, as studied in the previous section, from the mode-shift Wilson-Dirac operator. One can see the great improvement in the convergence of the cumulative average of the zero mode. The large statistical fluctuations over hundreds of sweeps have disappeared. The pion propagators at the three points have integrated autocorrelation times 17, 3, and 1, in order of the increasing momentum. Note that the autocorrelation time of the zero momentum mode has dropped from 171 to 17. The mode-shifting has almost completely removed the long-range fluctuation that comes from the smallest eigenvalues.

We calculated the full pion propagator in momentum space (Fig. 2.8). With the mode-shift improvement the propagator is obtained accurately at all momenta. From the momentum space propagator one can obtain an all-point propagator in coordinate space with any source points and any sink points. For example, one can calculate the timeslice propagator, in which spatial momentum $\mathbf{p}$ is set to zero:

$$\Delta(t) \equiv \sum_{\mathbf{x}} \Delta_{ps-ps}(\mathbf{x}, t)\,. \tag{2.34}$$

This propagator is used to compute the mass of the pions, since it decays as e^{-mt} with pion mass m for large Euclidean time t. Using the propagator in momentum space, one can easily get

$$\begin{aligned} \Delta(t) &= \sum_{\mathbf{x}} \frac{1}{V} \sum_{p} \mathrm{e}^{-ipx}\, \Delta_{ps-ps}(p) & (2.35)\\ &= \frac{1}{T} \sum_{p_0} \mathrm{e}^{-ip_0 t}\, \Delta_{ps-ps}(\mathbf{p}=\mathbf{0}, p_0)\,. & (2.36) \end{aligned}$$

With the same gauge configuration this timeslice propagator is calculated (Fig. 2.9). This propagator obtained from the all-point propagator should be the average over all $6^4 = 1296$ single-source propagators that are obtained from the conventional method. Fig. 2.9 compares this all-point propagator with a few single-source propagators. Thus, an all-point propagator extracts the full physical content from the gauge configurations, in a computationally feasible way.

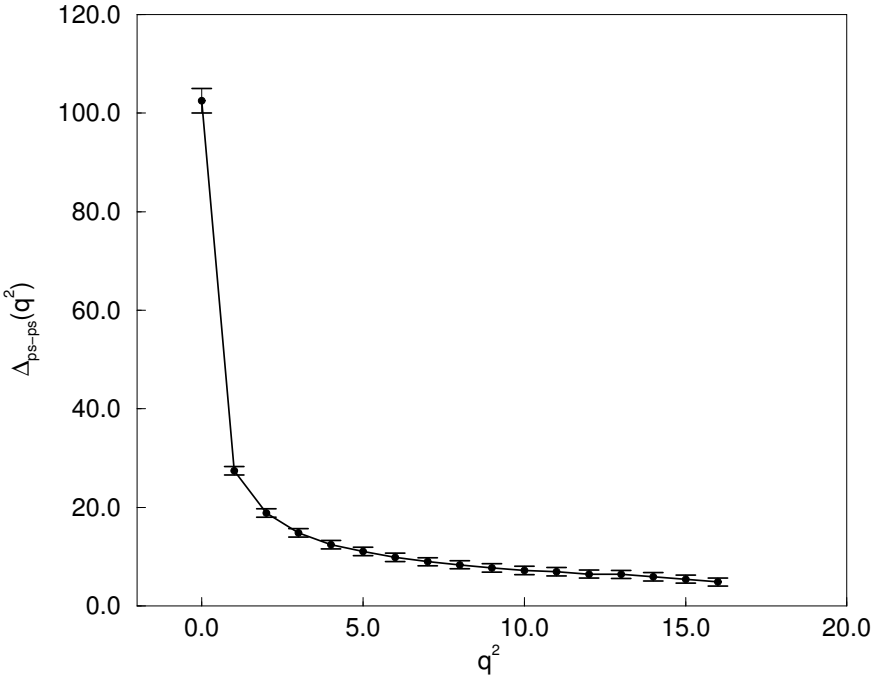

Figure 2.8: A pion propagator in momentum space from the mode shift

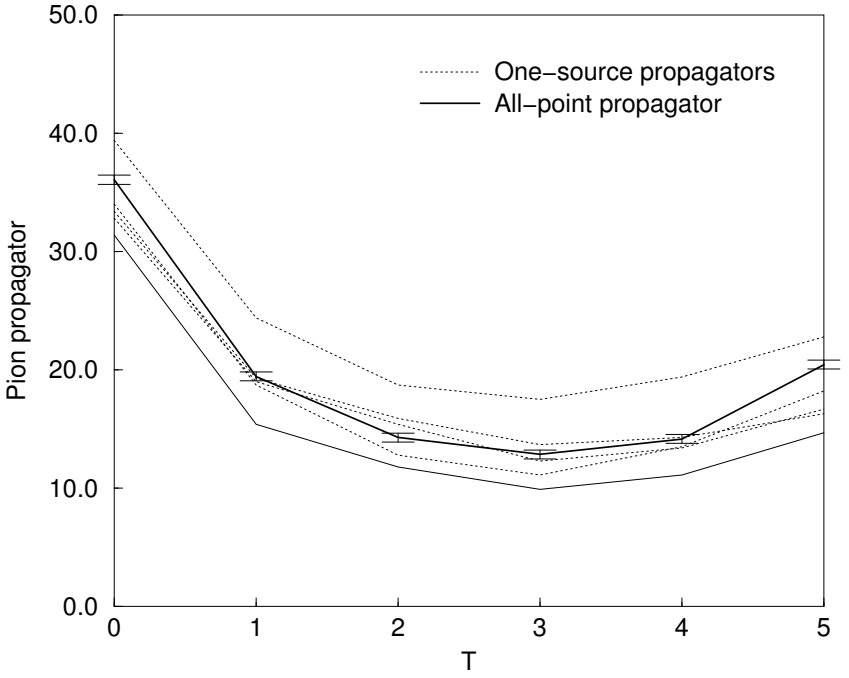

Figure 2.9: An all-point propagator from the mode shift

2.4 IMPROVEMENT BY OVERRELAXING PSEUDOFERMIONS

The gaussian heatbath used in the previous section updates the fields at one site at a time. After one sweep over the entire sites in the lattice, the field is strongly correlated to the old field. The overrelaxation method is a standard technique to reduce the autocorrelation of the gaussian local updates [10, 11]. Consider the quadratic action of a one-dimensional variable x, for simplicity:

$$S(x) = ax^2 + bx + c,\ a > 0\,, \tag{2.37}$$

where a, b, and c are constant. Instead of $e^{-S(x)}$ the overrelaxation algorithm uses the probability transition function:

$$P(x_i \to x_i') \propto \mathrm{e}^{-\frac{a}{\omega(2-\omega)}\left[\omega\overline{x}+(1-\omega)x_i-x_i'\right]^2}\,, \tag{2.38}$$

where $\overline{x}$ is the minimum, $-b/2a$, of the $S(x)$, and ω is a number between 1 and 2. When $\omega = 1$, the update is the ordinary heatbath. For $\omega > 1$, the new minimum of the exponent becomes $\omega\overline{x} + (1-\omega)x_i$, which is in the other side of the original minimum. Therefore, the updated x' tends to go away from x. As ω increases, this tendency increases. In this way the overrelaxation reduces the correlations between x and x'. For the special case of $\omega = 2$, the action does not change so that every possible configuration is not accessible with the update process (i.e., the update process does not satisfy ergodicity). One needs to combine the overrelaxation of $\omega = 2$ with a separate update process which is chosen to ensure the ergodicity (in particular, to change the action). So in this case, there is an additional computational cost.

Using this overrelaxation method one can improve autocorrelation arising in a pure heatbath update of the pseudofermion fields. The new updated field is obtained as follows: ($A = (1+16\kappa^2)\mathbf{1}$ for Wilson fermions, but a nondiagonal 12×12 matrix for more complicated quark actions)

$$\phi_x^{new} = (1-\omega)\phi_x + \omega A^{-1}b_x + \sqrt{\omega(2-\omega)}A^{-1/2}\xi_x\,. \tag{2.39}$$

Table 2.1: Integrated autocorrelations versus ω

ω	1.0	1.3	1.6	1.9	2.0
τ_{int}	171	76	41	17	26

The test runs with $\omega = 1.3$, 1.6, 1.9, and 2.0 were performed with a total of 20000 sweeps. The propagators were measured at every sweep after the first 1000 sweeps. For the $\omega = 2.0$ run the ordinary heatbath and the overrelaxation were alternated to ensure the ergodicity for a total of 40000 sweeps, in which the measurements were made after every combined heatbath and overrelaxation after the first 2000 sweeps. The autocorrelations and the errors of the pion propagator at the point $p_\mu = 0$ are shown in the table (2.1). In the simulation, the matrix A in Eq. (2.39) at each site is diagonalized in the beginning before starting the update, although A is a multiple of the identity in the present case , as we use the simplest QCD action, namely Wilson action. Then, ϕ^{new} in Eq. (2.39) can be calculated during the update without additional cost. i.e., the speed with overrelaxation remains the same as the pure heatbath. Note that even though the run with $\omega = 2.0$ is twice as slow as the others, the autocorrelation and error are not better than for $\omega = 1.9$. The case of $\omega = 1.9$ will be chosen for the later simulation.

With $\omega = 1.9$ we checked the cumulative average and the autocorrelation of the propagator at $q_\mu = (0, 0, 0, 0)$. The results of a comparison of the mode shifting and overrelaxation methods are shown in Fig. 2.10 and 2.11. The integrated autocorrelation time at the lowest momentum value is 17 with overrelaxation. The cumulative average and the autocorrelation of the lowest momentum mode are greatly improved compared to the simple heatbath algorithm. The mode shifting(3 modes) and overrelaxation methods($\omega = 1.9$) decorrelate fields at roughly the same rate.

Let us compare the speed of the two algorithms, the mode-shift and overrelaxation. As said, the overrelaxation update has the same speed as the pure heatbath. But the mode-shift method takes longer for both the update of the pseudofermion fields and the measurement of the correlator.

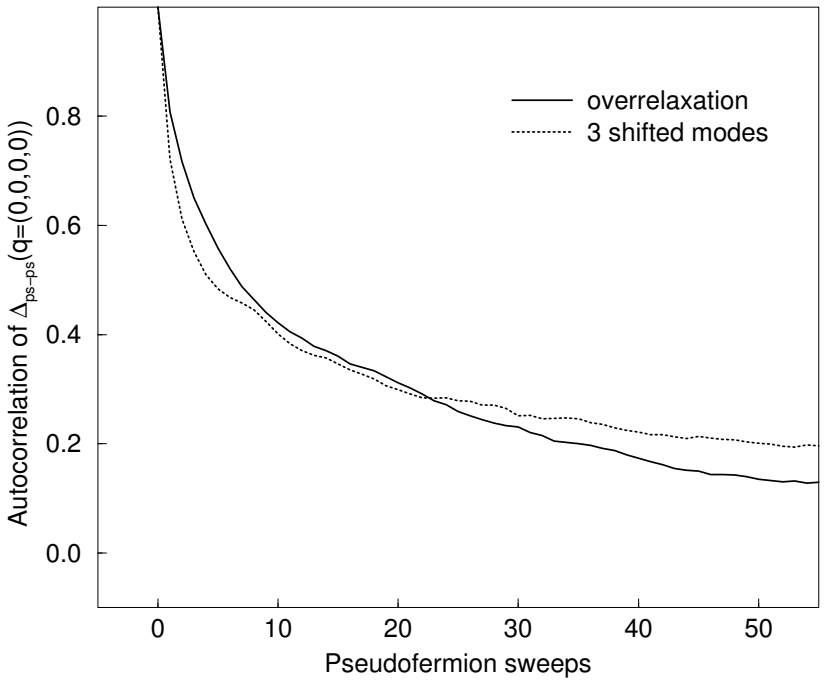

Figure 2.10: Autocorrelations of the pion propagator at zero momentum point with the overrelaxation and mode-shift methods

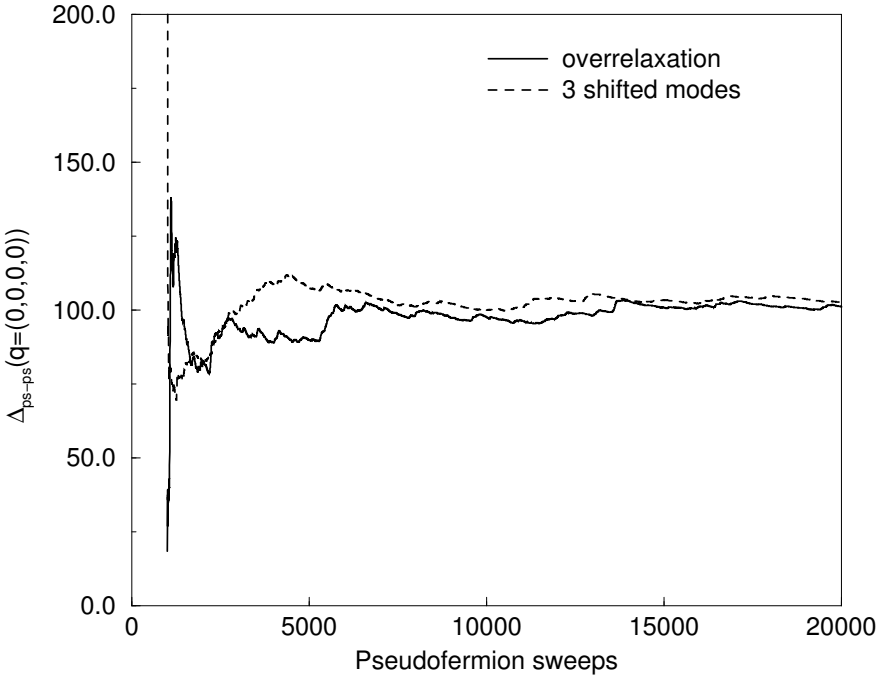

Figure 2.11: Cumulative averages of the pion propagator at zero momentum point with the overrelaxation and mode-shift methods

	update	measurement
overrelaxation	0.182 ms/site	0.020 ms/site
mode-shift	0.190 ms/site	0.156 ms/site

With the overrelaxation an update per site takes 0.182 ms but a measurement per site is only 0.020 ms. The measurement needs very little time compared to the update. However, with the mode-shift method an update per site takes 0.190 ms, and a measurement per site is 0.156 ms. The update time increases by 15 percent, but the measurement time increases by a factor 8, and becomes comparable with the update time. Now let us take into account the time of calculating the eigenmodes. The mode-shift method has to find the eigenvalues and eigenvector to be shifted before starting the Monte Carlo simulation. For a 6^4 lattice, with the same computer, each eigenvector with the eigenvalue takes 8.8min. With 3 modes, the total time is 26min. Considering the time for finding the eigenmodes, the overrelaxation method works better than the mode-shift method.

Finally, let us combine the mode-shift with the overrelaxation. Since the overrelaxation does not require an additional cost, this runs at the same speed as the mode-shift. Again, the cumulative averages and the autocorrelations of the three points were computed (Fig. 2.12 and 2.13). One can see that the cumulative average at the zero point becomes flat faster than that of the mode-shift, or the overrelaxation method. The integrated autocorrelation times were measured as 9, 2, and 1. With the overrelaxation and mode-shift methods combined one can reduce autocorrelation time by a factor 2 from the mode-shift or overrelaxation. Let us measure the propagator at every five sweeps. Then, the updated new fields of all non-zero momentum modes are completely decorrelated from the field at the preceding measurement. Then, with the overrelaxation method, five sweeps plus one measurement takes $0.93V\,ms$, and with the combined mode-shift/ overrelaxation method $1.106V\,ms$ with the lattice volume V. With the 6^4 lattice, doing 20000 sweeps with measurements every five sweeps after the 1000 sweeps, the overrelaxation method takes 80 min. The mode-shift method combined with the overrelaxation takes 95 min plus 26 min for the calculation of eigenmodes. Since the mode-shift method combined with the overrelaxation is twice as good with respect to the autocorrelation time, for example, running $121(= 95 + 26)$min for the total sweeps of 20000 with this method is more efficient than $160(2 \times 80)$min for 4000 sweeps with the

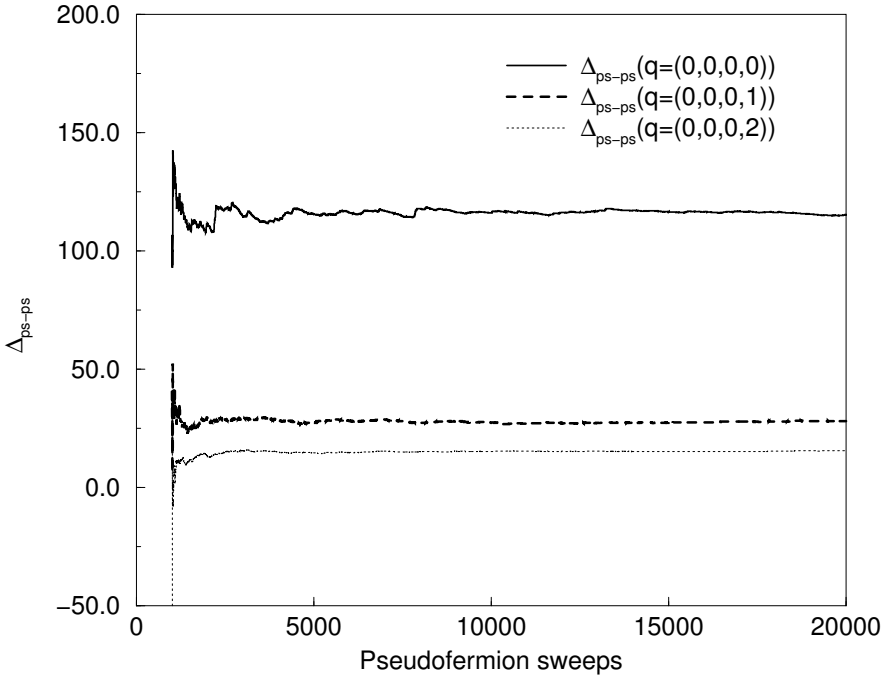

Figure 2.12: Cumulative averages of the pseudoscalar correlator with the 3 mode shifted Wilson-Dirac operator and the overrelaxation combined

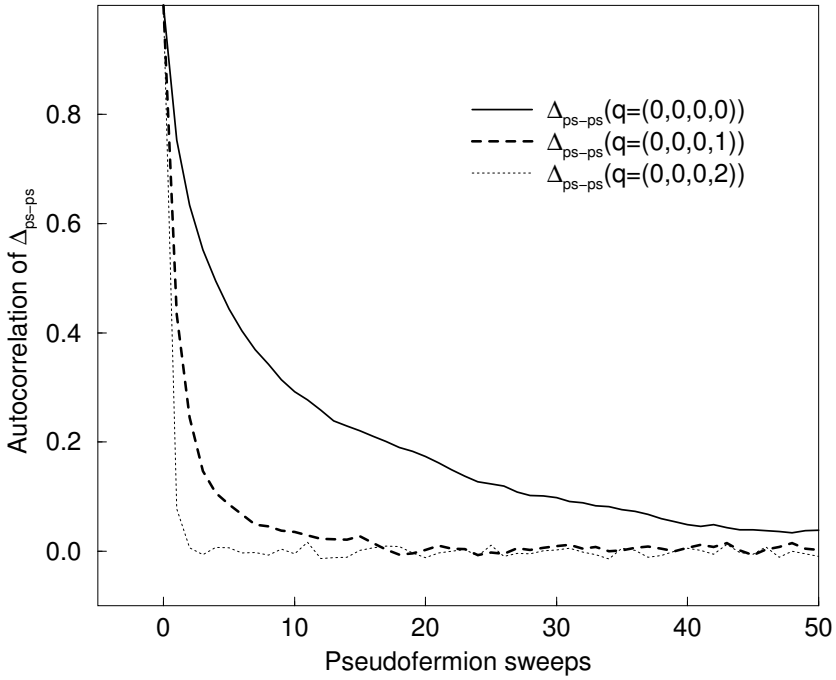

Figure 2.13: Autocorrelations of the pseudoscalar correlator with the 3 mode shifted Wilson-Dirac operator and the overrelaxation combined

overrelaxation to get the same statistical error. As measurements are done less frequently, which is needed for the case of longer autocorrelation, this combined method becomes much more efficient. That is, the combined mode-shift/overrelaxed method is the most efficient heatbath algorithm among the algorithms considered here for the pseudofermion simulation of a pion propagator.

The optimal number of eigenmodes required for the mode-shift varies as the smallest eigenvalues of the Wilson-Dirac operator, which depends on the quark mass in simulation, and the autocorrelation time is also dependent on a specific problem, especially on observables. Thus, the efficiency should be determined for each problem under consideration separately.

3.0 CHIRAL LAGRANGIAN AND CURRENT CORRELATORS

Many phenomenological investigations of low energy QCD employ the effective Lagrangian of chiral perturbation theory. The parameters(couplings) in this effective Lagrangian are in principle determined - in a completely nonperturbative way - from the underlying QCD Lagrangian, via methods of lattice QCD (cf. Ch. 4). In this chapter, we review the basic features of chiral perturbation theory [13, 14, 15, 16, 17].

3.1 CHIRAL SYMMETRY

The QCD Lagrangian for N flavors of quarks in the continuum theory is

$$\mathcal{L}_{QCD} = \frac{1}{4} F^a_{\mu\nu} F^a_{\mu\nu} + \sum_f^N \bar{\psi}_f (i\not{D} - m_f)\psi_f \,. \tag{3.1}$$

We are interested in low energy QCD with the two lightest quarks, up and down quarks, ignoring the other heavy quarks. Since the mass difference between up and down quarks is negligible, it is assumed that the two quarks are degenerate. From now on, QCD with two degenerate up and down quarks will be considered.

Let us denote the quark field by a column vector as follows:

$$q(x) = \begin{pmatrix} u(x) \\ d(x) \end{pmatrix} , \tag{3.2}$$

where $u(x)$ and $d(x)$ represent up and down quark fields, respectively. Let us define the left-handed quark field q_L and the right-handed quarks field q_R:

$$q_L = \frac{1-\gamma_5}{2} q \,, \qquad q_R = \frac{1+\gamma_5}{2} q \,, \tag{3.3}$$

respectively, and so their conjugates become

$$\bar{q}_L = \bar{q}\frac{1+\gamma_5}{2}\,, \qquad \bar{q}_R = \bar{q}\frac{1-\gamma_5}{2}\,. \tag{3.4}$$

In terms of q_L and q_R, the quark part of the QCD Lagrangian can be written as follows:

$$\mathcal{L}_q = \bar{q}_L i D q_L + \bar{q}_R i D q_R + m(\bar{q}_L q_R + \bar{q}_R q_L)\,, \tag{3.5}$$

where m is the mass of degenerate up and down quarks. When the mass term is ignored, the Lagrangian is invariant under the following global symmetry:

$$q_L \to U_L q_L \qquad q_R \to U_R q_R\,, \tag{3.6}$$

where U_L and U_R are any two independent $SU(2)$ matrices. This symmetry group is a product $U_L \times U_R$ of the two subgroups, U_L and U_R. This symmetry is called the chiral symmetry. The currents associated with the separate symmetries, U_L and U_R are

$$j_L^{\mu i} = \bar{q}_L \gamma^\mu T^i q_L\,, \qquad j_R^{\mu i} = \bar{q}_R \gamma^\mu T^i q_R\,, \tag{3.7}$$

where $T^i \equiv \tau^i/2$ for the Pauli matrix τ^i, $i = 1, 2, 3$. For the above currents, there are conserved charges:

$$Q_L^i = \int d^3x\, j_L^{0i}\,, \qquad Q_R^i = \int d^3x\, j_R^{0i}\,. \tag{3.8}$$

In the Lagrangian of the real QCD, the chiral symmetry is broken by the mass term. Let us ask a purely mathematical question. When the masses of the quark are taken to zero in the limit mathematically, is the ground state of the QCD degenerate under the chiral symmetry or not? This can be formulated in the following mathematical terms. Let $|0'\rangle$ be a state transformed from the ground state $|0\rangle$ under the $SU(2)_L \times SU(2)_R$ chiral symmetry. Since $|0'\rangle$ and $|0\rangle$ are degenerate ground states if and only if $\langle 0'|H|0'\rangle = \langle 0|H|0\rangle$, the above question is equivalent to whether

$$Q_L^i|0\rangle = Q_R^i|0\rangle = 0, \tag{3.9}$$

or not. Since the quarks in the real world are massive, this question can only be checked in the mathematical limit of $m = 0$.

When the left-hand and right-hand quarks are rotated in the same or opposite directions under the symmetry $SU(2)_L \times SU(2)_R$, the quark field transforms as follows:

$$q \to \mathrm{e}^{iT^i\alpha_i} q\,, \qquad\qquad q \to \mathrm{e}^{i\gamma^5 T^i\alpha_i} q\,, \tag{3.10}$$

respectively. The Lagrangian of the massless QCD is invariant under these transformations. The currents associated with these symmetries are

$$j^{\mu i} = \bar{q}\gamma^\mu T^i q\,, \qquad\qquad j^{\mu 5 i} = \bar{q}\gamma^\mu\gamma^5 T^i q\,, \tag{3.11}$$

respectively, where $j^{\mu i}$ is called the isospin current, and $j^{\mu 5 i}$ the axial isospin current. Thus, the chiral symmetry group of the product of U_L and U_R is equivalent to the the product group of the isospin and axial isospin symmetry group. Namely,

$$SU(2)_R \times SU(2)_L \equiv SU(2)_V \times SU(2)_A\,. \tag{3.12}$$

These currents have the conserved charges:

$$Q^i = Q^i_L + Q^i_R\,, \qquad\qquad Q^{5i} = Q^i_R - Q^i_L. \tag{3.13}$$

In the QCD ground state, pairs of the quark and antiquark are expected to form a condensate similar to electron pairs in a superconductor. The result is that the expectation value of the scalar operator $\bar{q}q$ becomes nonzero:

$$\langle 0|\bar{q}q|0\rangle \neq 0\,. \tag{3.14}$$

The chiral symmetry is affected by the nonvanishing quark condensate. Let us see how the operator $A^i = \bar{q}\gamma_5 T^i q$ transforms under the axial isospin symmetry. For an infinitesimal ϵ_k,

$$\mathrm{e}^{iQ^{5k}\epsilon_k} A^i \mathrm{e}^{-iQ^{5k}\epsilon_k} \;\; = \;\; (\bar{q}\mathrm{e}^{-i\gamma^5 T^k\epsilon_k})\gamma^5 T^i(\mathrm{e}^{-i\gamma^5 T^k\epsilon_k} q) \tag{3.15}$$

where the repeated index k should not be summed. Expanding both sides up to the first order of ϵ yields

$$A^i + i\epsilon_i[Q^{5k}, A^i] = A^i - i\epsilon_k\bar{q}\{T^k, T^i\}q\,. \tag{3.16}$$

This gives

$$[Q^{5k}, A^i] = -\bar{q}\{T^k, T^i\}q \tag{3.17}$$

Setting $i = k$,

$$[Q^{5k}, A^k] = -\frac{1}{4}\bar{q}q \tag{3.18}$$

Thus, when the quark condensate does not vanish,

$$\langle 0|[Q^{5i}, A^i]|0\rangle \neq 0, \tag{3.19}$$

i.e.,

$$Q^{5i}|0\rangle \neq 0 \tag{3.20}$$

That is, a nonvanishing quark condensate (3.14) implies that the chiral symmetry is spontaneously broken as follows:

$$SU(2)_V \times SU(2)_A \rightarrow SU(2)_V \tag{3.21}$$

The Goldstone theorem says that when a continuous global symmetry is spontaneously broken in the ground state, for each broken generator of the symmetry group, there exists a massless spinless particle of the same quantum numbers as the current associated with the symmetry. Therefore, due to the broken SU_A symmetry, massless particles with odd parity and zero spin are expected to exist in the massless limit of the quarks (for the two flavors, the three generators of $SU(2)$ imply that the number of these particles should be three).

In real QCD the quarks are massive, and there are no massless bosonic particles with odd parity, but three light pions with the expected quantum numbers. Since the masses of the up and down quarks are small, the chiral symmetry is still a very good symmetry. Thus, the mass term can be treated a perturbation to the Lagrangian of the massless quarks in the low energy region. Then the Goldstone particles can get small masses from this perturbation, still having the same quantum numbers.

3.2 CHIRAL PERTURBATION THEORY

Pions are Goldstone boson particles coming from the approximate chiral symmetry spontaneously broken. The masses of up and down quarks are only $\sim$ 7MeV, though the characteristic hadronic scale is $\sim$ 500MeV. So it is expected that there is a low energy regime in which high energy degrees of freedom are negligible and the relevant degrees of freedom are the pion fields only. The idea of chiral perturbation theory is that one ignores(integrates out) those high energy degrees of freedom, and writes the Lagrangian with the low energy (pionic) degrees of freedom only. This effective Lagrangian can be determined from the symmetries of QCD including the chiral symmetry (it is written as the most general Lagrangian satisfying the required symmetries). Gasser and Leutwyler [16] derived the chiral effective Lagrangian, and calculated various low energy field correlators including the two-point current correlators.

Let us sketch briefly how the current correlators are calculated from chiral perturbation theory as we follow Ref. [16] closely. As demonstrated with the scalar field in Ch. 1, a field correlator can be obtained from the generating functional by differentiating with respect to the external source. With the source fields v_μ, a_μ, s, p for the vector, axial vector, scalar, and pseudoscalar currents, respectively, the QCD Lagrangian can be written as follows [16]:

$$\mathcal{L} = \mathcal{L}^{QCD}_{m_{quark}=0} + \bar{q}\gamma^\mu(v_\mu + a_\mu\gamma_5)q - \bar{q}(s - i\gamma_5 p)q\,, \tag{3.22}$$

where the source field s fluctuates around the quark mass matrix. This Lagrangian is invariant under the chiral symmetry $SU(2)_L \times SU(2)_R$ with the appropriately chosen transformation properties of the external source fields under the symmetry.

Consider a $O(4)$ vector field $U(x)$ with the unit length, i.e., $U^T U = 1$. The chiral symmetry $SU_L(2) \times SU_R(2)$ can be realized as follows:

$$U \to U' : U'(x)\cdot\tau = V_L U(x)\cdot\tau V_R\,, \tag{3.23}$$

where V_L, V_R are symmetry transformations for $SU_L(2)$, $SU_R(2)$, respectively. One can write the most general Lagrangian satisfying the chiral symmetry with the scalar field $U(x)$ in an

expansion in order of the pion momentum p. The order counting rule is that

$$\begin{aligned} & U(x) \sim 1, \\ & v_\mu(x),\, a_\mu(x),\, \partial_\mu U(x) \sim p, \\ & s(x),\, p(x),\, \partial_\nu v_\mu(x),\, \partial_\mu \partial_\nu U(x) \sim p^2\,. \end{aligned} \tag{3.24}$$

With this rule, one can obtain the effective chiral Lagrangian in order of p. The leading order of the chiral effective Lagrangian is p^2:

$$\mathcal{L}_1 = \frac{F^2}{2} \nabla_\mu U^T \nabla^\mu U + 2BF^2 (s^0 U^0 + p^i U^i)\,, \tag{3.25}$$

where ∇_μ is the covariant derivative under the symmetry transformation of $SU(2)_L \times SU(2)_R$. Gasser and Leutwyler [16] obtained the next-to-leading order Lagrangian of p^4 and using this Lagrangian, they calculated various two-point and three-point functions in pion physics including the one-loop corrections, such as pseudoscalar and axial-vector current correlators, pion form factor, etc.

From [16] the effective Lagrangian of order p^4 is

$$\begin{aligned} \mathcal{L}_2 &= l_1 (\nabla^\mu U^T \nabla_\mu U)^2 + l_2 (\nabla^\mu U^T \nabla^\nu U)(\nabla_\mu U^T \nabla_\nu U) \\ &+ l_3 (\chi^T U)^2 + l_4 (\nabla^\mu \chi^T \nabla_\mu U) \\ &+ l_5 (U^T F^{\mu\nu} F_{\mu\nu} U) + l_6 (\nabla^\mu U^T F_{\mu\nu} \nabla^\nu U) \\ &+ l_7 (\widetilde{\chi}^T U)^2 + h_1 \chi^T \chi + h_2 \mathrm{Tr}(F_{\mu\nu} F^{\mu\nu}) + h_3 \widetilde{\chi}^T \widetilde{\chi}\,, \end{aligned} \tag{3.26}$$

where $F_{\mu\nu}$ is defined by

$$(\nabla_\mu \nabla_\nu - \nabla_\nu \nabla_\mu) U = F_{\mu\nu} U \tag{3.27}$$

and

$$\chi = 2B(s^0, p^i) \qquad \widetilde{\chi} = 2B(p^0, -s^i)\,. \tag{3.28}$$

With the above Lagrangian in hand, one can apply the standard perturbation technique to calculate field correlators. In order to see how the loop integrals shift the chiral parameters in the current correlators, let us present the calculation of the pseudoscalar correlator of

Gasser and Leutwyler in some detail here. In Ch. 5, the loop integrals in the infinite space-time will be replaced for the finite volume integral to derive the finite volume effect. This is important as all calculations in lattice QCD necessarily involve a finite volume space-time effect. The basic results, which will be compared with the results of lattice QCD calculations in the next Chapter, are (3.38-3.41), for the reader who wishes to skip the details.

Since we are only concerned with the pseudoscalar correlator, $v_\mu, a_\mu, s^i, F^{\mu\nu}$ in Eq. (3.26) are set to zero, and

$$s^0 = m, \tag{3.29}$$

$$\nabla \to \partial_\mu \tag{3.30}$$

Then the Lagrangian becomes at $O(p^2)$

$$\begin{aligned}
\mathcal{L}_1 &= \frac{F^2}{2}\left(\partial^\mu U^i \partial_\mu U^i + U^i \partial^\mu U^i U^k \partial_\mu U^k\right) \\
&\qquad +2BF^2\left(-\frac{1}{2}mU^{i2} - \frac{1}{8}m(U^{i2})^2 + p^i U^i\right) \\
&= \frac{F^2}{2}\left(\partial^\mu U^i \partial_\mu U^i + M^2 U^{i2}\right) \\
&\qquad +\frac{F^2}{2}\left(U^i \partial^\mu U^i U^k \partial_\mu U^k - \frac{1}{4}M^2(U^{i2})^2 + 4Bp^i U^i\right),
\end{aligned} \tag{3.31}$$

and at $O(p^4)$:

$$\begin{aligned}
\mathcal{L}_2 &= l_3(2B)^2\left[-m^2 U^{i2} + (p^i U^i)^2 + 2mp^i U^i\right] \\
&\qquad +l_4(2B)(-p^i \Box U^i) + h_1(2B)^2 p^{i2} \\
&= l_3\left[-M^4 U^{i2} + (2B)^2(p^i U^i)^2 + 4BM^2 p^i U^i\right] \\
&\qquad +l_4(2B)(-p^i \Box U^i) + h_1(2B)^2 p^{i2}
\end{aligned} \tag{3.32}$$

The correlator of the pseudoscalar $P^i = \bar{\psi}\gamma_5 \frac{\tau^i}{2}\psi$ is obtained by differentiating the generating functional with respect to p^i twice:

$$\begin{aligned}
i < P^i(x) P^k(j) > &= 8i\delta^{ik}\delta(x-y)B^2 h_1 \\
&\qquad -\left[(2BF^2)^2 + l_3(4BFM)^2\right] < U^i(x) U^k(y) > \\
&\qquad +l_4 2(2BF)^2 < \Box U^i(x) U^k(y) >
\end{aligned} \tag{3.33}$$

The Lagrangian $\mathcal{L}_1$ of p^2 order is used to generate the Feynman graphs up to one loop, and the Lagrangian of p^4 order only at level of the tree graphs for the next-leading order contribution. $< U^i(x)U^k(y) >$ only in (3.33) can get the contributions of the loop integral because according to (3.24) $< \Box U^i(x)U^k(y) >$ is already of higher order.

Expanding e^{iL} in the path integral up to the next-to-leading order yields

$$\begin{aligned} i < U^i(x)U^k(y) > &= i < U^i(x)U^k(y) >_0 \\ &- \frac{F^2}{2}\int d^4z \ < U^i(x)U^k(y)U^l(z)\partial^\mu U^l(z)U^m(z)\partial_\mu U^m(z) >_0 \\ &+ \frac{1}{8}(MF)^2\int d^4z \ < U^i(x)U^k(y)U^{l^4}(z) >_0 \\ &+ l_3M^4\int d^4z \ < U^i(x)U^k(y)U^{l^2}(z) >_0 , \end{aligned} \tag{3.34}$$

where the subscript $_0$ indicates that the expectation values are taken with the free vacuum of field U.

The second and the third terms in (3.34) can be expressed graphically as

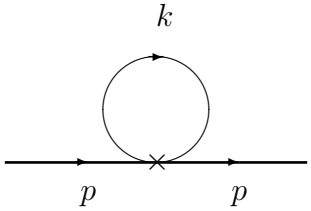

The one-loop integral above is

$$\mu^{4-d}\int \frac{d^d\,k}{(2\pi)^d}\,\frac{1}{k^2+M^2} \quad = \quad \frac{\mu^{4-d}m^{d-2}}{(4\pi)^{d/2}}\Gamma(1-\frac{d}{2}). \tag{3.35}$$

Using

$$\Gamma(1-\frac{d}{2}) = -\frac{1}{2-\frac{d}{2}} + \lambda_E - 1 \tag{3.36}$$

this loop integral becomes

$$\frac{M^2}{16\pi^2}\left(-\frac{1}{2-\frac{d}{2}} + \lambda_E - 1 - \ln 4\pi\right) + \frac{M^2}{16\pi^2}\ln\frac{M^2}{\mu^2} \tag{3.37}$$

The renormalization scheme used is that the terms with the first part in (3.37) in the perturbative calculation are subtracted by shifting the chiral parameters. Then the calculation of the above Feynman graph containing the one-loop is straightforward.

Calculating all contributions in (3.33), one gets the pseudoscalar-pseudoscalar correlator up to the next-leading order as follows:

$$i\int d^4x\, \mathrm{e}^{ip(x-y)} < P^i(x)P^k(y) > \; = \delta^{ik}\left[\frac{G_\pi^2}{M_\pi^2-p^2}+\frac{B^2}{2\pi^2}(\bar{h_1}-\bar{l_4})\right] \tag{3.38}$$

with

$$\begin{aligned} M_\pi^2 &= M^2\{1-\frac{M^2}{32\pi^2F^2}\bar{l}_3+O(M^4)\} \\ G_\pi &= 2BF\{1-\frac{M^2}{32\pi^2F^2}(\bar{l}_3-2\bar{l}_4)+O(M^4)\}\,, \end{aligned} \tag{3.39}$$

and constants $\bar{l}_3, \bar{l}_4, \bar{h}_1$.

Similarly, one can compute the axial vector-axial vector correlator with the one-loop correction:

$$\begin{aligned} & i\int d^4x \mathrm{e}^{ip(x-y)} < A_\mu^i(x)A_\nu^k(y) > \\ & \quad = \delta^{ik}\{\frac{p_\mu p_\nu F_\pi^2}{M_\pi^2-p^2}+g_{\mu\nu}F_\pi^2+(p_\mu p_\nu-g_{\mu\nu}p^2)\frac{1}{48\pi^2}(\bar{h}_2-\bar{l}_5\}+O(p^4) \end{aligned} \tag{3.40}$$

with

$$F_\pi = F\{1+\frac{M^2}{16\pi^2F^2}\bar{l}_4+O(M^4)\}\,, \tag{3.41}$$

and constants $\bar{l}_5, \bar{h}_2$.

The importance of calculations of this kind is that they provide a direct link between the QCD Lagrangian, used to calculate correlators like (3.38) and (3.40) via lattice QCD, and the parameters (such as $\bar{l}_3, \bar{h}_1$) of the effective Lagrangian, which is of great phenomenological importance.

4.0 MATCHING CURRENT CORRELATORS IN LATTICE QCD TO CHIRAL PERTURBATION THEORY

Pseudoscalar and axial-vector current correlators in momentum space were calculated with gauge configurations on a 6^4 lattice using the pseudofermion method to compute all-point propagators [7, 19]. Chiral perturbation theory gives the expansion of current correlators at low energy in order of pion momentum. By fitting the lattice data to the chiral expansions of up to the next-to-leading order the chiral parameters were extracted.

4.1 SIMULATION

This simulation has been carried out on a 6^4 lattice using the 800 unquenched gauge configurations generated with the Truncated Determinant Approximation algorithm(TDA). This algorithm will be explained in detail in a later chapter. Its main feature is that, instead of calculating the full quark determinant of the matrix Q in Eq. (1.43), $\det Q$, which is equal to $\det H$ with $H = \gamma_5 Q$ a hermitian matrix, is replaced with the product of a fixed number of lowest eigenvalues of H, called the infrared determinant. The eigenvalues of H correspond physically to the off-shellness of quarks in virtual quark loops: by including exactly all eigenvalues up to ~ 500MeV, the low energy physics relevant to chiral perturbation theory should be properly included. The objective of the calculations presented here is twofold: to check the adequacy of the TDA approximation in representing low energy chiral theory, and to test the practicality of all-point methods for computing chiral current correlators. These issues can be tested on small lattices. The effect of high modes of Q is believed to be a renormalization of the bare QCD coupling [20]. Though the simple Wilson quark action is

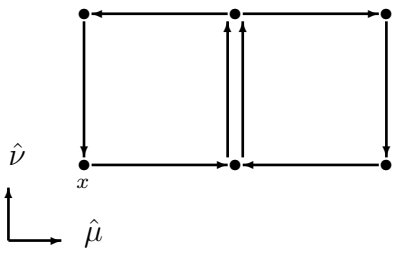

$$\mathrm{Tr}\left[U^{\dagger}_{x,\nu}U^{\dagger}_{x+\nu,\mu}U_{x+\mu,\nu}U^{\dagger}_{x+\mu,\mu}U^{\dagger}_{x+2\mu,\nu}U_{x+\mu+\nu,\mu}U_{x+\mu,\nu}U_{x\mu}\right]$$

Figure 4.1: A twisted rectangle

used for the quark part of the lattice QCD action, the twisted rectangle term(Fig.4.1) is added to the Wilson gauge action to remove the errors of order $O(a^2)$ from the finite lattice spacing [21]. For this 6^4 run, the 860 lowest eigenvalues(up to $\sim$ 420MeV) are included in the infrared determinant. The kappa value for the quark mass is chosen as 0.2050, which is equivalent to the pion mass $M_\pi = 0.396$ in lattice unit from the analysis of smeared-local pion propagators. The lattice spacing is measured as $a = 0.4$F from calculations of the string tension [22].

The two-point current correlators, pseudoscalar and axial-vector, are calculated using the two pseudofermion fields as explained in Sec. 2.2. The correlators were measured every two pseudofermion sweeps after the first 1000 sweeps. A total of 20000 sweeps were performed for each gauge configuration, which takes 2.1 hrs with a Pentium 1.5 GHz CPU.

4.2 EXTRACTING CHIRAL PARAMETERS FROM PSEUDOSCALAR CORRELATORS

In this section we show the lattice data of the pseudoscalar current correlator, and their fit to the chiral formula. The isovector pseudoscalar current correlator in momentum space is the Fourier transform of the two-point function of field $\bar{q}\tau_i\gamma_5 q$:

$$\int d^4x \langle \bar{q}\tau_i\gamma_5 q(x)\bar{q}\tau_j\gamma_5 q(y)\rangle e^{iq(x-y)}, \tag{4.1}$$

where τ_i are the Pauli matrices for $SU(2)$ flavor space. $q(x)$ is a two component quark field of up and down quarks. In our calculation the masses of up and down quarks are assumed equal. This current correlator can be related to the pion propagator in Ch. 2. The pion propagator $\Delta_{ps-ps}(q)$ in momentum space in Ch. 2 is defined as

$$\Delta_{ps-ps}(q) = \int d^4x \, \langle \bar{\psi}\gamma_5\psi(x)\bar{\psi}\gamma_5\psi(y)\rangle e^{iq(x-y)} \tag{4.2}$$

for quark field ψ. With $\tau_\pm = \frac{1}{2}(\tau_1 \pm i\tau_2)$, this is equal to

$$\int d^4x \langle \bar{q}\tau_-\gamma_5 q(x)\bar{q}\tau_+\gamma_5 q(y)\rangle e^{iq(x-y)}. \tag{4.3}$$

Thus,

$$\Delta_{ps-ps}(q) = \frac{1}{2}\int d^4x \langle \bar{q}\tau_i\gamma_5 q(x)\bar{q}\tau_i\gamma_5 q(y)\rangle e^{iq(x-y)}, \tag{4.4}$$

for any i. In the previous chapter, we have obtained the low energy expansion of the current correlator in the right side of (4.4). So Δ_{ps-ps} has a low energy expansion in terms of pion momentum:

$$\Delta_{ps-ps}(q^2) \simeq \frac{1}{2}\left(\frac{G_\pi^2}{q^2+M_\pi^2} + \frac{B^2}{2\pi^2}(\bar{l}_4 - \bar{h}_1) + O(q^2)\right). \tag{4.5}$$

We have calculated $\Delta_{ps-ps}(q^2)$ from 800 gauge configurations using the pseudofermion method. Points in Fig. 4.2 show the average values of $\Delta_{ps-ps}(q^2)$ for this ensemble. The statistical errors of momentum modes were obtained from the fluctuations between configurations, ignoring the statistical error in each configuration. The statistical errors are smaller than the symbol sizes. The pseudofermion simulation causes a statistical error in $\Delta_{ps-ps}(q^2)$ for each gauge configuration. The errors are very small except for the zero momentum mode.

Thus in our data analysis this zero-momentum point is discarded. The natural lattice momentum is $2\sin(\frac{\pi n_\mu}{L})$ at the lattice point n_μ in the Fourier transformed space from lattice coordinate space. To calculate q^2, this formula for lattice momentum is used. The entire range of q^2 is from 0 to 16 in lattice unit. A lattice momentum unit corresponds to 0.25 GeV^2 in physical unit.

Let us first describe the conventional way to calculate the pion mass. First one calculates the timeslice operator of pion fields for each gauge configuration:

$$\sum_{\mathbf{x}} < \bar{\psi}\gamma_5\psi(\mathbf{x},t)\bar{\psi}\gamma_5\psi(0) > . \tag{4.6}$$

For large t, the lowest energy state at zero spatial momentum(as a result of the sum over $\mathbf{x}$) is dominant in (4.6). This decays as $e^{-M_\pi t}$ for large t in infinite space-time. But in finite volume with the periodic boundary condition, this timeslice operator becomes $\sim (e^{-M_\pi t} + e^{-M_\pi(T-t)})(\propto \cosh(M_\pi(t-T/2)))$ for large t due to the periodicity. One fits data of the timeslice operators to this formula to get the pion mass. Lattice simulations are performed on a finite lattice, and for intermediate t, the expectation value (4.6) has contributions from the excited states. To extract better signals, normally one uses a smeared operator to create the pion:

$$\sum_{\mathbf{z}} f(\mathbf{z})\bar{\psi}(\mathbf{x}+\mathbf{z},t)\gamma_5\psi(\mathbf{x},t), \tag{4.7}$$

where $f(\mathbf{z})$ is a spatial wavefunction. This wavefunction is chosen to maximize the overlapping of the field operator with the lowest energy state. This conventional method with the smeared pion operator gives $M_\pi = 0.396 \pm 0.007$ in lattice unit with the same set of gauge configurations.

Now the fit results of the pseudoscalar correlators from the pseudofermion simulation to the chiral form will be described. From (4.5), the following fitting formula is obtained:

$$\Delta(q^2) = \frac{A_1}{q^2 + M_\pi^2} + A_2 + A_3 q^2 + A_4 (q^2)^2 \tag{4.8}$$

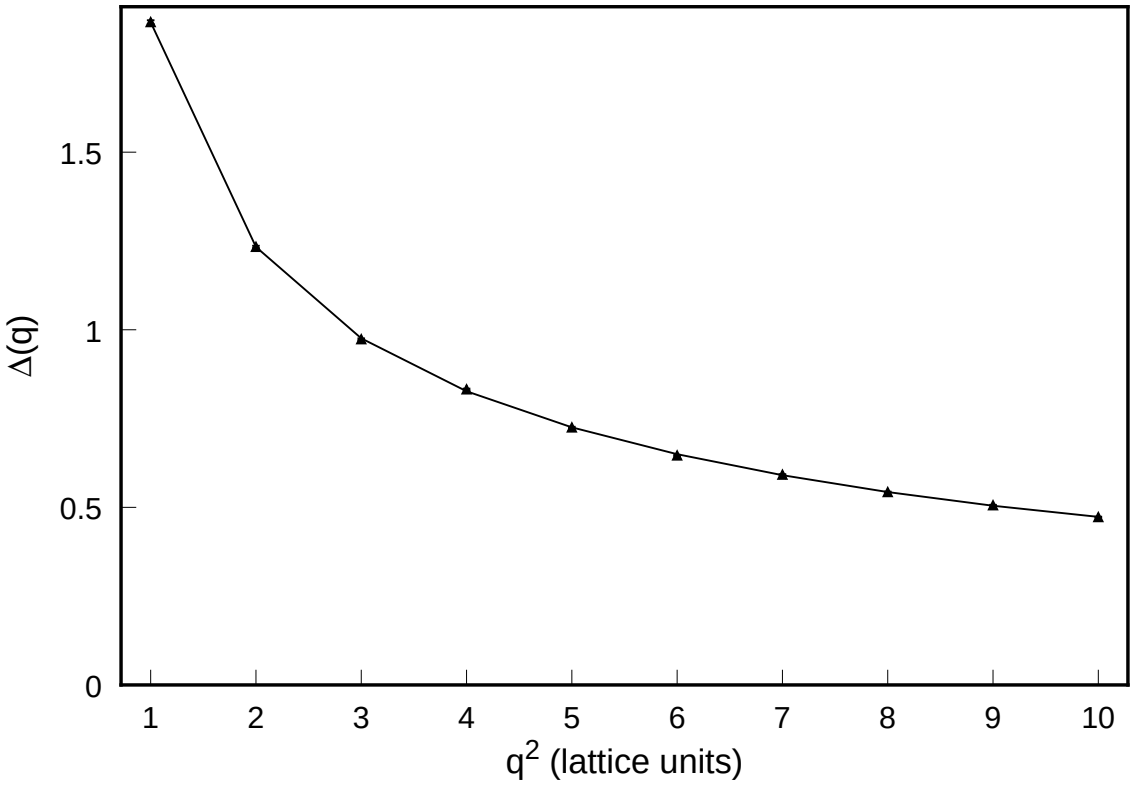

Figure 4.2: Fit of measured pseudoscalar correlator $\Delta(q^2)$, $1 \leq q^2 \leq 10$

Table 4.1: Dependence of fitted pion mass on momentum fitting range.

q^2range	M_π	χ^2/d.o.f
1-8	0.324± 0.033	3.6
1-9	0.352± 0.026	2.7
1-10	0.422± 0.020	2.6
1-11	0.449± 0.017	2.3
1-12	0.480± 0.015	2.2
1-13	0.530± 0.013	2.7

The pion masses from the fits over various ranges of q^2 are shown in Table 4.1. The $\chi^2/d.o.f.$ has a minimum in the region $10 \leq q^2 \leq 12$. We have picked the fitting range $q^2 = 1 - 10$ for analysis. The fitting for this range gives

$$\begin{aligned} A_1 &= 1.52 \pm 0.029 \\ M_\pi &= 0.422 \pm 0.020 \\ A_2 &= 0.622 \pm 0.010 \\ A_3 &= -0.0460 \pm 0.0015 \\ A_4 &= 0.00163 \pm 0.00007 \end{aligned} \tag{4.9}$$

with χ^2/d.o.f = 2.6. Fig. 4.2 shows the fitting graph with the data. The pion mass from this fit is consistent with that from the analysis of the smeared-local correlators. In this fit, the term of order q^4 is important. From the fit with up to terms of only order q^2, χ^2/d.o.f. is large(> 5), and M_π becomes very different from the value from the smeared-local operators, if the momentum extends over 6. One should note that parameters in higher order terms are calculated with very small statistical errors as well as in the leading order term, and are small. So chiral perturbation is accurate even at quite high momenta. From A_1 we find $G_\pi = 1.74 \pm 0.02$.

4.3 EXTRACTING CHIRAL PARAMETERS FROM AXIAL CURRENT CORRELATORS

The axial-vector current correlator is defined as

$$\int d^4x \langle \bar{q}\tau_i\gamma_5\gamma_\mu q(x)\bar{q}\tau_j\gamma_5\gamma_\nu q(y)\rangle e^{iq(x-y)}. \tag{4.10}$$

Following the same approach as in the case of the pseudoscalar correlator, define

$$\Delta_{ax-ax}(q) \equiv 2g_{\mu\nu}\int d^4x < \bar{\psi}\gamma_5\gamma^\mu\psi(x)\bar{\psi}\gamma_5\gamma^\nu\psi(y) > e^{iq(x-y)} \tag{4.11}$$

for a quark field ψ. Using the τ_+ and τ_-, this can be related to the axial-vector correlator of degenerate up and down quarks:

$$\begin{aligned}\Delta_{ax-ax}(q) &= 2g_{\mu\nu}\int d^4x < \bar{q}\tau_-\gamma_5\gamma^\mu q(x)\bar{q}\tau_+\gamma_5\gamma^\nu q(y) > e^{iq\cdot(x-y)} \\ &= g_{\mu\nu}\int d^4x < \bar{q}\tau_i\gamma_5\gamma^\mu q(x)\bar{q}\tau_i\gamma_5\gamma^\nu q(y) > e^{iq\cdot(x-y)}\end{aligned} \tag{4.12}$$

for any i. The chiral expansion at low momentum gives [16] :

$$\Delta_{ax-ax}(q) \simeq \frac{F_\pi^2 q^2}{q^2+M_\pi^2} - 4F_\pi^2 + \frac{1}{16\pi^2}(\bar{l}_5 - \bar{h}_2)q^2 + O(q^4) \tag{4.13}$$

From (4.13) we have the fitting formula:

$$\Delta_{ax-ax}(q) = \frac{F_\pi^2 q^2}{q^2+M_\pi^2} + A_1 + A_2 q^2 + A_3 q^4, \tag{4.14}$$

where A_1 corresponds to $-4F_\pi$ but is made a free parameter because this comes from a contact term $\propto \delta^4(x-y)$ in the coordinate space correlator which is highly UV-divergent and not accessible from our lattice calculation. The pion mass is fixed at $M_\pi = 0.422$ from the analysis of pseudoscalar correlator.

With the fitting range $0 \le q^2 \le 10$, the parameters are obtained as

$$\begin{aligned}F_\pi &= 0.187 \pm 0.011 \\ A_1 &= 0.8148 \pm 0.0038 \\ A_2 &= 0.0777 \pm 0.0003 \\ A_3 &= -0.00442 \pm 0.00002\end{aligned} \tag{4.15}$$

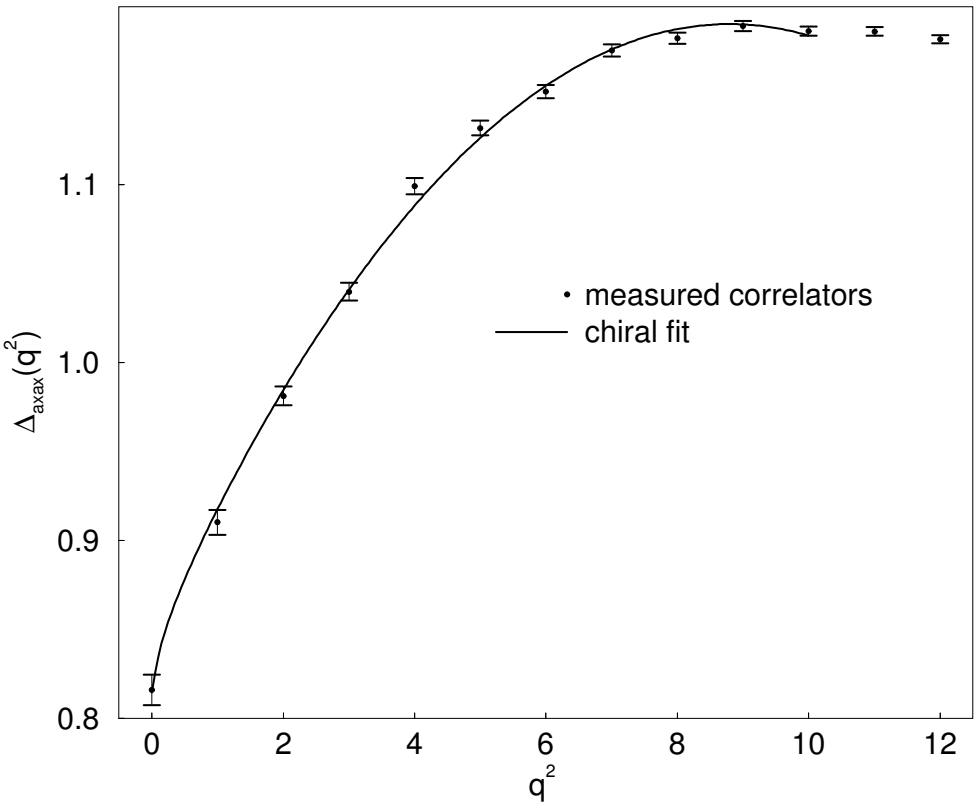

Figure 4.3: Fit of measured axial-vector correlator $\Delta_{ax-ax}(q^2)$, $0 \leq q^2 \leq 10$

with $\chi^2/d.o.f. = 2.0$. These values have very small statistical errors. The higher order parameters are very small. This shows that at least for axial current correlators the chiral perturbation theory is accurate at up to 2.5GeV^2, consistent with the case of the pseudoscalar correlator.

The chiral Ward identity relates the bare quark mass to M_π, F_π, G_π:

$$\hat{m} = \frac{F_\pi M_\pi^2}{G_\pi} \tag{4.16}$$

The values of $G_\pi = 1.74 \pm 0.02, F_\pi = 0.187 \pm 0.011, M_\pi = 0.422 \pm 0.020$ give the bare quark mass $\hat{m} = 0.0191 \pm 0.0021$. Independently the quark mass can be obtained from a calculation of topological charge. Topological charge on a lattice can be defined in terms of the quark propagator as follows:

$$Q = \hat{m} < \bar{\psi}\psi(x) >= \hat{m}\text{Tr}H. \tag{4.17}$$

With the lattice definition of quark mass $m = 1/2\kappa - 1/2\kappa_c$, the topological charge is [18]

$$Q = (\frac{1}{2\kappa} - \frac{1}{2\kappa_c}) \sum_i \frac{1}{\lambda_i}, \tag{4.18}$$

where λ_i are eigenvalues of H. This method gives $\hat{m} = 0.020$ [23, 24]. The two quark masses from the two independent methods are consistent.

In summary, the chiral parameters with very small statistical errors have been extracted from the fits of the lattice current correlators in momentum space. The pion mass and quark mass are consistent with results from other methods, i.e., analysis of smeared-local pion propagators and topological charges. The parameters in higher order terms are very small compared to the parameters in the leading order term.

5.0 FINITE VOLUME EFFECTS

5.1 DIMENSIONAL REGULARIZATION IN A FOUR-DIMENSIONAL HYPERCUBIC BOX

Lattice calculations of QCD are performed on a finite space-time. Thus a path integral of the correlator of hadronic field $O(x)$ is calculated with gauge field U and quark field ψ defined on the volume V:

$$Z^{-1}\int_V D\bar{\psi}D\psi DU\, O(x)\bar{O}(y)e^{-\int_V d^4x\, L} \equiv \langle O(x)\bar{O}(y)\rangle_V, \tag{5.1}$$

where to emphasize the finite volume a subscript V is added to the right side of (5.1). This path integral is not equal to the expectation value with respect to the vacuum of the finite space-time system, i.e.,

$$\langle O(x)\bar{O}(y)\rangle_V \neq \langle 0_V|O(x)\bar{O}(y)|0_V\rangle, \tag{5.2}$$

where $|0_V\rangle$ is the vacuum state of the finite space-time system. These two are equal only in the limit of $T \to \infty$ (where T is the Euclidean time extent of the lattice).

Even though in lattice QCD $\langle O(x)\bar{O}(y)\rangle_V$ is calculated on a finite volume, and is not a vacuum expectation value, the assumptions used in chiral perturbation theory can be still applied [25]. That is, there should be a regime at low energy and large T such that the hadronic correlators are dominated by pion fields, and the Lagrangian can be expanded in terms of pion momentum in such regime. However, coordinates x in integrals are restricted to the finite volume V. To extract the errors coming from the finiteness of space-time, let us consider the continuous four-dimensional box ($V = L^3T$). Since the rotational symmetry in the finite box is lost, when one writes the most general effective Lagrangian, it could contain

a term only satisfying the discrete rotation by a multiple of $\pi/2$ like $\sum_{\mu=1}^{4}(\nabla^\mu\phi\nabla_\mu\phi)^2$ for the theory of scalar fields ϕ. Those terms could appear from p^4 order so that it is expected that the contributions from those terms are comparable with terms at that order satisfying the continuous rotation symmetry. As the chiral parameters of the terms of order p^4 in the lattice calculation in Ch. 4 were very small compared to those of the leading-order terms, the terms with the discrete rotational symmetry are expected to be also very small. In this study of chiral perturbation in a finite box, those terms are ignored.

The free propagator of the scalar field ϕ in the infinite Euclidean space-time is

$$\langle 0|\phi(x)\phi(y)|0\rangle = \int \frac{d^4k}{(2\pi)^2}\frac{e^{ik(x-y)}}{k^2+M^2}. \tag{5.3}$$

The momentum k is continuous from $-\infty$ to $+\infty$. In a four dimensional box, the momentum becomes discrete:

$$k_{n_\mu} = \frac{2\pi}{L_\mu}n_\mu, \quad n_\mu = -\infty\cdots,-1,0,1,\cdots\infty \tag{5.4}$$

so the free propagator of the scalar field in finite V is a discrete sum:

$$\langle\phi(x)\phi(y)\rangle_V = \frac{1}{L^3T}\sum_{n_\mu}\frac{e^{ik(x-y)}}{k_{n_\mu}^2+M^2} \tag{5.5}$$

In our lattice study of chiral perturbation theory, we calculated current correlators in momentum space. The Fourier transform of (5.5) is $1/(k_{n_\mu}^2+M^2)$. Finite volume effects arise from the discrete momenta appearing in sums like (5.5), which appear in loop integrals. Our task is to compare the sums for finite box V with the integrals for infinite space-time in the loop integrals.

A loop integral appearing in the chiral perturbation calculations(this is the only loop integral contained in the pseudoscalar and axial-vector current correlators up to the next-to-leading order) is

$$\int \frac{d^4x}{(2\pi)^2}\frac{1}{k^2+M^2} \to \frac{1}{L^3T}\sum_{n_\mu}\frac{1}{k_{n_\mu}^2+M^2} \tag{5.6}$$

This loop integral in infinite volume is regularized by the dimensional regularization. Likewise, we do the dimensional regularization on a hypercubic box of (d-1) space dimension and one time-dimension:

$$\mu^{4-d}\int \frac{d^dk}{(2\pi)^d}\frac{1}{k^2+M^2} \to \frac{\mu^{4-d}}{L^{d-1}T}\sum_{n_\mu}\frac{1}{k_{n_\mu}^2+M^2} \tag{5.7}$$

To do this summation, first let us convert it to a exponential form using a Schwinger parameter λ:

$$\frac{1}{k^2+M^2} = \int_0^\infty d\lambda e^{-\lambda(k^2+M^2)} \tag{5.8}$$

This yields

$$\frac{\mu^{4-d}}{L^{d-1}T} \int_0^\infty d\lambda\, e^{-\lambda M^2} \sum_{n_\mu} e^{-\lambda k_{n_\mu}^2} \tag{5.9}$$

By changing the integration variable $\lambda \to 4\pi^2\lambda/L^2$, this integral becomes

$$\frac{\mu^{4-d}}{(2\pi)^2 L^{d-3}T} \int_0^\infty d\lambda e^{-\frac{M^2L^2}{4\pi^2}\lambda} \left(\sum_{n=-\infty}^{\infty} e^{-\lambda n^2}\right)^3 \left(\sum_{n_4=-\infty}^{\infty} e^{-L^2\lambda n_4^2/T^2}\right) \tag{5.10}$$

One needs to evaluate the sum:

$$\sum_{n=-\infty}^{+\infty} e^{-\lambda n^2} \equiv \sqrt{\pi}\mathcal{I}(\lambda) \tag{5.11}$$

The Poisson sum formula is [26]

$$\sum_{n=-\infty}^{\infty} f(2\pi n) = \frac{1}{2\pi} \sum_{n=-\infty}^{\infty} \int_{-\infty}^{\infty} f(\tau) e^{-in\tau}\, d\tau \tag{5.12}$$

where f is any smooth function. Using the Poisson sum formula,

$$\mathcal{I}(\lambda) \;=\; \frac{1}{2\pi^{3/2}} \sum_{n=-\infty}^{\infty} \int_{-\infty}^{\infty} e^{-\lambda\tau^2/4\pi^2} e^{-in\tau}\, d\tau$$

The integral in the above equation becomes

$$\int_{-\infty}^{\infty} e^{-\lambda\tau^2/4\pi^2} e^{-in\tau}\, d\tau = \sqrt{\frac{4\pi^3}{\lambda}} e^{-\pi^2 n^2/\lambda}$$

Thus,

$$\mathcal{I}(\lambda) = \frac{1}{\sqrt{\lambda}} \sum_{n=-\infty}^{+\infty} e^{-\frac{\pi^2 n^2}{\lambda}} \tag{5.13}$$

This can be expanded for large λ:

$$\frac{1}{\sqrt{\lambda}} \sum_{n=-\infty}^{+\infty} e^{-\frac{\pi^2 n^2}{\lambda}} = \frac{1}{\sqrt{\lambda}} \left(1 + 2\sum_{n=1}^{\infty} e^{-\pi^2 n^2/\lambda}\right) \simeq \frac{1}{\sqrt{\lambda}}(1 + 2e^{-\frac{\pi^2}{\lambda}} + ...) \tag{5.14}$$

Then, the loop integral in d dimensional hypercubic box becomes

$$S_2 \equiv \frac{\mu^{4-d}}{4\pi^{2-\frac{d}{2}}L^{d-3}T}\int_0^\infty d\lambda e^{-\frac{M^2L^2}{4\pi^2}\lambda}\mathcal{I}^{d-1}(\lambda)\mathcal{I}(\lambda\frac{L^2}{T^2}) \tag{5.15}$$

For large volume, $\mathcal{I}^{d-1}(\lambda)\mathcal{I}(\lambda\frac{L^2}{T^2})$ can be expanded:

$$\mathcal{I}^{d-1}(\lambda)\mathcal{I}(\lambda\frac{L^2}{T^2}) \simeq \left(\frac{T}{L}\right)\frac{1}{\lambda^{d/2}}(1+2(d-1)e^{-\frac{\pi^2}{\lambda}}+2e^{-\frac{\pi^2}{\lambda}(\frac{T}{L})^2}+...) \tag{5.16}$$

One can show that the first term in (5.16) gives the infinite volume singularity:

$$\begin{aligned} S_2 &= \frac{\mu^{4-d}}{4\pi^{2-\frac{d}{2}}L^{d-3}T}(\frac{T}{L})\int_0^\infty d\lambda e^{-\frac{M^2L^2}{4\pi^2}\lambda}\frac{1}{\lambda^{d/2}} \\ &= \frac{\mu^{4-d}}{4\pi^{2-\frac{d}{2}}L^{d-3}T}(\frac{T}{L})(\frac{ML}{2\pi})^{d-2}\Gamma(1-\frac{d}{2}) \\ &= \frac{\mu^{4-d}M^{d-2}}{(4\pi)^{d/2}}\Gamma(1-\frac{d}{2}), \end{aligned} \tag{5.17}$$

which is exactly the same as (3.35) for infinite space-time. The remaining of the integral (5.15) can be shown to be finite. For $d=4$,

$$S_2^F \equiv \frac{1}{4LT}\int_0^\infty d\lambda e^{-\frac{M^2L^2}{4\pi^2}\lambda}\left[\mathcal{I}^3(\lambda)\mathcal{I}(\lambda\frac{L^2}{T^2})-(\frac{T}{L})\frac{1}{\lambda^2}\right] \tag{5.18}$$

Since

$$\sum_{n=-\infty}^{\infty}e^{-\pi^2n^2/\lambda} < \sum_{n=-\infty}^{\infty}e^{-\pi^2n/\lambda}, \tag{5.19}$$

S_2^F is bounded from above:

$$S_2^F < \frac{T}{4L^3}\int_0^\infty d\lambda e^{-\frac{M^2T^2}{4\pi^2}\lambda}\left[\frac{1}{\lambda^2}\left(\sum_{n=-\infty}^{\infty}e^{-\pi^2n/\lambda}\right)^4-\frac{1}{\lambda^2}\right]. \tag{5.20}$$

After doing the geometrical sum, the quantity in the bracket becomes

$$\frac{1}{\lambda^2}\left(\sum_{n=-\infty}^{\infty}e^{-\pi^2n/\lambda}\right)^4-\frac{1}{\lambda^2}=\frac{1}{\lambda^2}\left(1+\frac{1}{e^{\pi^2/\lambda}-1}\right)^4-\frac{1}{\lambda^2}. \tag{5.21}$$

Let us check how this behaves in the limits of $\lambda\to 0$ and $\lambda\to\infty$. First, for $\lambda\to 0$, this becomes

$$\frac{1}{\lambda^2}(1+e^{-\pi^2/\lambda})^4-\frac{1}{\lambda^2}\simeq\frac{4}{\lambda^2}e^{-\pi^2/\lambda}\to 0 \tag{5.22}$$

So the integrand in (5.20) is well behaved at $\lambda = 0$. In the other limit of $\lambda \to \infty$,

$$\frac{1}{\lambda^2}\left(1 + \frac{1}{1 + \frac{\pi^2}{\lambda} \cdots - 1}\right)^4 - \frac{1}{\lambda^2} \sim \lambda^2 \tag{5.23}$$

When this factor is multiplied with $e^{-\frac{m^2T^2}{4\pi^2}\lambda}$, the whole integrand vanishes fast enough as $\lambda \to \infty$ that the integral (5.20) exists. Thus as S_F is bounded by a finite number, it must be finite.

For a large volume, the leading term in S_2^F is a good approximation. It has a closed form. For the case of $L = T$, the leading-order S_2^F becomes

$$S_2^{F,\text{leading}} = \frac{2}{L^2}\int_0^\infty d\lambda \frac{e^{-\frac{M^2L^2}{4\pi^2}\lambda - \frac{\pi^2}{\lambda}}}{\lambda^2} = \frac{2}{\pi^2}\frac{M}{L}K_1(ML) \tag{5.24}$$

where $K_1(x)$ is a modified Bessel function. For the limit of large ML,

$$K_1(ML) \sim \sqrt{\frac{\pi}{2ML}}e^{-ML}$$

so

$$S_2^{F,\text{leading}} \sim \frac{\sqrt{2ML/\pi^3}}{L^2}e^{-ML} \tag{5.25}$$

5.2 FINITE VOLUME CORRECTIONS TO TWO-POINT HADRONIC CORRELATORS

When we fit current correlators to the chiral formula in Ch. 4, we used the formulas for infinite volume, ignoring the errors from the finite volume. By doing the dimensional regularization in a finite hypercubic box, we can derive the corrections to these values due to finite volume. The one-loop integral in the pseudoscalar and axial-vector current calculators up to the next-to-leading order involves (5.6) only so that the finite volume corrections come from this loop integral. In infinite volume, with the same renormalization scheme as in Sec. 3.2 the loop integral gives a logarithmic term:

$$\int \frac{d^4k}{(2\pi)^4}\frac{1}{k^2 + M^2} \quad \longrightarrow \quad \frac{M^2}{16\pi^2}\ln M^2. \tag{5.26}$$

Table 5.1: Finite volume corrections $G_\pi^F, M_\pi^F, F_\pi^F$ on a 6^4 lattice with $G_\pi = 1.87, F_\pi = 0.187$

ML	1.0	2.0	3.0	4.0	5.0	6.0
S_2^F	0.0244	0.0044	0.0013	0.00041	0.00015	0.000053
G_π^F	0.607	0.109	0.032	0.010	0.0037	0.0013
M_π^F	-0.196	-0.018	-0.0035	-0.00082	-0.00024	-0.00007
F_π^F	0.130	0.024	0.0070	0.0022	0.00080	0.00028

Using the same renormalization scheme for finite volume, the finite volume loop integral gives

$$\sum_{n_\mu=-\infty}^{\infty} \frac{1}{k_{n_\mu}^2 + M^2} \quad \longrightarrow \quad \frac{M^2}{16\pi^2} \ln M^2 + S_2^F. \tag{5.27}$$

Using this rule, the finite volume corrections to M_π, G_π, F_π can be calculated as follows:

$$\begin{aligned} G_\pi &\rightarrow G_\pi^{\text{inf.vol.}} - \frac{B}{F} S_2^F \\ M_\pi &\rightarrow M_\pi^{\text{inf.vol.}} + \frac{M}{4F^2} S_2^F \\ F_\pi &\rightarrow F_\pi^{\text{inf.vol.}} - \frac{1}{F} S_2^F \end{aligned} \tag{5.28}$$

So we only need to calculate the integral S_2^F to find the finite volume corrections to leading order in chiral perturbation theory. In our simulation in Ch. 4, $M^2L^2/4\pi^2 (\simeq 0.40, ML \simeq 2.5)$ is small so that the accurate calculation of the integral in the region of small λ is necessary. Thus $S_2^{F,\text{leading}}$ can not be used in this case. *Mathematica* is used to calculate the sum in S_2^F numerically to include more terms in the expansion. This yields $S_F^2 = 0.0022$. For the case of $L = T = 6$, the values of S_2^F and the finite volume corrections (denoted by $G_\pi^F, M_\pi^F, F_\pi^F$) to G_π, M_π, F_π for several different values of ML are shown in Table 5.1. $ML = 1.0$ corresponds to that the correlation length $1/M$ is equal to L, and for $ML = 6.0$, $1/M$ is the lattice spacing. From this table, one can see that for $\frac{1}{M} \lesssim 3$ (corresponding to pion mass $\lesssim$ 200MeV on these lattices), the finite volume effect is very small.

The finite volume contribution terms become $-B_\pi S_2^F/F_\pi$, $M_\pi S_2^F/4F_\pi$, and $-S_2^F/F_\pi$ to the leading order. G_π, M_π, F_π obtained in Ch. 4 contain the finite volume errors. To get the

Table 5.2: Finite volume corrections M_π^F on a 6^4 lattice with $F_\pi = 0.187$ for the conventional smeared-local operator method in coordinate space

ML	1.0	2.0	3.0	4.0	5.0	6.0
S_2^{Fs}	0.00823	0.00221	0.000742	0.000268	0.000100	0.000038
M_π^F	0.066	0.0089	0.0020	0.00054	0.00016	0.00005

values corresponding to infinite volume one needs to subtract the finite correction terms in (5.28) from the fitting results obtained in the previous chapter.

From $F_\pi = 0.187 \pm 0.011, M_\pi = 0.422 \pm 0.020$, the finite volume corrections to M_π, F_π are 0.007 and -0.012, respectively. The finite volume correction term of G_π includes a constant B. This constant cannot be obtained from the data fits. So we use the relation $G = 2BF$, which becomes $G_\pi = 2BF$ to the leading order. Then the finite volume correction of G_π becomes $G_\pi S_2^F / 2F_\pi^2$. Using the value of $G_\pi = 1.74$, this correction is 0.05. We see that the finite volume corrections at leading order of chiral perturbation theory to M_π, G_π, F_π are very small in this simulation.

Let us comment on the finite volume corrections to the pion mass when it is calculated in coordinate space using smeared-local correlators and cosh fit. The normal way to calculate F_π, M_π is to calculate quark propagators in coordinate space, and then fit the pion propagators with the fit formula of $\cosh(M(t - L/2)$ with Euclidean time t. When one uses local pion operators, the finite volume corrections in (5.28) are still applied. To make the operator more overlap with the lowest energy state, normally one uses smeared operators. With an optimal choice of the smearing function the overlap of the pion creation operator with excited states with pionic quantum numbers would be zero and the sensitivity of the pion propagator to the finite extent in the Euclidean time direction could be eliminated. Thus, the effect of smeared operators corresponds to making the ratio of T/L large. When T/L is large, the factor $\mathcal{I}(\frac{L^2}{T^2}\lambda)$ in (5.18) becomes $\simeq \frac{L}{T}\frac{1}{\sqrt{\lambda}}$. Thus the finite part of the integral becomes

$$S_2^{Fs} \equiv \frac{1}{4L^2}\int_0^\infty d\lambda e^{-\frac{M^2L^2}{4\pi^2}\lambda}\left(\mathcal{I}^3(\lambda)\frac{1}{\sqrt{\lambda}} - \frac{1}{\lambda^2}\right) \tag{5.29}$$

The leading correction for large L regardless of the actual ratio of T/L is

$$S^{Fs,\text{leading}} = \frac{3}{2L^2}\int_0^\infty d\lambda \frac{e^{-\frac{M^2L^2}{4\pi^2}\lambda - \frac{\pi^2}{\lambda}}}{\lambda^2} = \frac{3}{2\pi^2}\frac{M}{L}K_1(ML) \tag{5.30}$$

Using this (5.29),(5.30), finite corrections to M_π, F_π which are calculated from smeared operators in coordinates space can be calculated. With this new formula (5.29), the finite volume corrections to M_π are calculated for several values of ML in Table 5.2. As one can see, using the smeared operator greatly reduces the finite volume corrections.

6.0 TRUNCATED DETERMINANT APPROXIMATION

In this chapter the truncated determinant approximation(TDA) method, which was introduced by Duncan, *et al.* [18] to simulate QCD with a small quark mass efficiently, will be reviewed.

6.1 TRUNCATED DETERMINANT APPROXIMATION

In a simulation to generate a ensemble of gauge configurations U on a lattice, U is updated according to the following probability weight: (for the case of QCD with the two degenerate quarks)

$$\mathrm{P}(U) \propto \det(Q^2) e^{-S_g},$$

where Q is the Wilson-Dirac operator, and S_g is a gauge action. The determinant of a nonhermitian matrix Q is equal to the determinant of a hermitian matrix $H = \gamma_5 Q$(as $\det(\gamma_5) = 1$). For the free theory, eigenvalues of the operator H are $\pm\sqrt{p^2 + m^2}$, which corresponds to exactly the off-shellness of the virtual quark loops.

To see the effect of high modes of H, the high modes are gradually switched off by defining a effective action as

$$\mathcal{D}(\mu) \equiv \mathrm{Tr}\ \ln \tanh(\frac{H^2}{\mu}),$$

with a constant μ. As μ becomes much larger than the largest eigenvalues of H, $e^{\mathcal{D}(\mu)}$ becomes $\propto \det H^2$, whereas as μ becomes much smaller than the smallest eigenvalue, $e^{\mathcal{D}(\mu)}$ becomes 1. For an intermediate μ, high modes with eigenvalues $\lambda >> \mu$ are suppressed.

Let μ be much larger than $\Lambda_{QCD}(\simeq 250\text{MeV})$ so that as μ is varied, the number of high modes of H included in $\mathcal{D}$ are controlled. Ref. [18] performed an analytic calculation for the case of QED at weak coupling to show that the dependence of $\mathcal{D}(\mu)$ at large μ is

$$\mathcal{D}(\mu) \simeq \beta_F \ln \frac{\mu^2}{m_q^2} \int d^4x \, F_{\mu\nu}^2 + O(\frac{1}{\mu^2}(DF)^2),$$

where β_F is the one-loop quark contribution to the beta function. That is, varying the number of high modes is equivalent to the renormalization of the coupling constant. Thus, the quark determinant $\det H^2$ can be split into the ultraviolet determinant U_{UR} from those high modes and the infrared determinant U_{IR}:

$$\begin{aligned} \det(H^2) &= \prod_{|\lambda_i|<\mu} \lambda_i^2 \prod_{|\lambda_i|>\mu} \lambda_i^2 \\ &\equiv D_{IR} D_{UR} \end{aligned}$$

So it is expected that D_{IR} well describes low energy QCD in which virtual quark off-shellness is typically lower than μ. In lattice simulations, μ is chosen as $2\Lambda_{QCD}$. Eigenvalues in D_{IR} are calculated with the Lanczos algorithm.

6.2 LANCZOS ALGORITHM

The Lanczos algorithm is an standard technique to calculate eigenvalues of a matrix. Given a hermitian matrix A, it find a tridiagonal matrix:

$$T = \begin{pmatrix} \alpha_1 & \beta_1 & & & \\ \beta_1 & \alpha_2 & \beta_2 & & \\ & \ddots & \ddots & \ddots & \\ & & \beta_{n-2} & \alpha_{n-1} & \beta_{n-1} \\ & & & \beta_{n-1} & \alpha_n \end{pmatrix} \tag{6.1}$$

A tridiagonal matrix can be easily diagonalized with standard numerical techniques. T can be written as $T = V^{-1}AV$ with an unitary matrix V. The unitary matrix V can be written as

$V = (\mathbf{v}_1, \cdots, \mathbf{v}_n)$ with orthonormal column vectors $\mathbf{v}_i$. Then, $\alpha_i, \beta_i, \mathbf{v}_i$ satisfy the following relations:

$$\begin{aligned} A\mathbf{v}_1 &= \alpha_1\mathbf{v}_1 + \beta_1\mathbf{v}_2, \\ A\mathbf{v}_i &= \beta_{i-1}\mathbf{v}_{i-1} + \alpha_i\mathbf{v}_i + \beta_i\mathbf{v}_{i+1} \quad \text{for} \quad i = 2, \cdots n-1, \\ A\mathbf{v}_n &= \beta_{n-1}\mathbf{v}_{n-1} + \alpha_n\mathbf{v}_n \end{aligned} \tag{6.2}$$

This relation with the orthogonality of $\mathbf{v}_i$ tells that if one has α_i, β_i, and $\mathbf{v}_i$, one can get α_{i+1}, β_{i+1}, and $\mathbf{v}_{i+1}$. So starting with a random vector ω_0, one can generate all α_i, β_i by repeating the following process:

$$\begin{aligned} \mathbf{v}_i &= \omega_{i-1}/\beta_{i-1} \\ \alpha_i &= < \mathbf{v}_i, A\mathbf{v}_i >, \\ \omega_i &= (A - \alpha_i)\mathbf{v}_i - \beta_{i-1}\mathbf{v}_{i-1} \\ \beta_i &= \sqrt{< \omega_i, \omega_i >} \\ i &\leftarrow i + 1, \end{aligned} \tag{6.3}$$

where $<,>$ means the scalar product of two vectors. The initial β_0 and $\mathbf{v}_0$ are defined as $\beta_0 =< \omega_0, \omega_0 >$, $\mathbf{v}_0 = \mathbf{0}$. Theoretically this recursion should find all α_i, β_i after n times of iteration, unless $\beta_i = 0$ terminates process, but in real computation, accumulated roundoff errors in the iterations prevent all $\mathbf{v}_i$ from being orthogonal, which causes that the matrix T contains not only eigenvalues of the matrix A but also eigenvalues which are not those of the matrix A, called the spurious eigenvalues. Cullum and Willoughby [27] proposed a solution in which the recursions can be done any number of times. One finds good eigenvalues by removing spurious eigenvalues with the following recipe. Construct another tridiagonal matrix T_2 by removing the first row and column from the original tridiagonal matrix T. Then, spurious eigenvalues are all common simple eigenvalues of T (i.e., those unchanged by the deletion with multiplicity=1), and all of the other eigenvalues of T are good eigenvalues of A.

6.3 TDA SIMULATIONS

In lattice simulation, new gauge configurations U' are generated from old U according to e^{-S_g}, and then one does a Metropolis update with $e^{-\Delta\mathcal{D}_{IR}}$, where

$$\Delta\mathcal{D}_{IR} \equiv \ln \prod_{i=1}^{N_{eig}} \frac{\lambda_i^2}{\lambda_i'^2}. \tag{6.4}$$

λ_i' are eigenvalues of H with the new gauge configuration U'. Namely, a new gauge configuration U' is accepted/rejected by comparing $e^{-\Delta\mathcal{D}_{IR}}$ with a random number r. If $e^{-\mathcal{D}_{IR}} > r$, U' is accepted, and otherwise U is rejected.

Gauge configurations used in our study of chiral perturbation theory in Ch. 4 were generated from the TDA method. As shown there, the chiral parameters were extracted consistently with the results from independent methods. As another example, Fig. 6.1 shows the static energy on 6^4 lattices obtained from the TDA simulations from Ref. [28]. One can see that the static energy shows stringbreaking with an asymptotic value which agrees well with twice the heavy-light meson mass. Thus, the TDA method reproduces important aspects of low energy unquenched QCD.

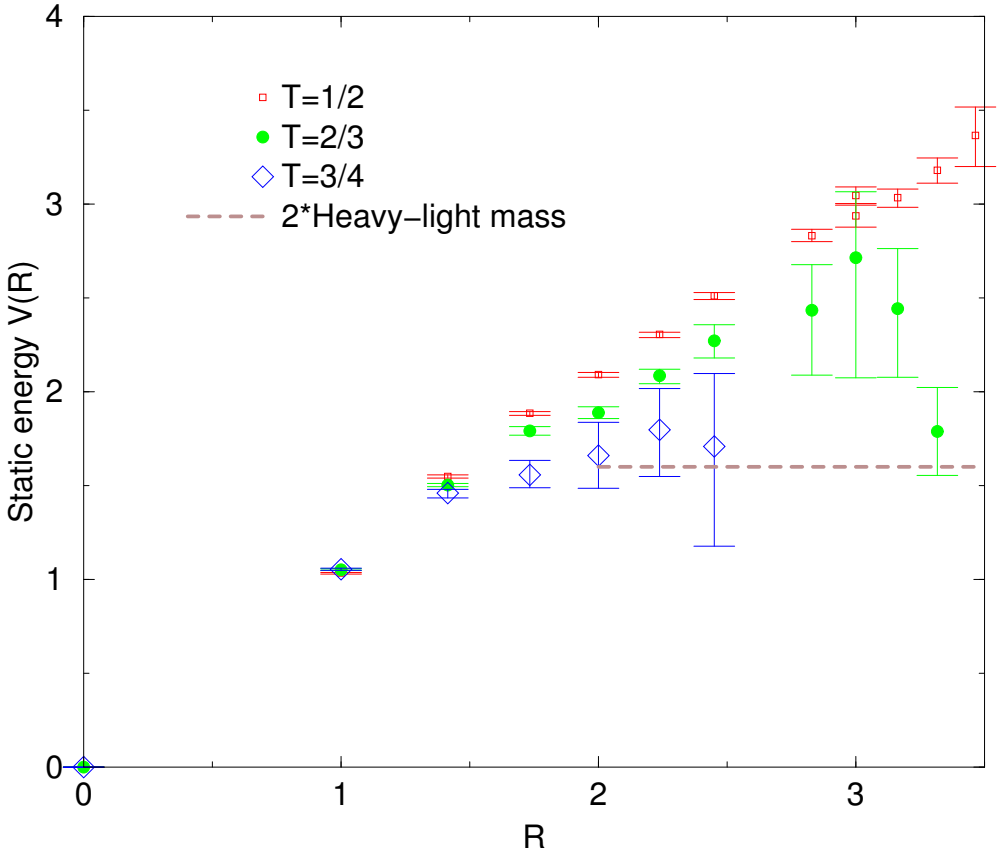

Figure 6.1: Static energy $V(R)$ for κ=0.2050

7.0 EXACT ALGORITHM WITH TDA+MULTIBOSON METHOD

7.1 MULTIBOSON METHOD

The multiboson method [30, 31] was proposed to simulate unquenched QCD of two degenerate quarks. For the case of two degenerate quarks, the probability density for a gauge configuration U is

$$P_{eff}[U] \propto \det H^2 e^{-S_g[U]}.$$

By introducing bosonic fields, the multiboson method converts $\det H^2$ to an effective action e^{-S_b} such that S_b is a local action of bosonic fields. The absolute value of the spectrum of the hermitian Wilson-Dirac operator H is bounded by $1 + 8\kappa$ so the operator

$$\overline{H} \equiv \frac{H}{1 + 8\kappa} \tag{7.1}$$

has a spectrum between -1 and 1. One can rewrite $P_{eff}[U]$ in terms of this normalized operator:

$$P_{eff}[U] \propto \det \overline{H}^2 e^{-S_g[U]}.$$

One wants to approximate $\det \overline{H}^2$ in terms of a polynomial P_N which has N complex roots:

$$\det \overline{H}^2 \simeq \frac{1}{\det P_N(\overline{H}^2)}.$$

The polynomial $P_N(s)$ is approximating $1/s$:

$$P_N(s) \simeq \frac{1}{s}, \quad \epsilon \leq s \leq 1,$$

where the lower limit ϵ of the convergence should be less than the smallest eigenvalue of $\overline{H}^2$. By factorizing $P(\overline{H}^2)$ with complex roots z_k, $k = 1, \cdots, N$, one can write $\det(\overline{H}^2)$ as

$$\det\left(\overline{H}^2\right) \simeq \prod_{k=1}^{N/2} \frac{1}{\det\left((\overline{H}^2 - z_k)(\overline{H}^2 - \overline{z_k})\right)}$$

This can be written in terms of $\sqrt{z_k} = \mu_k + i\nu_k, \nu_k > 0$:

$$\det\left(\overline{H}^2\right) \simeq \prod_{k=1}^{N} \frac{1}{\det\left((\overline{H} - \mu_k)^2 - \nu_k^2\right)} \tag{7.2}$$

The determinant of each factor in the denominator in (7.2) can be converted to a bosonic integral with a gaussian action:

$$S_b = \sum_{k=1}^{N} \sum_{x} (|(\overline{H} - \mu_k)\phi_k(x)|^2 - \nu_k^2 |\phi_k(x)|^2)$$

Thus, the probability weight P_{eff} for the gauge configuration U becomes

$$P_{eff}[U] \propto \int D\phi D\phi^\dagger \, e^{-S_b[\phi] - S_g[U]} \tag{7.3}$$

Typically Chebyshev polynomials are used for P_N. Roots of Chebyshev polynomials can be expressed analytically as follows:

$$z_k = \frac{1+\epsilon}{2}(1 - \cos\frac{2\pi k}{N+1}) - i\sqrt{\epsilon}\sin\frac{2\pi k}{N+1} \tag{7.4}$$

The relative error for Chebyshev polynomial is bounded by $2(\frac{1-\sqrt{\epsilon}}{1+\sqrt{\epsilon}})^{N+1}$. Fig. 7.1 shows roots of Chebyshev polynomials for the cases of $N = 20$, $N = 60$ with the fixed maximum relative error$\simeq 0.005$.

When one simulates small quark mass, $\overline{H}^2$ has small eigenvalues. Then, a polynomial P_N of small ϵ and large N are necessary. The roots of P_N are densely concentrated near zero. This causes critical slowing down of multiboson fields: simulations based on (7.3) display long autocorrelations of the bosonic fields.

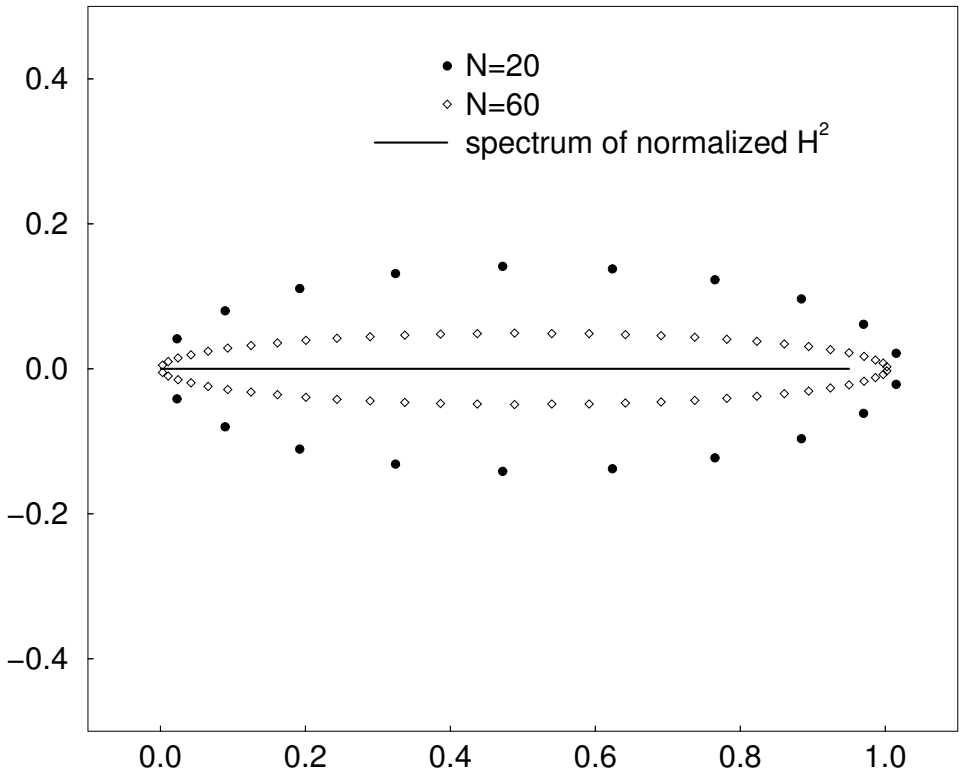

Figure 7.1: Roots of Chebyshev polynomials

7.2 TDA + MULTIBOSON

The exact unquenched simulation with the multiboson method requires a large number of bosonic fields in order to accurately reproduces the small eigenvalues of the quark determinant. For a finite N, the multiboson method is not exact. For a given P_N with a low convergence limit ϵ, the exact probability density for a gauge configuration U and bosonic fields $\phi_i\,, i = 1, \cdots, N$, can be expressed as

$$P(\phi, U) \propto \det\left[P_N(\overline{H}^2)\overline{H}^2\right] e^{-S_b - S_g} \tag{7.5}$$

The exact probability density $P(\phi, U)$ has a correction factor $\det\left[P_N(\overline{H}^2)\overline{H}^2\right]$. As first shown in [32], one can make the algorithm exact by evaluating the correction determinant with the eigenvalues of low modes of $\overline{H}$:

$$\det\left[P_N(\overline{H}^2)\overline{H}^2\right] \simeq \prod_i^{N_{eig}} P(\lambda_i^2)\lambda_i^2 \tag{7.6}$$

Namely, one applies the TDA method to evaluate the correction factor which comes from the infrared modes of H. So the TDA method takes care of the infrared modes while the multiboson method approximates the ultraviolet modes. The TDA method combined with the multiboson method can reduce the number of multiboson fields needed to make the algorithm exact by computing the exact infrared determinant so that the critical slowing down of multiboson fields in the continuum limit can be avoided. Even for the case of lattice simulation of relatively heavy quark mass, this combined method can reduce time required to generate decorrelated gauge configurations compared with the pure multiboson method. Moreover, as the errors in the multiboson method are eliminated by exact calculation of low eigenvalues, the method can be made effectively exact.

Define the determinant compensation factor as the logarithm of the correction factor from a N_{eig} lowest eigenvalues of $\overline{H}$:

$$D_{CF}(N, N_{eig}) \equiv \ln(\prod_{k=1}^{N_{eig}} \lambda_k^2 P_N(\lambda_k^2)).$$

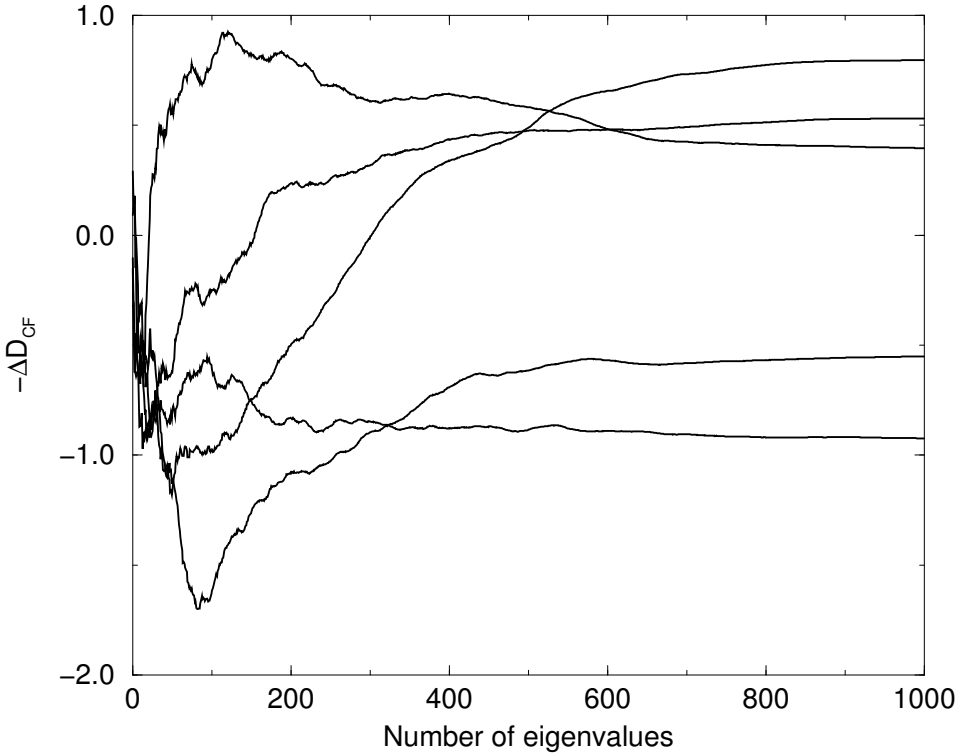

Figure 7.2: Convergence of determinant compensation factor on a 6^4 lattice ($N = 20, \epsilon = 0.02$)

The factor $e^{-\Delta D_{CF}}$ with $\Delta D_{CF} = D_{CF} - D'_{CF}$ will be used in Monte Carlo simulations to correct gauge configurations generated from the multiboson method. That is, this will be compared with a random number at the end of each update to decide the Metropolis accept/reject. To do this, this factor needs to converge with N_{eig} number of eigenvalues. Fig. 7.2 shows convergences of ΔD_{CF} on a 6^4 lattice with $N = 20$, $\epsilon = 0.02$. The number of the smallest eigenvalues up to $\epsilon = 0.02$ are around 850, but to ensure the convergence, in the following simulation we include 1000 smallest eigenvalues in D_{CF}.

7.3 SIMULATION

We have simulated the TDA + multiboson algorithm on a coarse and physically large 6^4 lattice. As in TDA simulation in Ch. 4, the gauge part of QCD action is $O(a^2)$ improved with a 8 link loop of twisted rectangle terms whereas the pure Wilson quark action is used:

$$\begin{aligned} S_g(U) &= \beta_{\rm plaq} \sum_{\rm plaq} \frac{1}{3} {\rm ReTr}(1 - U_{\rm plaq}) \\ &+ \beta_{\rm trt} \sum_{\rm trt} \frac{1}{3} {\rm ReTr}(1 - U_{\rm trt}), \end{aligned} \tag{7.7}$$

where "trt" refers to "twisted rectangles". $\beta_{plaq}, \beta_{trt}$ are chosen as 0.65, 0.75, respectively so that the lattice spacing is measured as $a^{-1} = 0.54$GeV. $N = 20$, $\epsilon = 0.02$ are used to generate the Chebyshev polynomial P_N. i.e., we have 20 multiboson fields. 1000 lowest eigenvalues are calculated exactly by the Lanczos algorithm and included in the determinant compensation factor.

The Monte Carlo simulation should update both gauge configuration U and multiboson fields ϕ. For the update of ϕ, the gaussian overrelaxation technique is used, and for U, the overrelaxation and the pure Metropolis are combined. After updating ϕ, U, the D_{CF} is computed to accept/reject updated U, ϕ. The update proceeds in the following order:

1. update of each multiboson field with 1 overrelaxation (overrelaxation parameter $\omega = 1.9$)
2. update of gauge field with 10 hit Metropolis, 1 overrelaxation and another 10 hit Metropolis.
3. update of each multiboson field with 1 overrelaxation ($\omega = 1.9$)

4. Metropolis accept/reject with the determinant compensation factor $e^{-\Delta D_{CF}}$.

The pure Metropolis and overrelaxation for gauge configurations U are standard. For the pure Metropolis of gauge configurations U, a table of random SU(3) matrices are generated, and a U from the table is picked randomly, and then the Metropolis accept/reject is done with $U^{new}_{x\mu} = UU^{old}_{x\mu}$. For overrelaxation of gauge field, one needs to find U_{min} minimizing the action with the environment fixed. At each overrelaxation U_{min} was found numerically. Then $U^{new}_{x\mu} = U^{old}_{x\mu}U^{-1}_{min}U^{old}_{x\mu}$ is used for the Metropolis accept/reject.

Fig. 7.3 shows the equilibrated D_{CF} versus sequence. One sweep including computation of D_{CF} takes $\sim$ 5min with a Pentium 1.6GHz CPU. The acceptance rate is $\sim 50\%$.

7.4 TDA+MULTIBOSON IN QQ+Q QCD

The TDA+Multiboson algorithm can be extended to the simulation of 2+1 quarks: degenerate up and down quarks, and relatively heavy strange quark. For this case, the probability density $P(U)$ contains two determinant factors from up and down quarks, and one factor from strange quark:

$$P_{eff}[U] \propto \det \overline{H}^2 \det \overline{H}_s e^{-S_g[U]},$$

where $\overline{H}_s$ is the normalized hermitian Wilson-Dirac operator for the strange quark. For the determinant of $\overline{H}^2$, one uses a Chebyshev polynomial P_N as obtained in Sec. 7.1. Since even at very small quark mass a quark determinant does not become negative, one has

$$\det \overline{H}_s = \det \sqrt{\overline{H}_s^2} \tag{7.8}$$

A polynomial $P^s_N(x)$ approximating $\sqrt{x}$ with N^s complex roots can be found from the standard Remes algorithm, which is fully implemented in *Mathematica* [33]. Fig. 7.4 shows the relative error of $P^s_N(x)$, i.e.,

$$R(x) = 1 - \sqrt{x}P^s_N(x)$$

for the case of the lower convergence limit $\epsilon = 0.02$ and the maximum relative error $max(R) = 0.003$. The exact algorithm now contains two compensation factors. In addition to D_{CF}

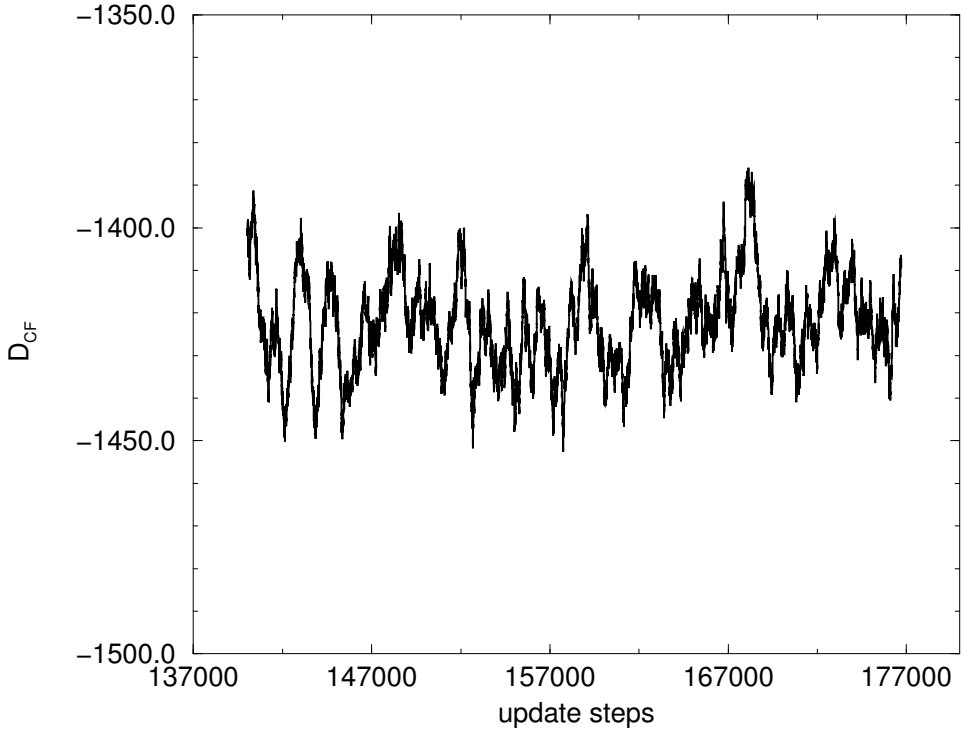

Figure 7.3: Monte Carlo sequence of D_{CF} on a 6^4 lattice with κ=0.1920 and 1000 lowest eigenvalues

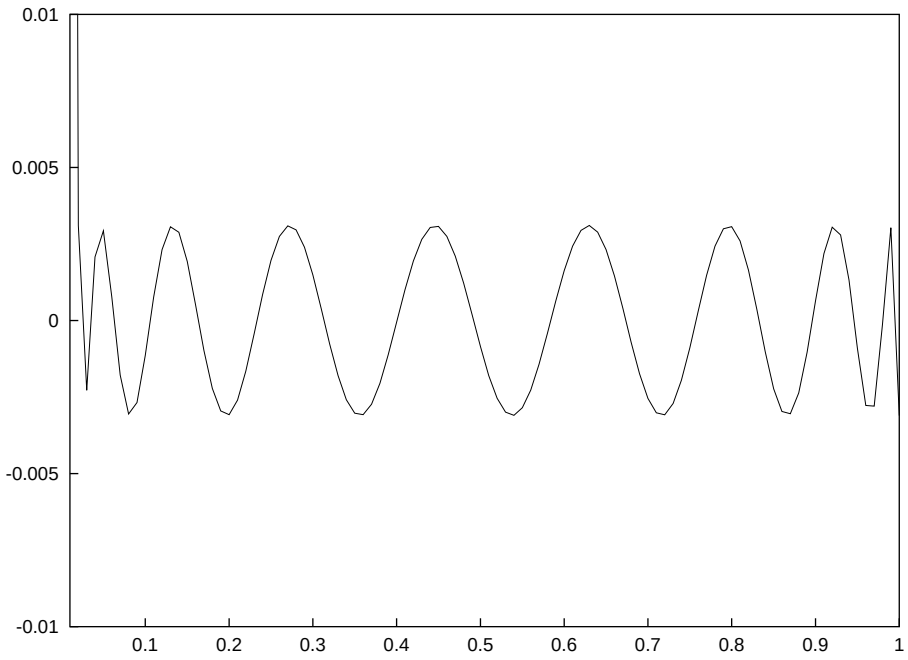

Figure 7.4: Relative error $R(x)$

for up and down quark, the compensation factor for strange quark determinant has to be computed:

$$D^s_{CF} = \ln \prod_{i=1}^{N^s_{eig}} P^s_N(\lambda^{s2}_i)\lambda^{s2}_i, \tag{7.9}$$

where λ^s_i is an eigenvalue of $\overline{H}_s$. In Monte Carlo simulation for this case, the product $e^{-\Delta(D_{CF}+D^s_{CF})}$ is used for the global accept/reject at the last step of each update of ϕ, U. Fig. 7.5 shows convergences of $\Delta(D_{CF} + D^s_{CF})$ from a qq+q simulation on a 8^4 lattice. Since the strange quark is heavier than up/down quark, $\overline{H}_s$ has fewer small eigenvalues. Thus, the low convergence limit ϵ for P^s can be larger than ϵ for P so that the strange quark needs a smaller number of multiboson fields. Fewer eigenvalues also need to be included in D^s_{CF}.

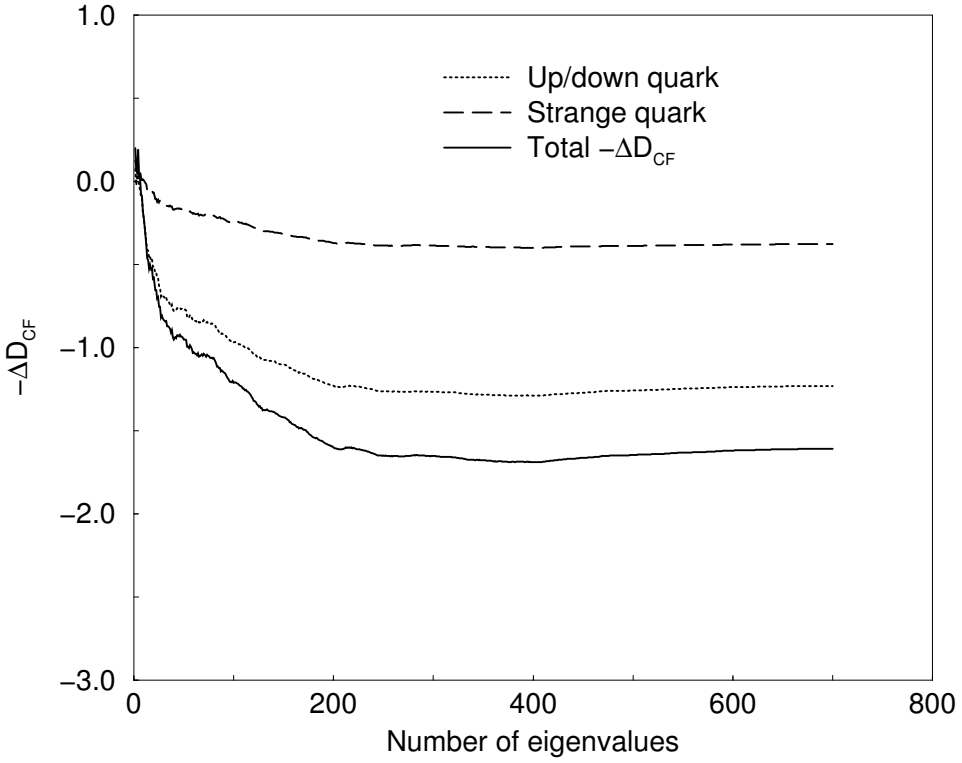

Figure 7.5: Determinant compensation factor from qq+q simulation

8.0 STATISTICAL PROPERTIES OF TDA+MULTIBOSON METHOD

8.1 AUTOCORRELATION IN PURE MULTIBOSON METHOD

In order to simulate QCD with the pure multiboson method only, the order of a polynomial $P_N(s)$ which approximates $1/s$ must become large, and ϵ become small. Then many ν_k, imaginary parts of square roots of z_k of P_N, become $\simeq 0$(see Fig. 7.1). The bosonic fields ϕ with such small ν_k's have bosonic actions $\sim e^{-\nu^2|\phi|^2}$, which has a width $1/\nu$. So the correlation length ξ of ϕ and U are $\sim 1/\nu_k$ with the smallest ν_k. From the analytical expression of roots of a Chebyshev polynomial Eq. (7.4), one can see that for small ν_k, $\nu_k^2 \sim \frac{\sqrt{\epsilon}}{N}$. Thus, $\xi^2 \sim \frac{N}{\sqrt{\epsilon}}$. The pure multiboson algorithm updates gauge field U and bosonic fields ϕ at each site at a time with a local effective action. The autocorrelation time with such local updates grows as ξ^2 [29]. So the autocorrelation time τ_{mb} with pure multiboson algorithm grows as [30, 32]

$$\tau_{mb} \sim \frac{N}{\sqrt{\epsilon}} \tag{8.1}$$

8.2 AUTOCORRELATIONS IN TDA+MULTIBOSON METHOD

To study the computational efficiency of the TDA+Multiboson algorithm we have simulated QCD with two degenerate quarks with different numbers of multiboson fields. Simple Wilson quark and gauge actions for the QCD action are used. The coupling constant β and the hopping parameter κ are chosen as $\beta = 5.3$ and $\kappa = 0.1620$. Six runs with different numbers of multiboson fields(14,20,30,40,50,60) were simulated to see statistical properties as the number of multiboson fields changes. ϵ, the low convergence limit of the Chebyshev polynomial for each run is chosen such that the polynomial have the same maximum relative

Table 8.1: ϵ and N_{eig} for each number of multiboson fields

N	14	20	30	40	50	60
ϵ	0.039	0.020	0.0092	0.0053	0.0034	0.0024
N_{eig}	1200	600	200	100	60	40

error $\delta(\simeq 0.005)$ (see Table 8.1). To check that every run simulates the same path integral, plaquette averages are measured. Every run gives a plaquette average value of ($\simeq 0.5$) consistently.

In the pure multiboson method an integrated autocorrelation time τ_{mb} of a general physical quantity is proportional to $\frac{N}{\sqrt{\epsilon}}$ with the number of multiboson fields N. In the TDA+Multiboson method one accepts or rejects a generated gauge configuration U and multiboson fields ϕ by comparing the determinant compensation factor with a random number. When they are rejected, the next U and ϕ are the same as the fields at the preceding step. Thus an autocorrelation time τ from the TDA+Multiboson method is expected to decrease by a factor of the acceptance rate r_a:

$$\tau = \frac{\tau_{mb}}{r_a}$$

Naively, when δ is fixed, one can see that the acceptance rate r_a decreases as the number of multiboson fields N decreases because more eigenvalues need to be included in the compensation factor D_{CF} for the smaller N so that D_{CF} fluctuates more. The measured acceptance rate for each run is shown in Fig. 8.4. The decreasing rate of r_a becomes faster as N gets smaller. This behavior can be understood approximately as follows.

At the last step of each Monte Carlo update, updated fields U' and ϕ' generated with the probability density $e^{-S_g - S_b}$(i.e, the multiboson part), where S_g is a QCD gauge action and S_b is an effective bosonic action, are accepted according to the factor $\min[1, e^{-\Delta D_{CF}}]$(i.e., the TDA part). This can be done by comparing the factor $e^{-\Delta D_{CF}}$ ($\Delta D_{CF} \equiv D_{CF} - D'_{CF}$) with a random number r_{rand} between 0 and 1 (if $e^{-\Delta D_{CF}} > r_{rand}$, accept U', ϕ', otherwise

reject), where primes($\prime$) indicate that D'_{CF} is calculated from the updated fields. Thus the acceptance rate r_a is the average of this factor in the course of a simulation:

$$r_a \;=\; << \min[1, e^{-\Delta D_{CF}}] >> \tag{8.2}$$

The average $<< \cdots >>$ in Eq. (8.2) is an average over the entire sequence of configurations (both accepted and rejected) generated as simulation proceeds. The average of $e^{-\Delta D_{CF}}$ can be shown to be equal to 1 [35]. The average of $e^{-\Delta D_{CF}}$ can be written as

$$<< e^{-\Delta D_{CF}} >>= \frac{1}{M} \sum_{(U,\phi),(U',\phi')} \frac{e^{D'_{CF}}}{e^{D_{CF}}} P[(U',\phi') \leftarrow (U,\phi)]\, e^{D_{CF}}\, e^{-S_g - S_b}, \tag{8.3}$$

where S'_g, S'_b are calculated with U', ϕ', and M is a normalization factor:

$$M = \sum_{U,\phi} e^{D_{CF}}\, e^{-S_g - S_b}.$$

Since

$$\sum_{(U,\phi)} P[(U',\phi') \leftarrow (U,\phi)]\, e^{-S_g - S_b} = e^{-S'_g - S'_b}, \tag{8.4}$$

it follows that

$$<< e^{-\Delta D_{CF}} >>= \frac{1}{M} \sum_{U',\phi'} e^{D'_{CF}}\, e^{-S'_g - S'_b}, \tag{8.5}$$

which is a sum of all probability, i.e., 1.

It is known from spectral theory [34] that eigenvalues of the Wilson-Dirac operator with random gauge configurations fluctuate more in the sparse region than in the dense region. The density of eigenvalues λ of the hermitian Wilson-Dirac operator H for $\lambda \ll \Lambda_{QCD}$ is believed to grow roughly linearly as the absolute value of λ [36] except for the smallest eigenvalues $\simeq 0$. We have checked the spectral density with a typical gauge configuration(see Fig. 8.1). Except for the region of $\lambda \simeq 0$, the spectral density is roughly linearly proportional to the magnitude of eigenvalues in the region of our interest. Let us assume this linearity of the spectral density for small eigenvalues to be included in the D_{CF}.

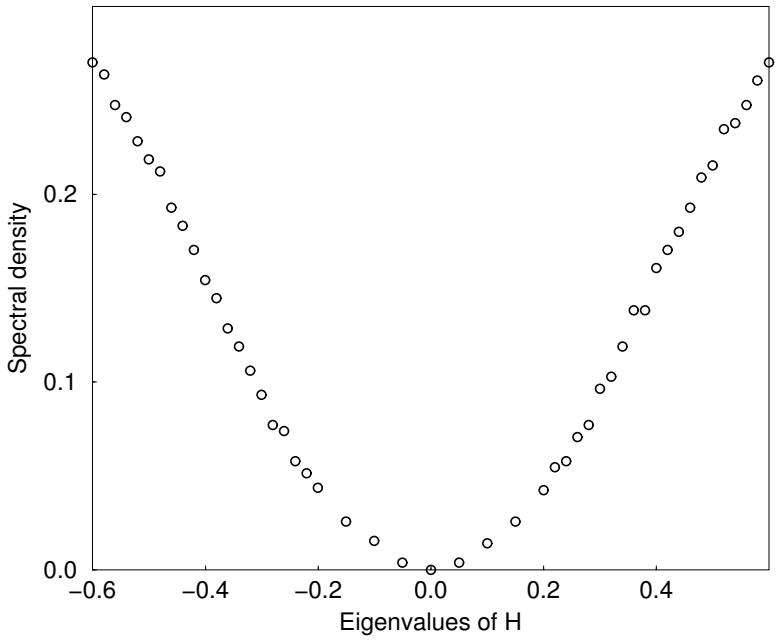

Figure 8.1: Spectral density of H from a gauge configuration. Except for the smallest eigenvalues the density grows linearly with magnitude of eigenvalues(fit gives roughly $0.63|\lambda| - 0.1$ for the linear part).

For each eigenvalue λ_i of $\overline{H}(=\frac{H}{1+8\kappa})$, the contribution to $e^{-\Delta D_{CF}}$ is

$$\frac{P_N(\lambda_i'^2)\lambda_i'^2}{P_N(\lambda_i^2)\lambda_i^2} \equiv (1+r_i) \tag{8.6}$$

where r_i is a relative change of $P(\lambda_i^2)\lambda_i^2$. These relative changes r_i are very small with the magnitude $\lesssim 0.01$. Taking the logarithm of (8.6) gives

$$\begin{aligned} \ln \frac{P_N(\lambda_i'^2)\lambda_i'^2}{P_N(\lambda_i^2)\lambda_i^2} &\equiv \ln(1+r_i) \\ &\simeq r_i \end{aligned} \tag{8.7}$$

Let us assume that r_i for each eigenvalue λ_i fluctuates randomly with a gaussian probability distribution with varying size l_i(although the fact is that the smallest eigenvalues of H are actually strongly correlated). Fluctuations of r_i should be large for small λ_i and disappear at around $\lambda_{N_{eig}}(\simeq \sqrt{\epsilon})$ because $P(s)s \simeq 1$ between ϵ and 1. So let us assume that l_i decays exponentially with a decay constant inversely proportional to N_{eig}:

$$l_i \propto e^{-C\lambda_i/N_{eig}} \tag{8.8}$$

From the linearity of the spectral density, N_{eig}, the number of eigenvalues needed for D_{CF} is proportional to ϵ.

Then summing of (8.7) is exactly a problem of random walk with varying step size r_i for i-th step. Then probability $P(\Delta D_{CF})$ can be obtained from the general formula for random walk [37]:

$$P(\Delta D_{CF}) \propto \exp\left(-\frac{(\Delta D_{CF})^2}{2N_{eig} < l_i^2 >}\right) \tag{8.9}$$

where $< l_i^2 >= \frac{1}{N_{eig}} \sum_i l_i^2$. But this probability distribution is not compatible with the condition $<< e^{-\Delta D_{CF}} >>= 1$, because for a gaussian distribution $<< e^{-\Delta D_{CF}} >>= 1$ requires $2 << D_{CF} >>=<< (D_{CF})^2 >>$. Thus to satisfy this condition, let us modify Eq. (8.9) as follows:

$$P(\Delta D_{CF}) \propto \exp\left(-\frac{(\Delta D_{CF} - \frac{N_{eig}<l_i^2>}{2})^2}{2N_{eig} < l_i^2 >}\right) \tag{8.10}$$

From (8.8), the mean-square of l_i can be easily calculated:

$$\begin{aligned} < l_i^2 > &= \frac{1}{N_{eig}} \sum_i^{N_{eig}} l_i^2 \\ &= \frac{\int_0^{\sqrt{\epsilon}} e^{-2C\lambda/N_{eig}} \lambda d\lambda}{\int_0^{\sqrt{\epsilon}} \lambda d\lambda} \\ &\propto N_{eig} \end{aligned} \tag{8.11}$$

Thus we obtain $P(\Delta D_{CF})$

$$P(\Delta D_{CF}) \propto \exp\left(-\frac{(\Delta D_{CF} - \frac{CN_{eig}^2}{2})^2}{2CN_{eig}^2} \right) \tag{8.12}$$

with a new constant C. Since $N_{eig} \propto \epsilon$, one can express $P(\Delta D_{CF})$ in terms of ϵ:

$$P(\Delta D_{CF}) \propto \exp\left(-\frac{(\Delta D_{CF} - \frac{C\epsilon^2}{2})^2}{2C\epsilon^2} \right) \tag{8.13}$$

with a redefined new constant C.

Fig. 8.2 shows the probability distribution $P(\Delta D_{CF})$ for each run. The measured probability distributions match very closely gaussian curves with one fitting parameter(standard deviation). The standard deviations from measurements grow roughly linearly(see Fig. 8.3) with ϵ. Thus, the prediction (8.13) from crude approximations agrees reasonably well with actual data.

The acceptance rate r_a can be calculated with $P(D_{CF})$ [35, 38]:

$$\begin{aligned} r_a &= << \min[1, e^{-\Delta D_{CF}}] >> \\ &= \frac{1}{Z} \int_{-\infty}^{0} P(\Delta D_{CF}) + \frac{1}{Z} \int_0^{\infty} e^{-\Delta D_{CF}} P(\Delta D_{CF}) \end{aligned} \tag{8.14}$$

where Z is a normalization for $P(\Delta D_{CF})$. With a new integration variable $x = \Delta D_{CF}$, Eq. (8.14) becomes

$$\begin{aligned} r_a &= \frac{1}{Z} \int_{-\infty}^{0} e^{-(x - C\epsilon^2/2)^2/2C\epsilon^2} \, dx + \frac{1}{Z} \int_0^{\infty} e^{-x} e^{-(x - C\epsilon^2/2)^2/2C\epsilon^2} \, dx \\ &= \text{erfc}(C\epsilon) \end{aligned} \tag{8.15}$$

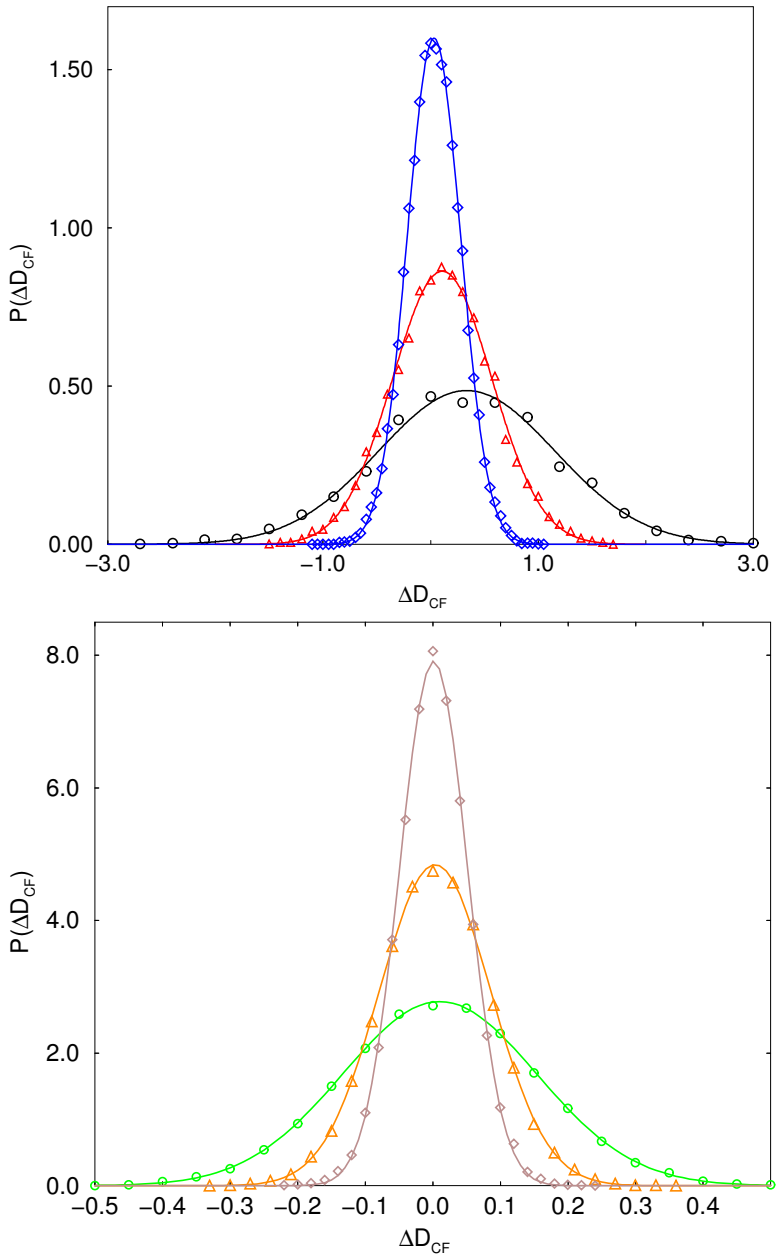

Figure 8.2: The probability distribution $P(\Delta D_{CF})$ for the cases of $\epsilon = 0.039$, 0.02, 0.0092, 0.0053, 0.0034, 0.0024 with $\sigma = 0.820$, 0.462, 0.249, 0.144, 0.0824, 0.0504, respectively (symbols are from measurements, and lines are from fits).

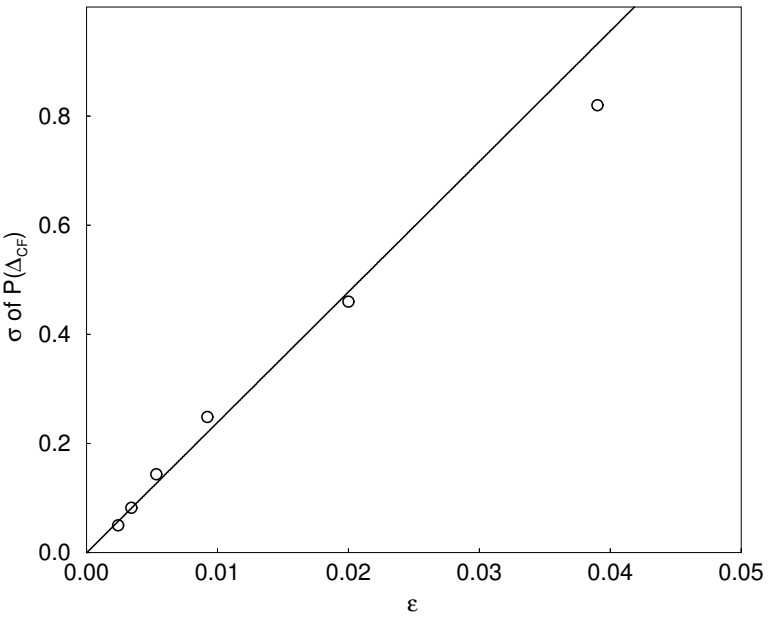

Figure 8.3: Standard deviations of the probability distribution $P(\Delta D_{CF})$. Circles are from measurements, and line is from fit(slope=23.9).

where erfc() is a error function and C is a constant. The maximum relative error δ in a Chebyshev polynomial is

$$\delta = 2\left(\frac{1-\sqrt{\epsilon}}{1+\sqrt{\epsilon}}\right)^{N+1} \tag{8.16}$$

This gives $\sqrt{\epsilon} \simeq \frac{\ln|\delta/2|}{2(N+1)}$. Thus, the number of multiboson fields N is proportional to $\sqrt{\epsilon}$ with a fixed maximum relative error δ of the Chebyshev polynomial P_N. So in terms of N, the acceptance rate r_a can be written as

$$r_a \quad = \quad \mathrm{erfc}(C'/N^2) \tag{8.17}$$

with a new constant C'. The line in Fig .8.4 shows a fit of the measured acceptance rates to this formula ($C' = 72$ is obtained). Both match reasonably well.

The constant C' should be dependent on the quark mass m because as m decreases, more small eigenvalues exist so that the standard deviation of $P(\Delta D_{CF})$ becomes larger. For small

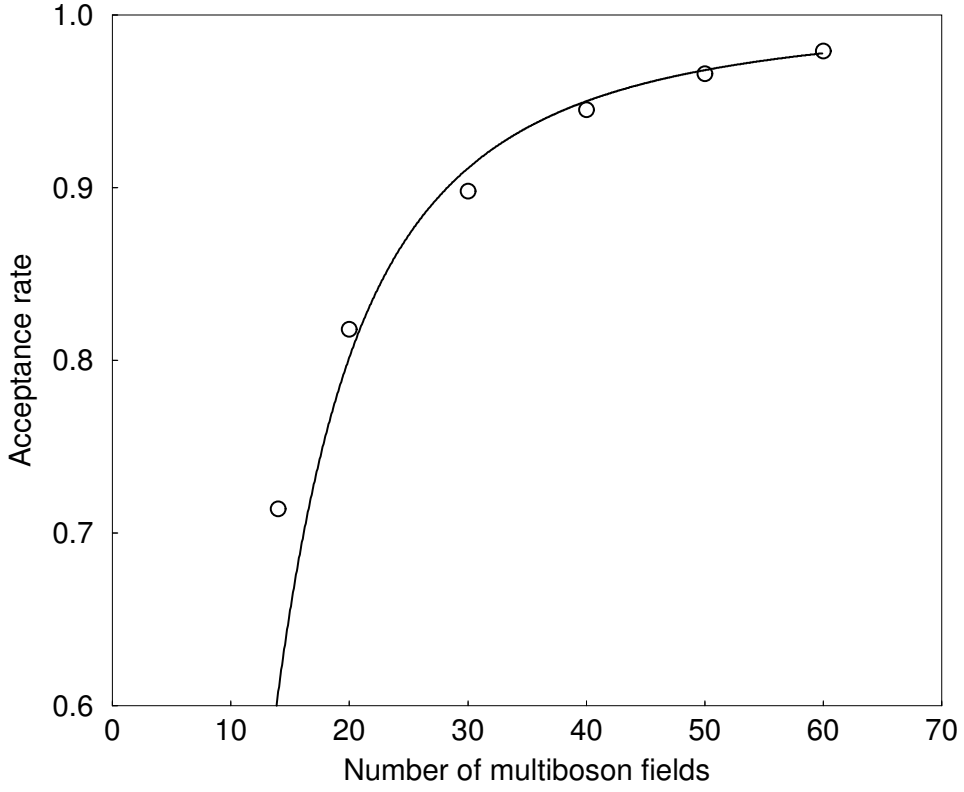

Figure 8.4: Acceptance rates with TDA+Multiboson method on a 6^4 lattice. Circles are from measurements, and line is from fit($C' = 72$).

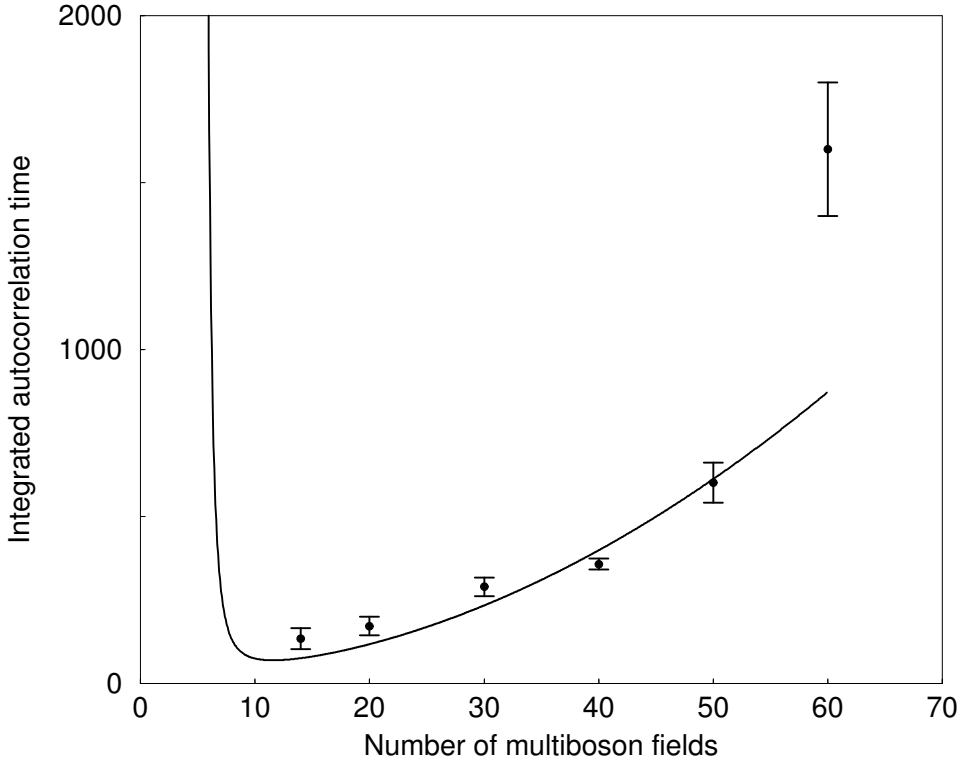

Figure 8.5: Integrated autocorrelation times with TDA+Multiboson method on a 6^4 lattice. Dots are from measurements, and line is from fit.

quark mass C' in Eq. (8.17) can be predicted to become large so that the acceptance rate drops faster for small m.

Putting the expression (8.15) for the acceptance rate in (8.1), one can estimate the behavior of autocorrelation times from the TDA+Multiboson method:

$$\tau \propto \frac{N}{\sqrt{\epsilon}\,\mathrm{erfc}(C\epsilon)} \tag{8.18}$$

With the maximum relative error δ of the Chebyshev polynomial fixed, the autocorrelation time becomes

$$\tau \propto N^2/\mathrm{erfc}(C'/N^2) \tag{8.19}$$

Fig. 8.5 shows the integrated autocorrelation times from measurements and fit (proportional constant = 0.24) as N is varied with δ fixed. For the case of 60 multiboson fields, the autocorrelation time is so large that the autocorrelation time and error bar are only roughly estimated. For large N, the autocorrelation time τ grows as N^2, which is equivalent to the pure multiboson algorithm. As N decreases, the decreasing rate of τ becomes slower than N^2, and at a certain number of multiboson fields, the autocorrelation has a minimum. For N smaller than the minimum, it sharply increases again.

8.3 COMPUTATIONAL EFFICIENCY WITH TDA+MULTIBOSON METHOD

Efficiency of a given algorithm for Monte Carlo simulation can be determined by the real computer time needed to generate a decorrelated gauge configuration. This is proportional to the autocorrelation time τ times computer time per sweep. Efficiency becomes better as this computer time decreases. Time per sweep for the case of each number of multiboson fields is measured with a Pentium Xeon 2.8 GHz CPU. The update time of gauge field and multiboson fields increases linearly with N. The increasing slope is measured as 0.18 seconds. Running the Lanczos part to calculate the determinant compensation factor D_{CF} takes most of the simulation time.

A-priori, one does not know how many low eigenvalues are obtained by Lanczos with a given number of sweeps. In order to check computer time as the magnitude of the largest eigenvalue λ_{max} changes, computer times are measured as the number of Lanczos sweeps are varied. Then the largest eigenvalues in the infrared part are checked. In this way, computer times versus the largest eigenvalues of H is plotted in Fig. 8.6. The curve roughly grows as λ_{max}^3. Fit with a dependence λ_{max}^3 gives proportionality constant 1480[s]. One needs to include eigenvalues of the normalized Wilson-Dirac operator $\overline{H}(=\frac{H}{N_{norm}})$ up to a little more than $\sqrt{\epsilon}$. So $\sqrt{\epsilon} \simeq \lambda_{max}/N_{norm}$ with normalization constant N_{norm}(=2.4 chosen here). So the computational time of the Lanczos part is roughly proportional to $(\sqrt{\epsilon})^3$. Since the low convergence limit of a Chebyshev polynomial $\sqrt{\epsilon} = \frac{\ln \frac{\delta}{2}}{2(N+1)}$, with δ fixed, the computational time of the Lanczos part is roughly proportional to $\frac{1}{N^3}$ with proportionality constant 687000.

Computer cost per decorrelated gauge configuration is proportional to autocorrelation time multiplied by time per sweep. Fig. 8.7 shows this computer cost for each run. As the number of multiboson fields decreases and simultaneously the number of eigenvalues included in D_{CF} increases, simulation with the TDA+Multiboson method achieves better efficiency. At $N = 30 - 40$ the computational cost has a minimum.

This shows that the TDA part in the combined method saves computer time. As N gets even smaller, the time per decorrelated fields increases again. Thus, when one uses the number of multiboson fields at which computer cost per decorrelated field is minimum, a lot of computer time can be saved compared to the pure multiboson method.

Let us try to understand the existence of the minimum in computer cost in terms of the approximate formulas for autocorrelation time and update time. The computational time $\mathcal{T}$ can be obtained as

$$\mathcal{T} \sim D \frac{N}{\sqrt{\epsilon}\,\mathrm{erfc}(C\epsilon)} \left[AN + B(\sqrt{\epsilon})^3\right] \tag{8.20}$$

For a fixed δ

$$\mathcal{T} \sim \frac{DN^2}{\mathrm{erfc}(C'/N^2)} \left[AN + B\frac{1}{N^3}\right] \tag{8.21}$$

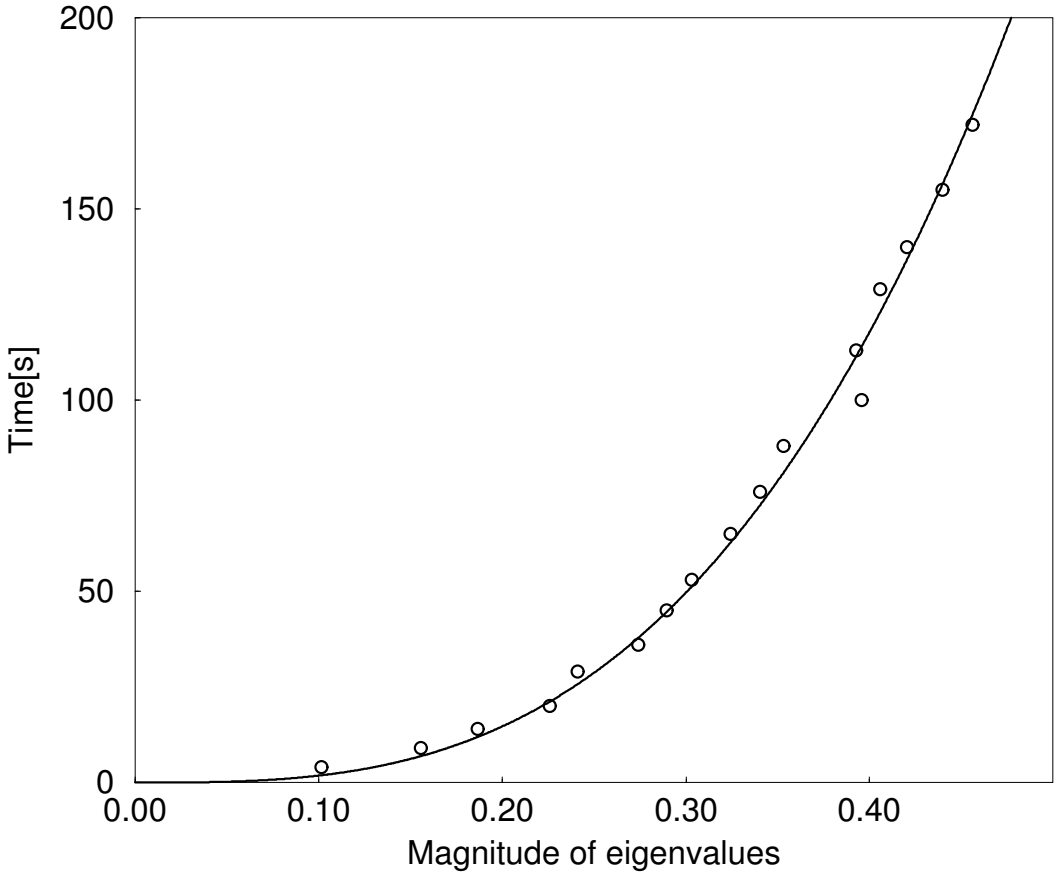

Figure 8.6: Computational time for running the Lanczos part versus the largest eigenvalues λ_{max}. Line is from fit with a formula λ_{max}^3 with the proportionality constant 1840[s]

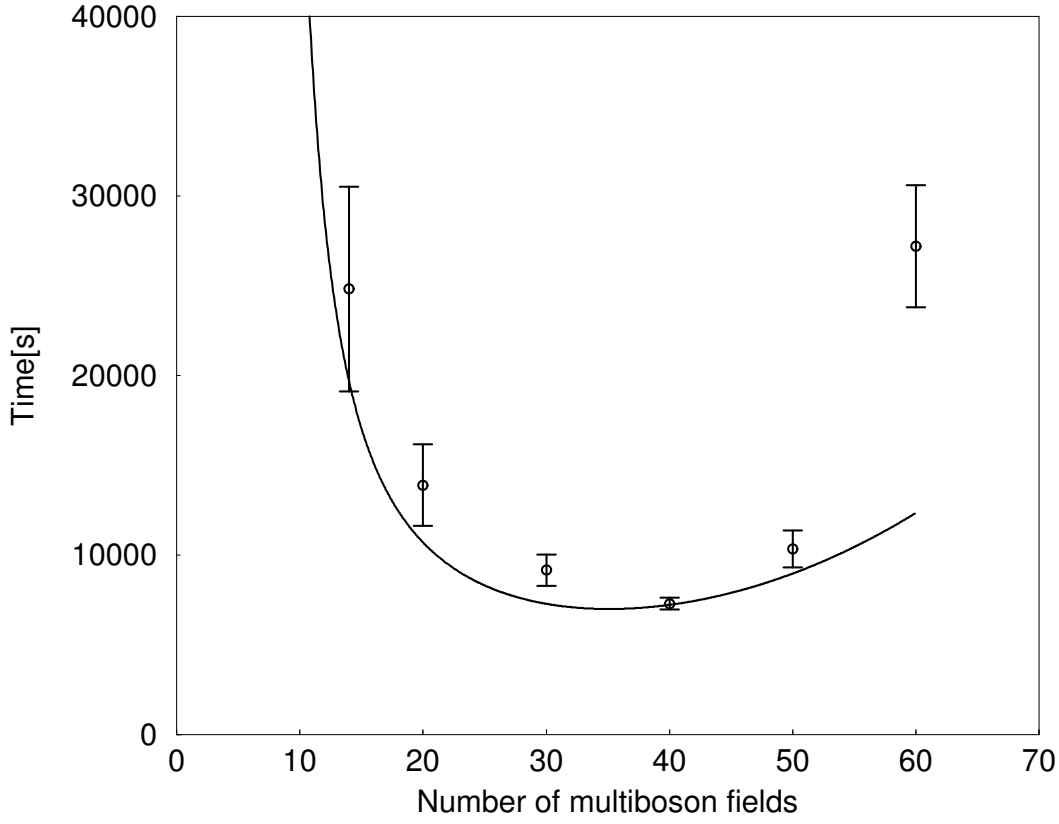

Figure 8.7: Computational cost to generate a decorrelated gauge configuration

with $A = 0.18$, $B = 687000$, $C' = 72$, and $D = 0.24$ as previous estimated. The estimation from this formula is shown in Fig. 8.7 as line. This formula gives a minimum $\mathcal{T}$ at $N = 35$, consistently with the real data.

Finally let us study the scaling behavior of $\mathcal{T}$ as the quark mass becomes small. With the lattice volume V and N,δ fixed, as the quark mass m goes to zero the computer time per sweep doesn't change. The quark mass dependence of $\mathcal{T}$ comes only from the acceptance rate r_a. As m decreases, the constant C in the acceptance rate should become large. Let us assume the scaling behavior of C of a form:

$$C \sim c' m^{-\gamma} \tag{8.22}$$

Putting (8.22) in (8.20), and neglecting the time of updating multiboson fields, one gets

$$\mathcal{T} \sim 1/\mathrm{erfc}(c' m^{-\gamma} \epsilon) \tag{8.23}$$

From this formula, one can estimate the scaling behavior of $\mathcal{T}$ with m. Since for large x, $\mathrm{erfc}(x) \sim e^{-x^2}/x$, as the quark mass m goes to zero, $\mathcal{T}$ behaves as

$$\mathcal{T} \sim m^{-\gamma} e^{m^{-2\gamma}\epsilon^2} \tag{8.24}$$

It is much worse than the pure multiboson method. If ϵ decreases as $\epsilon \sim m^\gamma$ with the relative δ of the Chebyshev polynomial fixed, the mass dependence of the acceptance rate can be eliminated. In this case(for small m, large N is needed), the multiboson computer time will be comparable to or much bigger than the Lanczos time. By neglecting the Lanczos computer time in (8.20), with δ fixed, the $\mathcal{T}$ scales as

$$\mathcal{T} \sim (\sqrt{\epsilon})^{-3} \sim m^{-3\gamma/2} \tag{8.25}$$

The smallest eigenvalues of H is proportional to m. If the pure multiboson method is used, ϵ should change such that $\sqrt{\epsilon} \sim m$ as m decreases. As long as γ <2, the TDA+Multiboson method is more efficient than the pure multiboson method as the pure multiboson algorithm scales as $1/m^3$, or $1/m^4$ [32]. Determination of γ requires extensive additional simulations, which will be performed in future work.

9.0 STRONG-COUPLING PHASE TRANSITION AT SMALL QUARK MASS

9.1 SHARPE AND SINGLETON'S TWO PHASE STRUCTURES

QCD simulation by a computer is performed on a finite discrete lattice with nonzero lattice spacing. So there is a discretization effect as well as finite volume effect (in Ch. 5 the finite volume effect was considered) at strong coupling. Because of asymptotic freedom, large lattice spacings correspond to the strong (bare) coupling regime. Sharpe and Singleton [39] studied the discretization effect on the pion mass qualitatively as the quark mass gets small, using chiral perturbation theory with the effective Lagrangian including the discretization effect. They have predicted that there are two different phase structures in the pion mass. In this section their argument will be reviewed.

When the lattice volume tends to infinity and lattice spacing tends to zero, lattice QCD approaches the continuum theory of QCD. At small lattice spacing a (and large volume such that the finite volume correction is negligible), lattice QCD is slightly different from the continuum theory so that the lattice theory can be described with the effective continuum theory which has the Lagrangian of the continuous QCD with small supplementary terms arising from the finite lattice spacing. Such supplementary terms can be determined by the symmetries of QCD on a lattice.

For QCD with two quarks of the same mass m, the Lagrangian of the effective continuum theory in the region where the lattice quark mass am is of the same order as $(a\Lambda_{QCD})^2$, becomes, up to the first order of the lattice spacing,

$$\mathcal{L}_{eff} = \mathcal{L}_g + \bar{\psi}(\not{D} + m)\psi + a\bar{\psi}i\sigma_{\mu\nu}F_{\mu\nu}\psi + O(a^2) \tag{9.1}$$

where $\mathcal{L}_g$ is the continuum QCD gauge action and the third, which is proportional to the lattice spacing a, is called a Pauli term (all constants of order one are ignored in this qualitative analysis).

Like the continuum QCD at low energy(see Ch. 3), low energy hadronic physics with terms proportional to a can be described by chiral perturbation theory. The effective chiral Lagrangian of this effective continuum theory can be written in terms of pion fields. Pion fields are excited around the nonvanishing vacuum expectation value Σ_0:

$$\Sigma = \Sigma_0 \exp\left(i \sum_{a=1}^{3} \pi_a \sigma_a / F_\pi\right) \tag{9.2}$$

where σ are Pauli matrices. One notes that the way the third term in Eq. (9.1) breaks the chiral symmetry is the same as the quark mass term (it is odd under $\psi \to \gamma_5 \psi$). Thus, the chiral Lagrangian is of the same form as that of the continuum QCD. The chiral parameters in this case will depend on the lattice spacing a. One just needs to substitute m for $m + a\Lambda_{QCD}$ (the subscripts on Λ_{QCD} will be dropped from now on). So the chiral potential energy becomes

$$\mathcal{V}_\chi = -\frac{c_1}{4}\mathrm{Tr}(\Sigma + \Sigma^\dagger) + \frac{c_2}{16}\{\mathrm{Tr}(\Sigma + \Sigma^\dagger)\}^2 \tag{9.3}$$

up to the order of m^2. The m, a dependencies of the coefficients are shown by Sharpe and Singleton [39] to be of order

$$c_1 \sim m\Lambda^3 + a\Lambda^5, \quad c_2 \sim m^2\Lambda^2 + ma\Lambda^4 + a^2\Lambda^6. \tag{9.4}$$

As the quark mass decreases, the pion mass decreases. When it reaches the region $am' \sim (a\Lambda)^3$, where $m' \equiv m - a\Lambda$, the coefficients become $c_1 \sim m'\Lambda^3, c_2 \sim a^2\Lambda^6$ so that $c_1 \sim c_2$. In this region the pion mass shows two different behaviors with the quark mass m, depending

on the sign of c_2. Parameterizing the condensate $\Sigma_0 = \cos\theta_0 + i\sin\theta_0\sigma_3$, one can expand Σ around Σ_0. This gives $\mathrm{Tr}(\Sigma + \Sigma^\dagger)$:

$$\begin{aligned}
&\mathrm{Tr}(\Sigma+\Sigma^\dagger) \\
&\quad = \mathrm{Tr}(\cos\theta_0 + i\sin\theta_0\sigma_3)\left[1 + \frac{i\sum_a^3 \pi_a\sigma_a}{F_\pi} + \frac{1}{2}\left(\frac{i\sum_a^3 \pi_a\sigma_a}{F_\pi}\right)^2 + \cdots\right] + C.C. \\
&\quad = 4\cos\theta_0 - 4\frac{\sin\theta_0}{F_\pi}\pi_3 - 4\frac{\cos\theta_0}{2F_\pi^2}\sum_a^3 \pi_a^2 + O(\pi_a^3).
\end{aligned}$$

This gives $\mathcal{V}_\chi$, the effective potential, as a function of pion fields $\pi(a = 1, 2, 3)$:

$$\begin{aligned}
\mathcal{V}_\chi &= -c_1\left(\cos\theta_0 - \frac{\sin\theta_0}{F_\pi}\pi_3 - \frac{\cos\theta_0}{2F_\pi^2}\sum_{a=1}^3 \pi_a^3\right) \\
&\quad + c_2\left(\cos^2\theta_0 - \frac{2\sin\theta_0\cos\theta_0}{F_\pi}\pi_3 + \frac{\sin^2\theta_0}{F_\pi^2}\pi_3^2 - \frac{\sin^2\theta_0}{F_\pi^2}\sum_{a=1}^3 \pi_a^2\right) + O(\pi_a^3) \\
&= -\cos\theta_0\,(c_1 - c_2\cos\theta_0) + \frac{\sin\theta_0(c_1 - 2c_2\cos\theta_0)}{F_\pi}\pi_3 \\
&\quad + c_2\frac{\sin^2\theta_0}{F_\pi^2}\pi_3^2 + \frac{c_1\cos\theta_0 - 2c_2\sin^2\theta_0}{2F_\pi^2}\sum_{a=1}^3 \pi_a^2 + O(\pi_a^3)
\end{aligned} \tag{9.5}$$

The vacuum expectation value of Σ, Σ_0 is a minimum of $\mathcal{V}_\chi$. The minimum can be found in terms of c_1, c_2 by parameterizing $\Sigma = A + i\mathbf{B}\cdot\sigma$ with $A^2 + B^2 = 1$. The chiral potential becomes

$$\mathcal{V}_\chi = -c_1 A + c_2 A^2 \tag{9.6}$$

where $-1 \le A \le 1$.

First, let us consider the case of $c_2 > 0$. Let us define $\epsilon \equiv c_1/2c_2 \sim m'/(a^2\Lambda^3)$. If ϵ is in the range $1 \le \epsilon \le 1$, ϵ is a minimum of $\mathcal{V}_\chi$ so $\Sigma_0 = \epsilon$. If $|\epsilon| \ge 1$, the minimum occurs at $A = 1$, or -1, depending of the sign of ϵ(i.e., the sign of c_1), so $\Sigma_0 = \pm 1$. So $\cos\theta_0$ can get three values:

$$\cos\theta_0 = \begin{cases} -1 & \epsilon \le -1 \\ \epsilon & |\epsilon| \le 1 \\ +1 & \epsilon \ge 1 \end{cases} \tag{9.7}$$

Using (9.7) with $\epsilon = c_1/2c_2$, the potential becomes

$$\mathcal{V}_\chi = \begin{cases} \frac{c_2}{F_\pi^2}(1-\epsilon^2)\pi_3^2 - c_2\epsilon^2 + O(\pi^3) & |\epsilon| < 1 \\ \frac{c_2}{F_\pi^2}(|\epsilon|-1)\sum_a \pi_a^2 & |\epsilon| \geq 1 \end{cases} \tag{9.8}$$

Identifying the factors in π_a^2 with the pion mass, one has the pion mass:

$$M_1^2 = M_2^2 = 0, \quad \frac{M_3^2 F_\pi^2}{2c_2} = 1-\epsilon^2 \qquad \text{for} \quad |\epsilon| < 1 \tag{9.9}$$

$$\frac{M_a^2 F_\pi^2}{2c_2} = |\epsilon| - 1 \qquad \text{for} \quad |\epsilon| \geq 1 \tag{9.10}$$

Fig. 9.1 shows the pion mass as a function of ϵ. The pion mass becomes zero at $\epsilon = 1$. Since m is proportional to ϵ, the graph can be considered as the pion mass as a function of the quark mass. As m decreases, the pion mass can reach zero. In the region $|\epsilon| < 1$, two pions remain massless, and the other becomes massive. This phase is called the Aoki phase [40]. The appropriate phase for the weak-coupling continuum limit of QCD lies to the left of $\epsilon = -1$(or right of $\epsilon = +1$) in Fig. 9.1, allowing us to tune the bare quark mass so that $M_\pi \to 0$.

Let us consider the other case:$c_2 < 0$. The minimum of $\mathcal{V}_\chi$ always occurs at $A = 1$, or -1 depending on the sign of c_1. $\mathcal{V}_\chi$ becomes

$$\mathcal{V}_\chi = \frac{|c_2|}{F_\pi^2}(1+|\epsilon|)\sum_{a=1}^{3}\pi_a^2 + c_2 - |c_1| + O(\pi^3) \tag{9.11}$$

and the pion masses are

$$\frac{M_a^2 F_\pi^2}{2|c_2|} = 1 + |\epsilon| \tag{9.12}$$

Fig. 9.2 shows the pion mass as a function of ϵ. The pion mass does not become zero for any quark mass. Of course, Fig. 9.2 represents a qualitative calculation, ignoring quark mass dependences in c_1, c_2 which will alter the symmetry around $\epsilon = 0$.

In summary, in lattice QCD near the continuum theory with a large volume such that the finite volume effect is negligible, chiral arguments of Sharpe and Singleton show two phase structures for the pion mass as the quark mass decreases, depending on the sign of the

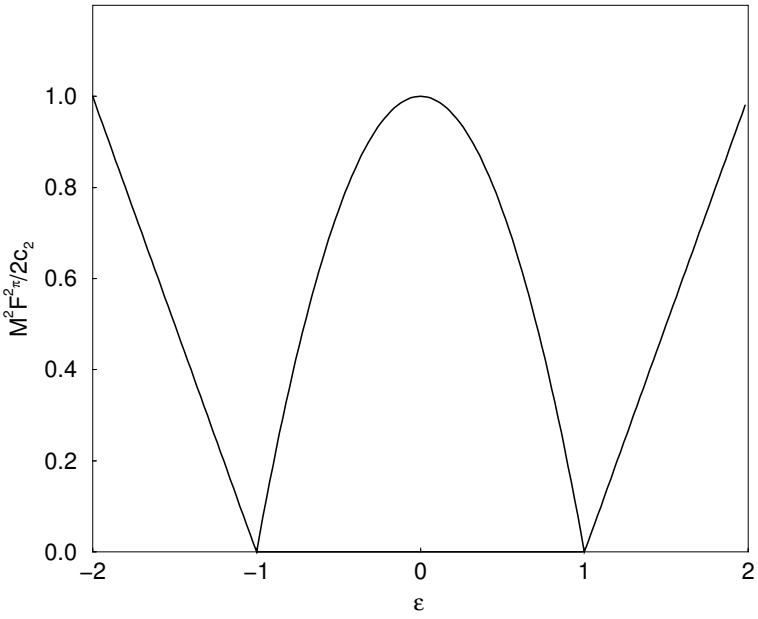

Figure 9.1: Pion mass for $c_2 > 0$

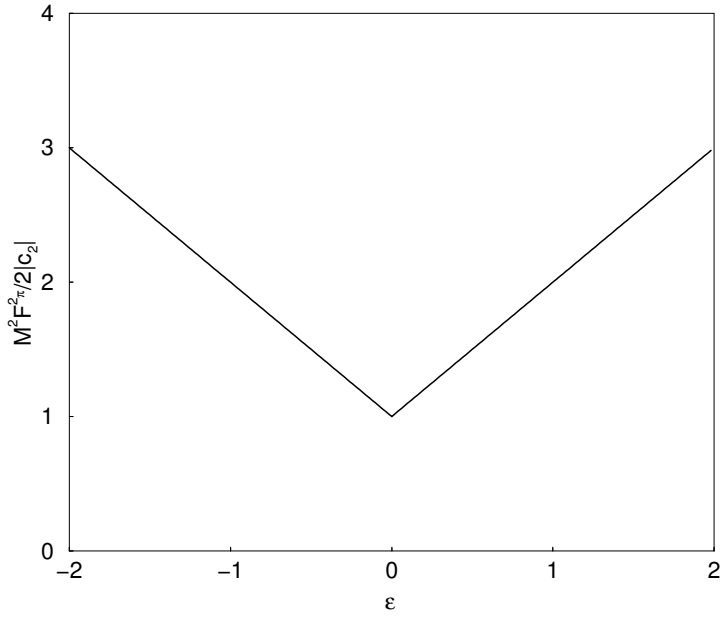

Figure 9.2: Pion mass for $c_2 < 0$

coefficient of the second order term in the chiral potential. When the coefficient is positive, the pion mass can reach zero, and when positive, the pion mass can not reach zero. As an application of the TDA+multiboson algorithm for full QCD described above, we have studied the strong coupling limit of lattice QCD with the light degenerate quarks in a search for the unconventional phase displayed in Fig. 9.2.

9.2 LATTICE SIMULATION

In this section we show the results from the lattice simulation of two light degenerate quarks on a 6^4 lattice (physically large but coarse) with the TDA+Multiboson method. The gauge action was improved at order of $O(a^2)$ with the twisted rectangle term (see Ch. 7), but the quark action used the simple Wilson quark action. The coupling constants β_{plaq} and β_{trt} for the plaquette term and the twisted rectangle term are chosen as 3.65 and 0.75, respectively. The lattice spacing was measured as $a^{-1} = 0.54$GeV from the string breaking.

For the multiboson part of the algorithm, we have used the 20-th order of the Chebyshev polynomial with the low convergence limit of P_N, $\epsilon = 0.02$, which gives the maximum relative error $\delta = 0.005$. For the TDA part, 1000 lowest eigenvalues are calculated to be included in the determination compensation factor D_{CF}(see Ch. 7).

In order to simulate small pion mass, we gradually increased κ from the free theory until the pion mass becomes reasonably small. Then, for four κ's (0.1900, 1915, 1920, 1925), long simulations were performed to extract the accurate pion masses. Fig. 9.3 shows the results from each kappa run. Since the lattice quark mass is defined as $m = \frac{1}{2\kappa} - \frac{1}{2\kappa_c}$ with the critical κ_c, where the quark mass vanishes, the pion masses squared are plotted as a function of $1/2\kappa$.

The smallest pion mass which we could get was $\sim$330MeV(0.62 in lattice unit) at around $\kappa \simeq 0.1920$. As the kappa increases to 0.1925, the pion mass suddenly jumps to $\sim$ 800MeV. From the three runs of $\kappa = 0.1900, 1915, 1920$, the critical kappa can be estimated as $\sim$ 0.1940. However, the pion mass at kappa values larger than 0.1920 was always $\gtrsim 0.6a^{-1}$.

Fig. 9.4 shows the plaquette average for the run at $\kappa = 0.1925$ as a function of Monte Carlo simulation time. As one can see, the plaquette average seemed stable for 7000-8000

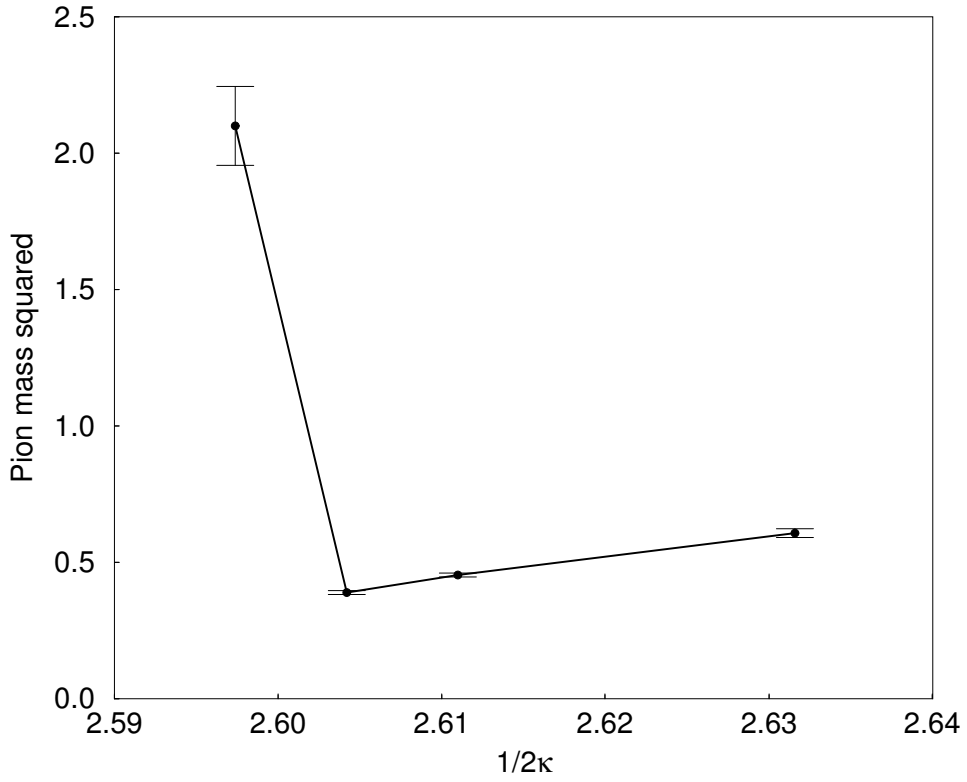

Figure 9.3: Pion mass as a function of $1/2\kappa$

sweeps, and then it has jumped to a new value. The mass also changed from 0.5 to 1.5(see Fig. 9.5). We believe that this behavior of the pion mass as a function of κ belongs to the second among the Sharpe and Singleton's two phase structures of the pion mass, in which as the quark mass decreases, the pion mass reaches a nonzero minimum, and after that, increases, due to the discretization effect of the lattice [39]. The sudden jump corresponds to a transition from the left to the right branch in Fig. 9.2: note that the starting configuration for $\kappa = 0.1925$ was the final configuration for $\kappa = 0.1920$. As pointed out previously, the qualitative symmetry of Fig. 9.2 depends on simplified assumptions (dependence of c_2/c_1 on ϵ) which are presumably only roughly valid in full QCD.

There is another reason to believe that this pion behavior is from the discretization effect. In the earlier simulation with the pure TDA algorithm [28], the same forms of gauge and quark actions were applied on a 6^4 lattice with almost the same physical lattice size. In that simulation, the pion mass of $\sim$ 200MeV could be obtained for the runs of the lightest quarks (~ 0.4 in lattice unit), and the finite volume effect on the pion mass was calculated as only $\sim$ 25MeV. Since the TDA method includes the infrared determinant only with the ultraviolet determinant ignored, the existence of a large minimum of the pion mass in the TDA+Multiboson simulation should come from the ultraviolet determinant, i.e., short-distance effects most influenced by lattice discretization.

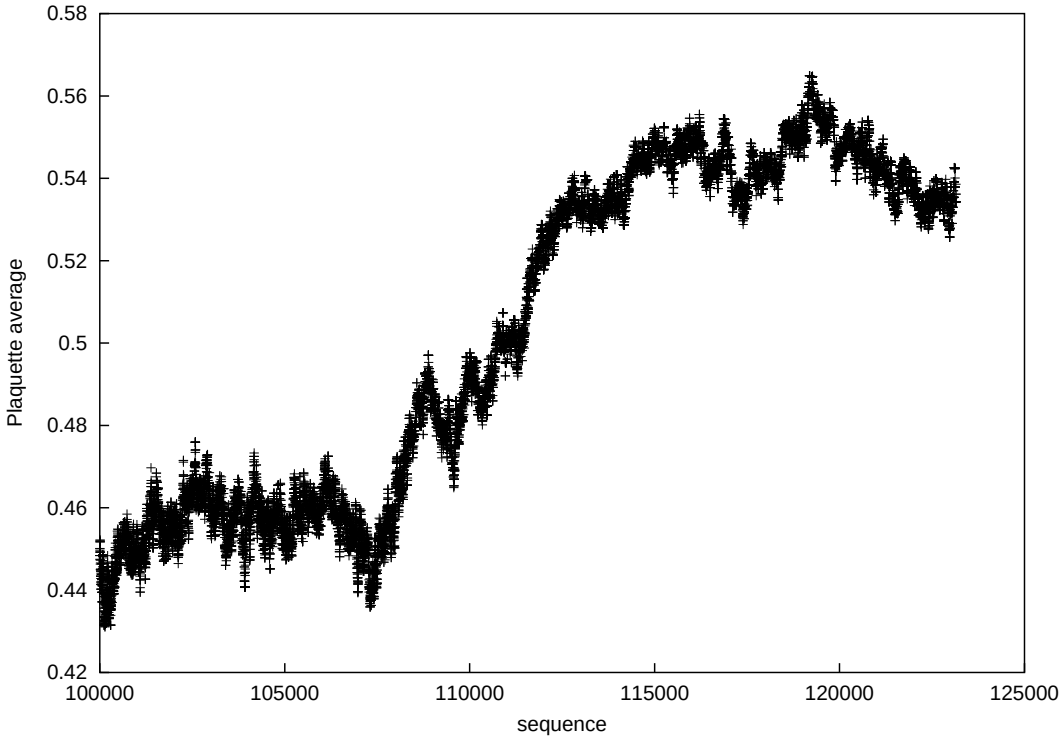

Figure 9.4: Plaquette average at κ=0.1925

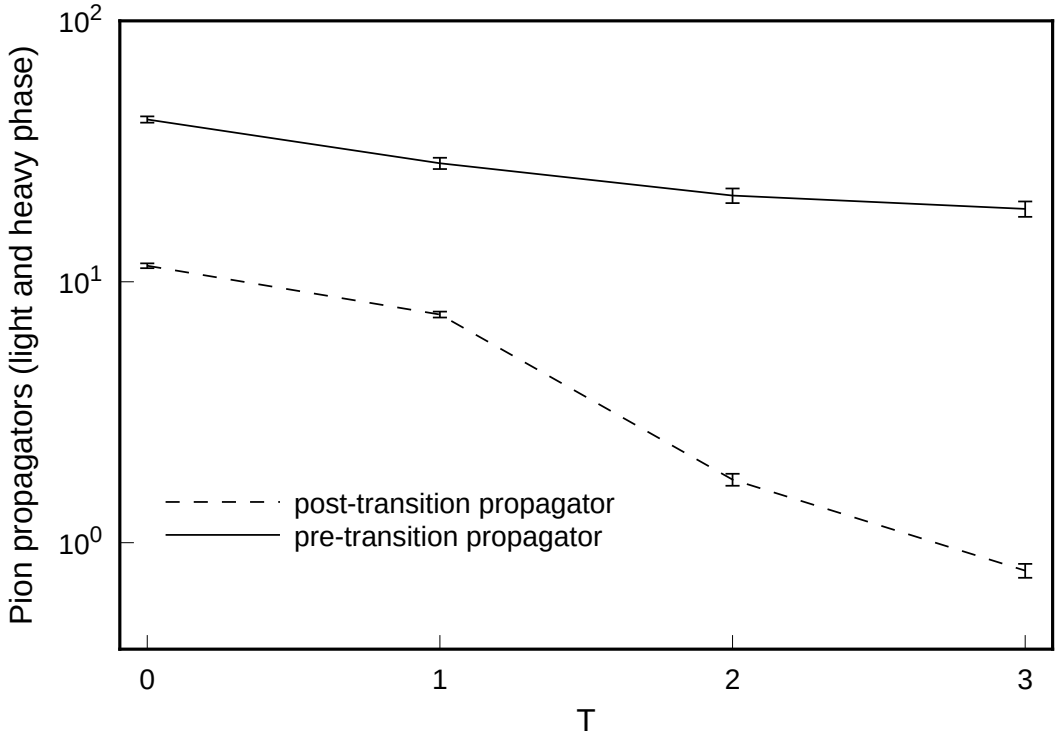

Figure 9.5: Pion propagators at κ=0.1925

10.0 SUMMARY

The strong interaction between hadronic particles are described by Quantum Chromodynamics(QCD). In order to perform nonperturbative calculations in QCD, the continuous space-time is regularized by a finite discrete lattice in lattice QCD, and gluon and quark fields are put on the lattice. Path integrals for hadronic field correlators are computed on the lattice by computer simulations. In this thesis, we have studied two algorithms which use bosonic fields to calculate path integrals involving anticommuting quark fields: the all-point quark propagator algorithm for extracting full quark propagators, and the combined truncated determinant/multiboson algorithm. In each case, the statistical properties of the algorithm were studied, and an application to a problem of physical interest in lattice QCD was presented.

Quark propagators are correlators between two quarks. Hadronic correlators can be constructed with quark propagators. Thus, in order to calculate hadronic correlators, first one needs to calculate quark propagators for each gauge configuration. The conventional method to calculate a quark propagator makes use of linear equation solvers. Such methods give a quark propagator with a single space-time source (i.e. correspond to computing the action of a matrix inverse on a single column vector). Calculation of some hadronic observables, however, requires quark propagators from any source point to any sink point. The pseudofermion method allows one to compute all-point quark propagators from any source to any sink, and hence to extract the full physical content from each gauge configuration, which is particularly important in unquenched lattice QCD as unquenched gauge configurations require a large amount of computational cost to generate. In this pseudofermion method, by introducing a bosonic pseudofermion field for each quark propagator in a hadronic correlator, the full matrix inverse, or all-point propagator, of the Wilson-Dirac operator can be calculated in a

Monte Carlo simulation. The actual simulation update is most simply implemented with the standard heatbath algorithm. However, this simplest approach leads to unacceptably large autocorrelations for low momentum correlators. Further improvements in the Monte Carlo update can be made with the mode-shift method, and by using overrelaxation. For each case, the computational effort required to generate fully decorrelated pseudofermion fields was studied. It was shown that the mode-shift method combined with the overrelaxation method is the most computationally efficient algorithm for the pseudofermion method to obtain all-point propagators.

The pseudofermion method for all-point quark propagators was applied to chiral perturbation theory. The pseudoscalar and axial-vector current correlators in momentum space were calculated. The all-point propagators required for these current correlators were calculated with the pseudofermion method. The chiral parameters up to the next-to-leading order were extracted with very small statistical errors. The lattice simulations were performed on a finite lattice. So there were finite volume effects from the finiteness of the lattice. These finite volume effects were calculated using dimensional regularization on a hypercubic box. Formulas to correct the finite volume effects in physical quantities relevant to pion physics were presented.

Unquenched QCD simulations on a lattice need to generate gauge configurations according to the effective Boltzmann factor involving the quark determinant of the Wilson-Dirac operator which comes from the quark term in the QCD Lagrangian. The nonlocality of the quark determinant results in a very heavy computational load to do the unquenched simulations. The truncated determinant algorithm(TDA) includes the effect from the quark loops of large size by calculating the infrared part of the quark determinant only. In the TDA method one computes the lowest eigenvalues (up to $\sim 2\Lambda_{QCD}$) of the hermitian Wilson-Dirac operator using the Lanczos algorithm, and calculates the infrared determinant from these eigenvalues. Then, the full quark determinant is replaced with the infrared determinant. To make the algorithm exact by including the ultraviolet part of the determinant one can combine the TDA method with Luescher's multiboson method. The multiboson method approximates the ultraviolet determinant with the determinant of the inverse of a polynomial of the hermitian Wilson-Dirac operator. The determinant of this polynomial is computed

with multidimensional gaussian integrals of bosonic fields. By doing this, the ultraviolet part of the nonlocal determinant factor is generated by local multiboson terms in the effective Lagrangian.

The statistical properties of this combined TDA+Multiboson method were studied. The computational simulations with this algorithm were performed varying the number of multiboson fields. As the quarks become light, since the number of multiboson fields required to cover the smallest eigenvalues becomes large, the autocorrelation of gauge configurations from the pure multiboson method becomes large. It was shown that the TDA part saves computational time compared to the pure multiboson method by calculating low eigenvalues of the hermitian Wilson-Dirac operators exactly. The basic result of these studies of the combined TDA/multiboson algorithm was that the computational cost per decorrelated gauge configuration has a minimum at a certain number of multiboson fields. A formula to roughly estimate this minimum was derived and confirmed numerically.

The TDA+Multiboson method was applied to a unquenched QCD simulation at strong coupling with two light degenerate quarks on a 6^4 lattice with the $O(a^2)$ improved gauge action with the twisted rectangle term, and simple Wilson quark action. It was found that for this strongly coupled system at large lattice spacing the pion mass does not become zero with any κ value, but rather has a large minimum as the bare quark mass is tuned through a critical value. According to the Sharpe and Singleton analysis of the pion mass as a function of quark mass, there are two possible phase structures of the pion mass. One is a ordinary phase structure expected to hold at weak coupling, and in the continuum limit, in which the pion mass becomes zero at a critical kappa. In the other strong coupling phase, the pion mass does not become zero for any kappa value. Our simulation results confirm the existence of the second Sharpe-Singleton phase at strong coupling.

BIBLIOGRAPHY

[1] K.G. Wilson, Phys. Rev. D10 (1974) 2445.

[2] A. Smilga, *Lectures on Quantum Chromodynamics* (World Scientific, Singapore, 2001).

[3] I. Montvay and G. Muenster, *Quantum Fields on a Lattice* (Cambridge Univ. Press, United Kingdom, 1997).

[4] M. Creutz, *Quarks, Gluons and Lattices*, (Cambridge Univ. Press, United Kingdom, 1983).

[5] H.J. Rothe, *Lattice Gauge Theories: an Introduction*, 2nd ed., (World Scientific, Singapore, 1997)

[6] C. Michael and J. Peisa, Phys. Rev. D58 (1998) 034506.

[7] A. Duncan, E. Eichten and J. Yoo, Nucl. Phys. Proc. Suppl. 106 (2002) 1061.

[8] N. Madras and A. Sokal, J. Stat. Phys. 50 (1988) 109.

[9] A. Duncan and E. Eichten, Phys. Rev. D 65 (2002) 114502

[10] S. Adler, Phys. Rev. D23 (1981) 2901.

[11] C. Whitmer, Phys. Rev. D29 (1984) 306.

[12] For the ARPACK library, see www.caam.rice.edu/software/ARPACK.

[13] C. Itzykson and J.B. Zuber, *Quantum Field Theory*, (McGraw-Hill, New York, 1980).

[14] S. Pokorski, *Gauge Field Theory*, (Cambridge Univ. Press, United Kingdom, 1987).

[15] J.F. Donoghue, E. Golowich and B.R. Holstein, *Dynamics of the Standard Model*, (Cambridge Univ. Press, United Kingdom, 1992).

[16] J. Gasser and H. Leutwyler, Ann. Phys. 158 (1984) 142.

[17] G. Ecker, arXiv:hep-ph/9805500.

[18] A. Duncan, E. Eichten and H. Thacker, Phys. Rev. D59 (1999) 014505.

[19] A. Duncan, E. Eichten and J. Yoo, Phys. Rev. D65 (2002) 094509.

[20] A. Duncan, E. Eichten, R. Roskies and H. Thacker, Phys. Rev. D60 (2002) 054505.

[21] M. Alford, W. Dimm, G.P. Lepage, G. Hockney and P.B. Mackenzie, Phys. Lett. B361 (1995) 87.

[22] A. Duncan, E. Eichten and H. Thacker, Phys. Rev. D63 (2001) 111501.

[23] H. Leutwyler and A. Smilga, Phys. Rev. D 46 (1992) 5607.

[24] A. Duncan, E. Eichten and H. Thacker, Nucl. Phys. Proc. Suppl. 106 (2002) 254.

[25] J. Gasser and H. Leutwyler, Nucl. Phys. B307 (1988) 763.

[26] R. Courant and D. Hilbert, *Methods of Mathematical Physics*, Vol. 1, (Interscience Publishers, Inc., New York, 1953).

[27] J. Cullum and R.A. Willoughby, J. Comp. Phys. 44 (1981) 329.

[28] A. Duncan, E. Eichten and J. Yoo, arXiv:hep-lat/0209123

[29] H. Mueller-Krumbhaar and K. Binder, J. Stat. Phys, 8 1973.

[30] M. Luescher, Nucl. Phys. B418 (1994) 637.

[31] B. Bunk, K. Jansen, B. Jegerlehner, M. Luescher, H. Simma and R. Sommer, Nucl. Phys. Proc. Suppl. 42 (1995) 49.

[32] C. Alexandrou, A. Borrelli, Ph. de Forcrand, A. Galli and F. Jegerlehner, Nucl. Phys. B456 (1995) 296.

[33] S. Wolfram, *Mathematica*, 4th ed., (Cambridge Univ. Press, 1999)

[34] M.A. Halasz and J.J.M. Verbaarshot, Phys. Rev. Lett. 74 (1995) 3920.

[35] A. Borrelli, Ph. de Forcrand and A. Galli, Nucl. Phys. B477 (1996) 809.

[36] A. Smilga and J. Stern, J. Phys. Lett. B318 (1993) 531.

[37] S. Chandrasekhar, Rev. Mod. Phys, 15 (1943) 1.

[38] A. Kennedy and B. Pendleton, Nucl. Phys. B607 (2001) 456.

[39] S. Sharpe and R. Singleton, Phys. Rev. D 48 (1998) 074501.

[40] S. Aoki, Phys. Rev. D 30 (1984) 2653.